OCEAN DRILLING PROGRAM

LEG 180 PRELIMINARY REPORT

ACTIVE CONTINENTAL EXTENSION IN THE WESTERN WOODLARK BASIN, PAPUA NEW GUINEA

Dr. Philippe Huchon
CNRS, Laboratoire de Géologie
École Normale Supérieure
24 rue Lhomond
75231 Paris Cedex 05
France

Dr. Brian Taylor
School of Ocean and Earth Science and Technology
University of Hawaii at Manoa
2525 Correa Road
Honolulu, HI 96822-2285
U.S.A.

Dr. Adam Klaus
Ocean Drilling Program
Texas A&M University Research Park
1000 Discovery Drive
College Station, TX 77845-9547
U.S.A.

Dr. Jack Baldauf
Deputy Director of
Science Operations
ODP/TAMU

Dr. Adam Klaus
Leg Project Manager
Science Services
ODP/TAMU

September 1998

This informal report was prepared from the shipboard files by the scientists who participated in the cruise. The report was assembled under time constraints and is not considered to be a formal publication that incorporates final works or conclusions of the participating scientists. The material contained herein is privileged proprietary information and cannot be used for publication or quotation.

Preliminary Report No. 80

First Printing 1998

Distribution

D I S C L A I M E R

This publication was prepared by the Ocean Drilling Program, Texas A&M University, as an account of work performed under the international Ocean Drilling Program, which is managed by Joint Oceanographic Institutions, Inc., under contract with the National Science Foundation. Funding for the program is provided by the following agencies:

Australia/Canada/Chinese Taipei/Korea Consortium for Ocean Drilling
Deutsche Forschungsgemeinschaft (Federal Republic of Germany)
Institut Français de Recherche pour l'Exploitation de la Mer (France)
Ocean Research Institute of the University of Tokyo (Japan)
National Science Foundation (United States)
Natural Environment Research Council (United Kingdom)
European Science Foundation Consortium for the Ocean Drilling Program (Belgium, Denmark, Finland, Iceland, Italy, The Netherlands, Norway, Portugal, Spain, Sweden, Switzerland, and Turkey)
Marine High-Technology Bureau of the State Science and Technology Commission of the People's Republic of China

The following scientists were aboard the *JOIDES Resolution* for Leg 180 of the Ocean Drilling Program:

Co-Chief Scientist
Philippe Huchon
CNRS, Laboratoire de Géologie
École Normale Supérieure
24 rue Lhomond
75231 Paris Cedex 05
France
Internet: huchon@ens.fr
Work: 33-1-44-32-22-54
Fax: 33-1-44-32-20-00

Co-Chief Scientist
Brian Taylor
School of Ocean and Earth Science and Technology
University of Hawaii at Manoa
2525 Correa Road
Honolulu, HI 96822-2285
U.S.A.
Internet: taylor@soest.hawaii.edu
Work: 808-956-6649
Fax: 808-956-3723

Staff Scientist
Adam Klaus
Ocean Drilling Program
Texas A&M University Research Park
1000 Discovery Drive
College Station, TX 77845-9547
U.S.A.
Internet: adam_klaus@odp.tamu.edu
Work: 409-845-3055
Fax: 409-845-0876

Sedimentologist
Stefania Gerbaudo
Dipartimento di Scienze della Terra
Università degli Studi di Genova
Corso Europa, 26
Genova 16132
Italy
Internet: andri@dister.unige.it
Work: 39-10-3538287
Fax: 39-10-352169

Sedimentologist
Klas S. Lackschewitz
Geologisch-Paläontologisches Institut
Christian-Albrechts-Universität zu Kiel
Olshausenstrasse 40
24118 Kiel
Federal Republic of Germany
Internet: klackschewitz@gpi.uni-kiel.de
Work: 49-431-880-2818
Fax: 49-431-880-4376

Sedimentologist
Alastair H.F. Robertson
Department of Geology and Geophysics
University of Edinburgh
West Mains Road
Edinburgh EH9 3JW
United Kingdom
Internet: alastair.robertson@glg.ed.ac.uk
Work: 44-131-650-8546
Fax: 44-131-668-3184

Sedimentologist
Sherif Abdel Moneim Awadallah
Earth Sciences Department
Memorial University of Newfoundland
St. John's, NF A1B 3X5
Canada
Internet: sherif@morgan.ucs.mun.ca
Work: 709-737-8142
Fax: 709-737-2589

Paleontologist (foraminifers)/Observer
Russell C.B. Perembo
Department of Geology
University of Papua New Guinea
Box 414
University P.O.
Papua New Guinea
Internet: russ.perembo@upng.ac.pg
Work: 675-267-395
Fax: 675-260-369

Paleontologist (foraminifers)
Johanna M. Resig
Department of Geology and
Geophysics/SOEST
University of Hawaii at Manoa
2525 Correa Road
Honolulu, HI 96822
U.S.A.
Internet: jresig@soest.hawaii.edu
Work: 808-956-7757
Fax: 808-956-5512

Sedimentologist
Timothy R. Sharp
Department of Environmental Sciences
University of Technology, Sydney
P.O. Box 123
Broadway,
Sydney 2007, New South Wales
Australia
Internet: tim.sharp@uts.edu.au
Work: 61-2-9514-1757
Fax: 61-2-9514-1755

Microbiologist
Peter Wellsbury
Department of Earth Sciences
University of Bristol
Wills Memorial Building, Queens Road
Bristol BS8 1RJ
United Kingdom
Internet: peter.wellsbury@bris.ac.uk
Work: 44-117-928-8859
Fax: 44-117-925-3385

Igneous Petrologist
Charles K. Brooks
Dansk Lithosfœrecenter
Øster Voldgade 10
København K 1350
Denmark
Internet: kentb@geo.geol.ku.dk
Work: 45-35-32-24-17
Fax: 45-33-11-08-78

Paleontologist (nannofossils)
William G. Siesser
Department of Geology
Vanderbilt University
Box 46 Station B
Nashville, TN 37235
U.S.A.
Internet: siesser@ctrvax.vanderbilt.edu
Work: 615-322-2984
Fax: 615-322-2138

Paleontologist (nannofossils)
Kyoma Takahashi
Department of Earth and Planetary Sciences
Graduate School of Science
Hokkaido University
N10 W8
Sapporo, Hokkaido 060-0810
Japan
Internet: kyoma@cosmos.sci.hokudai.ac.jp
Work: 81-11-716-2111, ext 3519
Fax: 81-11-746-0394

Structural Geologist
Bernard Le Gall
CNRS UMR 6538-IUEM
CNRS
Geosciences MarinesInstitut Universitaire
Européen du la Mer
Place Copernic
29280 Plouzane
France
Internet: blegall@univ-brest.fr
Work: 33-2 98 49 87 56
Fax: 33-2 98 49 87 60

Metamorphic Petrologist
Véronique Gardien
Laboratoire de Pétrologie et Tectonique
CNRS-UMR 5570
Université Claude Bernard Lyon I
43 Bl du 11 Nov. 1918
Villeurbanne, Cedex 69622
France
Internet: vgardien@univ-lyon1.fr
Work: 33-4-72-44-62-38
Fax: 33-4-72-44-85-93

Metamorphic Petrologist
Brian D. Monteleone
Department of Geosciences
Gould-Simpson Building 210
University of Arizona,
Tuscon, AZ 85721,
U.S.A.
Internet: monteleo@geo.arizona.edu
Work: 520-621-6024
Fax: 520-621-2672

Organic Geochemist
Ian D. Mather
Department of Geology
University of Bristol
Wills Memorial Building
Queens Road
Bristol BS8 1RJ
United Kingdom
Internet: i.d.mather@bris.ac.uk
Work: 44-117-928-8859
Fax: 44-117-925-3385

Paleomagnetist
Gina Marie Frost
Hawaii Institute of Geophysics
and Planetology
University of Hawaii at Manoa
1680 East West Road, Room 602
Honolulu, HI 96822
U.S.A.
Internet: gfrost@soest.hawaii.edu
Work: 808-956-4879
Fax: 808-956-3188

Paleomagnetist
Naoto Ishikawa
School of Earth Sciences
Kyoto University
Sakyo-ku
Kyoto 606-8501
Japan
Internet: ishikawa@gaia.h.kyoto-u.ac.jp
Work: 81-75-753-6871
Fax: 81-75-753-6872

Inorganic Geochemist
Eric H. DeCarlo
Department of Oceanography/SOEST
University of Hawaii at Manoa
1000 Pope Road
Honolulu, HI 96822
U.S.A.
Internet: edecarlo@soest.hawaii.edu
Work: 808-956-6473
Fax: 808-956-7112

Physical Properties Specialist
Garry D. Karner
Lamont-Doherty Earth Observatory
Columbia University
Palisades, NY 10964
U.S.A.
Internet: garry@ldeo.columbia.edu
Work: 914-365-8355
Fax: 914-365-8156

Physical Properties Specialist
Achim Kopf
GEOMAR
Christian-Albrechts-Universität zu Kiel
Wischhofstrasse 1-3
Kiel 24148
Federal Republic of Germany
Internet: akopf@geomar.de
Work: 49-431-600-2333
Fax: 49-431-600-2922

Physical Properties Specialist
Shannon C. Stover
JOIDES Logging Scientist Department
of Geological Sciences
University of Colorado at Boulder
Campus Box 399
Boulder, CO 80309
U.S.A.
Internet: shannon.stover@ucsu.colorado.edu
Work: 303-735-5032
Fax: 303-492-2606

JOIDES Logging Scientist
Elizabeth J. Screaton
Department of Geology
University of Florida
241 Williamson Hall
Gainesville, FL 32611
U.S.A.
Internet: screaton@geology.ufl.edu
Work: 352-392-4612
Fax: 352-392-9294

LDEO Logging Scientist
Bernard Célérier
ISTEEM-CC57
Université de Montpellier II
34095 Montpellier Cedex 05
France
Internet:
bernard.celerier@dstu.univ-montp2.fr
Work: 33-4-67-14-39-06
Fax: 33-4-67-14-47-74

LDEO Logging Trainee
Jacqueline Floyd
Lamont-Doherty Earth Observatory
Route 9W
Columbia University
Palisades, NY 10964
U.S.A.
Internet: jsfloyd@ldeo.columbia.edu
Work: 914-365-8318
Fax: 914-365-3181

Schlumberger Logging Engineer
Robert Laronga
Schlumberger Offshore Services
369 Tristar Drive
Webster, TX 77598
U.S.A.
Work: 281-480-2000
Fax: 281-480-9550

Geophysicist
Andrew M. Goodliffe
Department of Geology and
Geophysics/SOEST
University of Hawaii
1680 East-West Road
Honolulu, HI 96822
U.S.A.
Internet: andrew@soest.hawaii.edu
Work: 808-956-5238
Fax: 808-956-3723

Observer
Paul Kia
Private Mail Bag
Geological Survey
Port Moresby
Papua New Guinea
Internet: geosurv@online.net.pg
Work: 675-322-4259

Observer
Jimmy K. Haumu
Department of Petroleum and Energy
Petroleum Division
P.O. Box 1993
Port Moresby
Papua New Guinea
Work: +3224200/3224213

SCIENTIFIC REPORT

ODP LEG 180 INITIAL RESULTS: ACTIVE CONTINENTAL EXTENSION IN THE WESTERN WOODLARK BASIN, PAPUA NEW GUINEA

INTRODUCTION

The continuum of active extensional processes, laterally varying from continental rifting to seafloor spreading, in the western Woodlark Basin-Papuan Peninsula region of Papua New Guinea (Fig. 1) provides the opportunity to investigate the mechanics of lithospheric extension and continental breakup. Seafloor spreading magnetic anomalies indicate that during the last 6 m.y. the formerly contiguous, eastward extensions of the Papuan Peninsula (the Woodlark and Pocklington Rises) were separated as a westward propagating spreading center opened the Woodlark Basin (Weissel et al., 1982; Taylor et al., 1995, unpubl. data; Goodliffe et al., 1997; Goodliffe, 1998). The present spreading tip is at 9.8°S, 151.7°E. Farther west, extension is accommodated by continental rifting, with associated full and half graben, metamorphic core complexes, and peralkaline rhyolitic volcanism (Smith and Simpson, 1972; Smith, 1976; Davies, 1980; Hegner and Smith, 1992; Davies and Warren, 1992; Hill et al., 1992, 1995; Baldwin et al., 1993; Hill and Baldwin, 1993; Stolz et al., 1993; Lister and Baldwin, 1993; Hill, 1994). Current rifting and spreading are confirmed by kinematic measurements using Global Positioning System (GPS) observations (Tregoning et al., 1998**)**. Earthquake source parameters and seismic reflection data indicate that normal faulting is active at depths above 9 km in the region of incipient continental separation (Figs. 2, 3, 4, 5, 6; Abers, 1991; Taylor et al., 1995, 1996, unpubl. data; Mutter et al., 1996; Abers et al., 1997). A low-angle normal fault emerges along the northern flank of Moresby Seamount, a continental crustal block with greenschist metamorphic basement. Asymmetric basement fault blocks overlain by only minor ponded sediments characterize the margin to the south, whereas the margin to the north has a down-flexed pre-rift sedimentary basin and basement sequence unconformably beneath synrift sediments (Figs. 3–5).

The primary objectives of Ocean Drilling Program (ODP) Leg 180 were to (1) characterize the composition and in situ properties (stress, permeability, temperature, pressure, physical properties, and fluid pressure) of an active low-angle normal fault zone to understand how such faults slip, (2) determine the sedimentology, magnetobiostratigraphy, physical properties, and vertical motion history of the northern margin, including the nature of the forearc basin (and basement?) sequence and hence the pre-rift history, and (3) determine the internal structure and composition of Moresby Seamount, including the nature of basement (rock type, P-T-t, structural fabric, and deformation history). These parameters will be used as input into regional models for the extensional deformation of continental lithosphere, particularly the mode, timing, and amount of extension prior to spreading initiation.

DRILL SITES

During Leg 180 we drilled a transect of sites just ahead of the spreading tip: Sites 1109, 1115, and 1118 on the down-flexed northern margin; Sites 1108 and 1110–1113 into the rift basin sediments above the low-angle normal fault zone; and Sites 1114, 1116, and 1117 on the footwall fault block, Moresby Seamount —Site 1114 near the crest, 1116 on the southern flank, and 1117 into the upper fault face (Figs 3–6, 7, 8; Table 1).

The drill sites are located within a grid of multichannel seismic (MCS) lines and multibeam bathymetry (Figs. 7, 8). The northern margin sites (1109, 1115, and 1118), cored to 802, 803, and 927 meters below seafloor (mbsf), respectively, penetrated the synrift Pliocene–Pleistocene cover sequence and into pre-rift sections: dolerites at Sites 1109 and 1118, and Miocene forearc clastics at Site 1115. Penetration into greenschist metadiabase beneath the 286-m-thick Pliocene–Pleistocene section and 6-m-thick fault breccia at Site 1114 extended to 407 mbsf. Basement was not reached beneath the 159 m of coarse rift clastics at Site 1116. The planned triple casing reentry hole at Site 1108 was aborted because of hydrocarbon concerns after drilling Hole 1108B to 485 mbsf. The presence of higher molecular weight hydrocarbons at depth (Site 1108), and the extent of talus proximal to Moresby Seamount where the fault is shallow (Sites 1110–1113, which penetrated 25–174 mbsf), precluded use of the available technology to meet our primary objective. At Site 1117, however, the ~100-m-thick fault zone of gouge, mylonite, and breccia, was cored through (meta)gabbro. Sites 1109, 1114, 1115, and 1118 were all logged with triple combo geophysics and Formation MicroScanner (FMS) sonic tool strings, and vertical seismic profiles were obtained at Sites 1118 (complete), 1109 and 1115 (partial), making this one of the most successful ODP logging legs to date.

The primary results are presented first by site and then by theme. In the following section the site summaries are arranged in geographic order, progressing from north to south along the transect.

SITE SUMMARIES

Site 1115

Hole 1115A (APC [advanced hydraulic piston corer]):
9°11.389´S, 151°34.450´E; 1149.6 mbsl (meters below sea level)
0–4.40 mbsf cored; 4.43 m recovered (101%)

Hole 1115B (APC/XCB [extended core barrel]):
9°11.382´S, 151°34.437´E; 1148.8 mbsl
0–293.10 mbsf cored; 286.84 m recovered (98%)

Hole 1115C (RCB [rotary core barrel]):
9°11.383´S, 151°34.422´E; 1148.7 mbsl
0–283.5 mbsf drilled without coring; 283.5–802.5 mbsf cored; 291.56 m recovered (56%)

The objectives of our study at Site 1115 were to determine the sedimentology, biostratigraphy, and vertical motion history of the Woodlark Rise (the northern, upper plate margin to the Moresby detachment fault), including the pre-rift history of the Trobriand forearc basin sequence. The site was located ~35 km to the north of Site 1109 to (1) better characterize the slope sediments and provide widely spaced data from shallower water depths for flexural subsidence models, (2) avoid the thick dolerite that prevented sampling of the pre-rift forearc sequence at Site 1109, and (3) sample the upper ~150 m of section that has been eroded by a submarine channel further south.

From bottom to top, the sedimentary succession cored at Site 1115 shows (1) a shoaling and coarsening upward, middle Miocene forearc sequence, unconformably below (2) a late Miocene nonmarine (fluvial?) and lagoonal succession, and (3) a shallow marine, then progressively deepening and fining upward, latest Miocene (5.54 Ma) to Pleistocene sequence related to the subsidence of the margin during the rifting of the Woodlark Basin. The synrift sequence is undeformed, with bedding dips <10% throughout, whereas the forearc sequence below exhibits a few normal, reverse, and strike-slip faults.

We cored the upper ~230 m of the ~5-km-thick Trobriand forearc basin sequence. This section was deposited at >135 m/m.y. and is older than 12.1 Ma and younger than 15.1 Ma. The sequence comprises turbiditic sands, silts, and clays derived from calc-alkaline arc sources including distinctive clinopyroxene-phyric basic extrusives. The turbidites below 615 mbsf were deposited in upper bathyal depths (150–500 m). Above 659 mbsf they are joined by redeposited neritic carbonates and deposits marked by sediment instability, possibly related to local channeling and/or regional tectonism. Benthic foraminifers indicate a change to neritic deposition (50–150 m) above 615 mbsf and by 13.6 Ma. The sediments record substantial input of shallow-water carbonate. The upward shallowing of the forearc sequence may be attributed to both filling of the basin and tectonic uplift.

An unconformity and hiatus at 574 mbsf resulted from the emergence of the forearc sequence. The unconformity is seismically imaged throughout the Trobriand forearc basin and is younger than 9.63 Ma at the Nubiam-1 well ~100 km to the northwest. At Site 1115, the unconformity is older than 5.54 Ma, by which time sediments younger than 8.6 Ma had accumulated to 513 mbsf at rates >13 m/m.y. The basal sediments are nonmarine (fluvial?)

conglomerate (to 566 mbsf), topped by an organic-rich silty claystone (inner lagoonal), and capped by a siltstone with common to abundant shell fragments (open-marine lagoonal).

Margin subsidence is recorded by inner neritic (<50 m) sandy siltstone (to 475 mbsf) passing upward to silty sandstones (to 417 mbsf) deposited on an open shelf (50–150 m) influenced by traction currents. Sedimentation rates from 4.0–5.5 Ma averaged 45 m/m.y.

From 4 to 3 Ma, the average sediment accumulation dramatically increased to ~284 m/m.y. This resulted in undercompaction and anomalously high measured porosities between ~420 and ~300 mbsf. Above 417 mbsf, turbidites were deposited in deeper water, upper bathyal (150–500 m), and they fine upward from sandy silty claystone to silty claystone. Volcaniclastic sand and silt horizons, originating from a calc-alkaline arc source, remain little changed throughout the Pliocene. The pelagic carbonate component increases above 300 mbsf, with $CaCO_3$ concentrations increasing from ~20 to ~75 wt% at the seafloor.

Since 3 Ma the sedimentation rate markedly slowed, initially to ~79 m/m.y. (to 2 Ma) and then ~59 m/m.y. (to 0.5 Ma) and ~34 m/m.y. thereafter. The marked change in the sediment supply to the area corresponds in part to a decrease in the volcaniclastic sand deposited by turbidity currents. Above 169 mbsf (2.58 Ma), the input of fine metamorphic detritus marked by the presence of illite to 520 mbsf also ends. By this time and since then, the sedimentation rate was much slower than the margin subsidence and the surface deepened to upper middle bathyal (500–1150 m) depths. No record of the last 120 k.y. is preserved and this may be responsible for the low porosities (65% to 70%) near the surface. Pleistocene sedimentation was dominated by nannofossil ooze with volcanic ash. The Pleistocene ash and middle–late Pliocene volcanogenic turbidites record a marked increase in explosive Trobriand Arc volcanism since 3.7 Ma.

The thermal gradient determined from five temperature measurements between 26 and 227 mbsf is 28°C/km, yielding a heat flow of 28 mW/m^2 given the average thermal conductivity measured on cores from this interval of 1 W/(m•K).

The magnetostratigraphic record of the upper 400 m is very good. The Brunhes/Matuyama/Gauss/Gilbert polarity transitions, and the Jaramillo, Olduvai, and Kaena Subchrons are identified, as are the Cobb Mountain and Reunion events. Very low magnetic susceptibilities characterize the intervals 210–410 mbsf and 480–550 mbsf, without apparent correlation to grain size, lithology, or sedimentation rate. The variation of susceptibility with depth observed at Site 1115 between 120 and 550 mbsf is similar to that observed at Site 1109 between 80 and 705 mbsf, and the susceptibility boundaries at both sites are time correlative.

Hole 1115C was successfully logged above 784 mbsf with triple combo geophysics and FMS-sonic tool strings. The well seismic tool was used to record check shots near the base of the hole, allowing depth correlation with seismic reflection lines.

The longest profile to date of the deep subseafloor biosphere was made at this site. Bacteria were present in the deepest sample analyzed (801 mbsf) and both dividing and divided cells were present to 775 mbsf. The persistence of apparently living microbial life into indurated sedimentary rock ~15 m.y. old and 801 mbsf extends the limit of the biosphere, whose base remains undefined. Methane is present at levels above 1000 ppm from 250 to 450 mbsf and above 20,000 ppm from 572 to 802 mbsf. The C_1/C_2 ratios generally exceed 1500 and 3000 over the same intervals, and broad maxima in ammonia occur within 200–450 mbsf and at the base of the hole. These observations are consistent with a biogenic origin for the volatile hydrocarbons and the presence of a significant amount of bacteria at depth.

High-resolution pore-water sampling (63 whole rounds) comprehensively documents the interstitial water chemical variations. In the upper 300 mbsf of the cored section, pore-water variations primarily reflect the oxidation of organic matter and the concomitant early diagenesis of biogenic carbonate (including aragonite) leading to precipitation of dolomite, as well as alteration of detrital, mostly volcanic, matter. Further downhole, most of the pore-water variations are controlled largely by the alteration of volcanic minerals and the formation of clays and zeolites. Silicification appears to be a dominant process below 500 mbsf. The formation of calcite cements is significant in sediments of the forearc sequence.

Site 1109

Hole 1109A (APC):
9°30.390´S, 151°34.388´E; 2210.9 mbsl
0–9.50 mbsf cored; 9.96 m recovered (105%)

Hole 1109B (APC):
9°30.396´S, 151°34.391´E; 2211.1 mbsl
0–14.80 mbsf cored; 15.14 m recovered (102%)

Hole 1109C (APC/XCB):
9°30.392´S, 151°34.390´E; 2211.0 mbsl
0–375.70 mbsf cored; 323.11 m recovered (86%)

Hole 1109D (RCB):
9°30.380´S, 151°34.355´E; 2211.0 mbsl
0–352.80 mbsf drilled without coring; 352.80–802.00 m cored; 299.87 m recovered (67%)

Site 1109 is located on the Woodlark Rise, 11 km north of a major south-dipping normal fault system that is antithetic to the low-angle fault dipping north from Moresby Seamount. The site was positioned to cross a sequence boundary and an angular unconformity at about 350 and 770 mbsf, respectively, beneath which a lower stratified sequence, interpreted to be pre-rift forearc basin sediments, dips northward at ~10%.

Four holes were drilled at Site 1109: two short APC holes (1109A and 1109B), one APC/XCB (1109C), and one RCB (1109D). These allowed coring to a total depth of 802 mbsf, complete logging above 786 mbsf with the triple combo geophysical tool, logging two intervals (112–351 and 376–786 mbsf) with the FMS-sonic tools, and conducting a well seismic tool-vertical seismic profile (WST-VSP) with nine receiver locations from 378 to 460 mbsf. The following description uses unit boundaries derived from integrated core-log data interpretation.

Data from Site 1109 show a record of progressive subsidence (from subaerial to lagoonal, then shallow marine and deep water) over a period from the early Pliocene to late Pleistocene. These data provide the information to fulfill one of our primary objectives: to determine the sedimentology, biostratigraphy, and vertical motion history of the synrift sediments on the hanging wall margin to the Moresby low-angle normal fault.

A second objective, to determine the nature of the forearc basin sequence beneath the rift-onset angular unconformity, was thwarted by the unexpected presence of a massive dolerite with ophitic texture from 773 to 802 mbsf overlain to 730 mbsf by a conglomerate of dolerite and

some basalt cobbles in an altered clayey silty matrix with nonrecovered interbeds likely similar to the overlying unit. The dolerite has seismic velocities of 5–6 km/s. In hindsight, culminations observed on reflection seismic sections to be developed locally on the erosional unconformity—previously interpreted as reefs—are more likely to be volcanic constructions.

From 713 to 730 mbsf, a very altered, clay-rich siltstone and fine-grained sandstone were recovered, including goethite concretions. A nonmarine, swampy setting is inferred. These sediments contain scattered basalt/dolerite clasts that logging data indicate were derived from discrete conglomerate intercalations. The oogonia of charophyte algae present in Section 1109D-39R-CC indicate a locally freshwater environment at the top of this unit.

We envision deposition in a lagoonal setting of the silty claystone and clayey siltstone encountered between 672 and 713 mbsf. Shell, plant, and wood fragments are common to abundant. The lagoon was alternately brackish and, as indicated by the presence of dolomite, hypersaline. This unit has high natural gamma ray and porosity (45%–50%), low magnetic susceptibility, and velocities about 2 km/s.

The first (early Pliocene: NN13 and N19/20) shallow-marine (<150 m water depth) deposits occur at 588–664 mbsf and are mixed carbonate-siliciclastic rocks. From 599 to 672 mbsf the lithology consists dominantly of well cemented, 30%–40% porosity, sandy bioclastic packstone-grainstone. A lower limestone section (643–672 mbsf) with high resistivity (3 Ωm), has low natural gamma ray, 40–80 wt% carbonate, and average velocities of 2.5–3.0 km/s. An upper sandstone section with lower resistivity (<2 Ωm), has high natural gamma ray, 20–30 wt% carbonate, and average velocities of 2.0–2.5 km/s. Above this is an interval (570–599 mbsf) of calcareous (bioclastic) sandstone with 40–50 wt% carbonate and 45%–50% porosity. The entire sequence reflects relatively shallow-water sediments derived from both volcanic-related and neritic carbonate source materials that accumulated before 4 Ma at >70 m/m.y.

A succession of clay-rich siltstones and silty claystones, interlayered with thin (1–10 cm) medium/fine-grained sandstones, at 390–570 mbsf were rapidly deposited (312 m/m.y.) in upper bathyal (150–500 m) water depths until ~3.35 Ma. Porosity increases (to 60%) as carbonate decreases (to 25 wt%) upsection to ~480 mbsf, whereas velocities steadily decrease from 2.0 to 1.8 km/s up the unit, and magnetic susceptibilities are constantly low above 540 mbsf. These are hemipelagic carbonate muds with turbiditic sand interbeds from a dominantly unaltered basalt-andesite volcanic source with minor neritic carbonates, deposited on a well-oxygenated and extensively bioturbated slope.

Above 380 mbsf, significantly greater magnetic susceptibilities (that continue to 83 mbsf) correspond to the influx of clays and silts from an additional source terrane, one that is characterized by altered calc-alkaline volcaniclastic material and metamorphic detritus with mixed-layer, and probably smectite, clays. Between 330 and 390 mbsf (~3.07–3.35 Ma) the silty claystone is nearly devoid of sandy interbeds. The lower portion (up to 353 mbsf) has a high frequency of layers with unaltered volcaniclastics. The section from 295 to 330 mbsf was deposited at 69 m/m.y. between 2.57 and 3.07 Ma. Seismic reflection data show that this compressed section is part of a conformable slope sequence that substantially thickens downslope toward the rift basin to the south (i.e., there is a regional “onlap” relationship of flat basin turbidites laterally continuous with conformable slope deposits).

The margin continued to subside with an accumulation rate of 66 m/m.y. between 3.07 and 1.95 Ma (295–255 mbsf), and above 285 mbsf was at middle bathyal (500–2000 m) water depths. Distal silt-clay bioturbated turbidites, with volcanic, terrigenous and biogenic components, rapidly

onlapped the margin (225 m/m.y.) from 1.95 Ma until 1.00 Ma (~42 mbsf). These include a significant component of reworked slope sediments, as evidenced by dominantly upper Pliocene biota in the younger section. Volcaniclastic sands are most frequent from ~100 to 170 mbsf. Silt to coarse sand interbeds are common from 170 to 247 mbsf, including a poorly recovered sand from 218 to 233 mbsf. These sands are remarkable for their high thorium and potassium contents, producing high natural gamma ray counts, and lower porosities (40%–50%) and higher velocities (2 km/s) than adjacent intervals (60%–70% and 1.7 km/s, respectively).

Between 1.00 and 0.46 Ma the site was relatively sediment starved and/or intermittently eroded (the site is located in a submarine valley), with net accumulation rates of 21 m/m.y. of calcareous clayey silt and silty clay with some thin volcanic ash layers. Since 0.46 Ma, nannofossil-rich, calcareous sand, silt, and clay with volcaniclastic sand and volcanic ash, were deposited at 67 m/m.y. The site subsided to lower bathyal depths (>2 km) by NN21 (0.26 Ma).

Extensional deformation is very weak throughout the section, except for minor normal faults at about 260 and 360 mbsf and normal shear zones at 678–685 mbsf and in the dolerite. A folded region 36–55 mbsf is interpreted as a slump.

Velocities linearly increase with depth from 1.5 km/s at the surface to 1.9 km/s at 520 mbsf, and then more rapidly to 2.2 km/s at 590 mbsf with the increasing carbonate. Velocities increase up to 3–4 km/s and are more variable in the bioclastic sandstones and limestones between 590 and 672 mbsf, and then return to 2 km/s in the lagoonal sequence below that. Porosity decreases downward, but the usual negative exponential decay is interrupted at two levels (160–280 and 350–540 mbsf) where the higher porosity reflects undercompaction correlated with periods of high sedimentation rates (300–400 m/m.y.). The thermal conductivity generally mirrors the porosity-depth profile and ranges from 0.78 to 1.5 W/(m•K), except for the dolerite, which shows values up to 2 W/(m•K). Six temperature measurements down to 170 mbsf define a linear thermal gradient of 31°C/km and, when combined with an average thermal conductivity of 0.9 W/(m•K) over this interval, a heat flow of 28 mW/m^2.

Although their number rapidly decreases with depth, bacteria are present in all samples obtained down to 746 mbsf. Total populations and numbers of dividing and divided cells show obvious relationships to the sediment geochemistry. Pore-water constituent profiles show that carbonate diagenesis occurs at shallow depth (above 100 mbsf), aided by the bacterial decomposition of organic matter. Diagenetic transformation of pre-existing detrital clay minerals occurs to 300 mbsf. Bacterial activity further downhole is evidenced by deep-seated (430–550 mbsf) ammonia and alkalinity sub-maxima (the latter likely due to increased CO_2 production). Of note is a generally increasing pH downhole, from 7.8 to greater than 8.6. Pore-water composition also reflects the alteration of volcanic components, formation of authigenic clay minerals, silica diagenesis, and diffusion of elements above the shell-rich and freshwater units below 672 mbsf. A crossover of Ca and Mg profiles, as often observed above igneous sills, occurs at 661 mbsf.

Headspace gas analyses show a typical methane profile, with concentrations increasing rapidly at 100 mbsf from ~5 to ~6000 ppm, then remaining between 1000 and 10,000 ppm down to 600 mbsf. Below 600 mbsf, methane content begins to decrease, reaching 5 ppm by 720 mbsf. The only other hydrocarbon detected was C_2, but it remained below 3.2 ppm throughout the entire cored section. The C_1/C_2 ratios did not drop below 1000, and organic carbon was generally <1% throughout the core.

Site 1118

Hole 1118A (RCB):
9°35.110´S, 151°34.421´E; 2303.6 mbsl
0–205.0 mbsf drilled without coring;
205.0–926.6 mbsf cored; 466.21 m recovered (65%)

Site 1118 is located 1.8 km north of a major south-dipping normal fault system that is antithetic to, and bounds the rift basin above, the low-angle fault dipping north from Moresby Seamount. The location was selected in order to drill through the thick synrift section onlapping the northern margin and to penetrate an angular unconformity into north-dipping reflectors deep in the inferred pre-rift forearc basin sequence. The site is about 9 km due south of Site 1109 and has similar objectives in common to it and Site 1115, namely to determine (1) the sedimentology, biostratigraphy, and vertical motion history of the northern margin, and (2) the nature of the forearc basin and basement sequence.

Data from Site 1118 record the progressive subsidence of an early Pliocene, subaerially eroded and tropically weathered, landmass. A conglomerate of diabase with minor basalt was recovered and imaged with FMS below 873 mbsf. Iron oxides and well-rounded clasts reveal that the diabase, similar to that encountered at Site 1109 (although locally more pegmatitic), was exposed to subaerial alteration. Shearing and veining fragmented and partially brecciated the diabase, which was deposited as a poorly sorted, probably fluvial conglomerate mixed with various clasts and sediment, including paleosols.

The diabase conglomerate is overlain to 857 mbsf by a sequence of early Pliocene limestones, calcareous paraconglomerates, and a volcaniclastic sandstone that was deposited in a marine lagoon with abundant calcareous algae. This sequence is well marked in the geophysical logs and by highs in the $CaCO_3$ profile of >80 wt%. A VSP shows that the diabase-limestone section corresponds to a strong reflector at the base of the sedimentary sequence that mantles underlying northward-dipping reflectors, which were not penetrated.

The Gauss/Gilbert Chron boundary (3.58 Ma), occurring at 846–850 mbsf, dates an upward-fining sequence disconformably above the limestones as all middle Pliocene and younger, in agreement with paleontological data (Biozones N20–N21 and NN16A–NN19A through the top of the cored sequence at 205 mbsf). The lower sedimentary section records a significant terrestrial input, including wood fragments, confirmed by the C/N ratio, which indicates a mixed-marine and terrigeneous source of organic carbon. The whole sequence records turbiditic and hemipelagic sedimentation. It comprises mixed volcaniclastic sandstones, siltstones, and minor claystones, then mostly siltstones and claystones interbedded with turbiditic sandstones and siltstones that decrease in proportion upward. The orientations of the subhorizontal maximum axes of the ellipsoids of magnetic susceptibility (corrected for bedding dip and core orientation) between 490 and 680 mbsf suggest an east-southeast/west-northwest directed paleocurrent during sedimentation, almost perpendicular to the present-day slope.

The sedimentation rate from 3.58 to 2.58 Ma (387.5 mbsf) was 479 m/m.y., the highest encountered during Leg 180, with benthic foraminifers revealing an upper bathyal (150–500 m) paleowater depth. Between 2.58 and 1.95 Ma (288 mbsf), the sedimentation rate decreased to 155 m/m.y., and the paleodepth was middle bathyal (500–2000 m) to at least 205 mbsf. Apparently, rapid subsidence since 3.6 Ma was accompanied by sufficient sediment supply to limit deepening

of the seafloor until 2.6 Ma. High porosities, slowly decreasing from 50%–60% at 205 mbsf to 40%–50% at 800 mbsf, likely reflect underconsolidation related to the high sedimentation rates observed.

Volcanic ash and volcaniclastic sands are ubiquitous throughout the Pliocene sedimentary section, but especially so between 3.0–3.6 Ma when a predominance of rhyo-dacitic glass reflects explosive silicic volcanism probably associated with rifting of the continental arc.

Most of the sedimentary section is undeformed with nearly horizontal beds and shows compaction-related minor faults as well as common slump folds. The abundance of synsedimentary features on such nearly level seafloor suggests an unstable area periodically shaken by earthquakes and affected by mass movement.

As seen in other northern sites drilled during Leg 180, the variations in interstitial water constituents reflect the oxidation of organic matter mediated by microbial activity and the concomitant early diagenesis of biogenic carbonates. Volcanic alteration and authigenesis are important processes, particularly in the lower part of the hole. The abundance of volcaniclastic sands and the higher porosities in the lower part of the hole, when combined with the high temperature gradient (~63°C/km), greatly influence the pore-water chemistry. In particular, the dissolved silica, lithium, and strontium show higher concentrations than might otherwise be expected. In addition, temperature measurements in the open hole during a logging run suggest migration of warm fluids at 700–800 mbsf.

Both methane and ethane, whose ratio is between ~5000 and ~1600, are present down to ~700 mbsf, below which ethane is not detected. The highest concentrations in these two volatile hydrocarbons occur where sulfate disappears from the interstitial water, attesting to a biogenic origin.

Bacteria population numbers and dividing and divided cells decrease rapidly with increasing depth and conform to the general model for their distribution in marine sediments. In extending their known distribution to 842 mbsf at this site, the deepest samples so far obtained, there is an indication that numbers are decreasing more rapidly than the model predicts, resulting in a sigmoidal depth distribution in these sediments.

Site 1108

Hole 1108A (jet-in test only):
9°44.708´S, 151°37.514´E; 3162.7 mbsl
0–16.3 mbsf drilled without coring

Hole 1108B (RCB):
9°44.724´S, 151°37.543´E; 3177.2 mbsl
0–494.90 mbsf cored; 148.58 m recovered (30%)

Site 1108 is located in the seismically active region of incipient continental separation 1 nmi ahead of the neovolcanic zone of the Woodlark Basin spreading center, Papua New Guinea. Here, a continental fault block (Moresby Seamount: summit 120 mbsl) forms the footwall to a low-angle normal fault imaged to 9 km that dips 25%–30% beneath a 3.2-km-deep, asymmetric rift basin with more than 2 km of sediment fill. At Site 1108 we sought to drill through ~900 m of the rift basin sediments, the low-angle normal fault zone, and into the footwall metamorphics. The primary objectives at this site were to (1) characterize the composition and in situ properties

(stress, permeability, temperature, pressure, physical properties, and fluid pressure) of the active low-angle normal fault zone to understand how such faults slip and (2) determine the vertical motion history of the hanging wall and the footwall as local ground truth for models of the timing and amount of continental extension prior to spreading initiation. Hole 1108A was a jet-in test in anticipation of reentry operations. Hole 1108B was rotary cored to 485 mbsf, with ~60 m of open-hole logging using the triple combo and temperature tools, before unstable hole conditions terminated operations. The site was not deepened because of pollution prevention and safety concerns, and hence the primary objectives were not met.

The first core contained late Pleistocene nannofossil-bearing hemipelagic sediment: calcareous clay with minor volcaniclastic silt and sand. Talus from Moresby Seamount was recovered as isolated clasts from 14.5 to 62.7 mbsf, including dark siliciclastic sandstone and siltstone, volcanic breccia, microgranite, granodiorite, epidosite, greenschist mylonite, and biotite gneiss. Some glassy basalt fragments were incorporated from submarine eruptions. Trace amounts of adhering sediments reveal biostratigraphic ages >1.25 Ma by 24.1 mbsf. Quartzo-feldspathic-lithic sand from 62.7 to 63.4 mbsf may relate to and herald the overlying talus. Gas observed bubbling out of the top of the core barrel for this interval may reflect penetration of a gas hydrate layer.

Terrigenous turbidites, now lithified to sandstones, siltstones, claystones, and minor conglomerates, constitute the remainder of the section 72.3–485.2 mbsf. Ages increase from 1.67 to 1.75 Ma at 82.8 mbsf to less than 3.35 Ma at the base. Sedimentation rates increase downsection, from 325 m/m.y. at 1.7–2.0 Ma to 425 m/m.y. at 3.0–3.2 Ma. Benthic foraminifers indicate deposition in deep water (lower bathyal: >2000 m), except for middle (500–2000 m) to lower bathyal conditions below 410 mbsf.

The majority of the turbidites comprise interbedded sandstones, siltstones, and claystones in which medium- to coarse-grained sediments dominate. The sandstones above ~330 mbsf contain a high proportion of metamorphic-derived lithoclasts, related mineral grains, and altered igneous-rock-derived grains (volcanic and ophiolitic), whereas those below contain large amounts of material derived from basic and acidic volcanic and minor plutonic rocks. Planktonic foraminifers and bioclasts of shallow-water origin are common to both sections.

A subunit from 139.4 to 202.2 mbsf comprises foraminifer-bearing clayey siltstone and silty claystone with occasional fine-grained sandstone. Bioturbation is common. Minor disseminated pyrite is suggestive of relatively low-oxygen bottom conditions at times. Subunits of thin conglomerate were recovered near 313, 380, and 437 mbsf. The clayey siltstone subunit shows abundant evidence of brittle deformation characterized by bedding dips up to 35%, low- angle shearing, brecciation, and ubiquitous slickensides. The faults dip at moderate angles (~45%) and most of the structures indicate normal senses of displacement in an extensional fault zone. The greatest frequency of fractures and faults is concentrated between 158 and 173 mbsf. Within this interval there is an age offset from 2.0 to 2.58 Ma between 159.6–164.8 and 172 mbsf. Based on the sedimentation rates above and below, ~200 m of section appears to be cut out by this normal fault near 165 mbsf.

Within the more competent lithologies below, the intensity of tectonic deformation falls off markedly and bedding is subhorizontal. However, below 350 mbsf the turbidites become finer grained (more claystones, siltstones, and fine sandstones), and the section is once more deformed with scaly fabrics, fractures, and evidence of shear along fault planes. Tectonic deformation appears to be concentrated in the finer grained units.

Lab-measured porosities show an expected exponential decay with depth below ~160 mbsf, but the misfit of these values when extrapolated to the surface with the measured surface porosities indicates that about 400 m of sediments has been removed. Half this amount may be associated with throw on the fault near 165 mbsf; the other half, with erosion between the unconsolidated sands at 63 mbsf and the consolidated sandstones at 72 mbsf.

Temperature measurements suggest an average thermal gradient of 100°C/km to 390 mbsf. Alternatively, the same data may be explained by advection of fluids along the ~165-mbsf fault, and/or by a thermal gradient of 94°C/km above 160 mbsf and 65°C/km below 200 mbsf, with a 10°C offset formed in the last thousand years. Thermal conductivities in the upper several meters are 0.8–0.9 W/(m•K) and are 1.0–1.7 W/(m•K) below 130 mbsf.

Three processes appear to control the pore-water geochemistry. Bacterially mediated oxidation of organic matter depletes sulfate 75% by 83 mbsf (and totally below 172 mbsf), the depth where methane concentrations become elevated and there is a salinity minimum. The downhole decrease in K^+ and Mg^{2+} and the increase in salinity, Na^+, Cl^-, Ca^{2+}, Li^+, and Ca/Mg (locally modulated by the formation of calcite cements) are consistent with diagenesis of volcanic matter to form clay minerals. Depth profiles of all these ions show offsets or local deviations associated with the fault at ~165 mbsf.

Organic carbon contents average 0.5%. The C/N ratios mainly between 8 and 20 suggest a mixed terrigenous and marine origin for the organic matter. Headspace gas data show a C_1/C_2 ratio decreasing from ~2000 at 335 mbsf to 138–195 in the deepest samples (467 and 476 mbsf). Starting at 391 mbsf, there is an increasing presence of higher chain volatile hydrocarbons indicative of thermogenically derived gas.

Sites 1110 through 1113

Site 1110

Hole 1110A (APC):
9°43.599´S, 151°34.511´E; 3246.4 mbsl
0–9.50 mbsf cored; 9.50 m recovered (100%)

Hole 1110B (APC/XCB):
9°43.609´S, 151°34.508´E; 3246.3 mbsl
0–22.30 mbsf cored; 5.37 m recovered (24%)

Hole 1110C (RCB):
9°43.599´S, 151°34.498´E; 3245.8 mbsl
0–15.00 mbsf drilled; no cores taken

Hole 1110D (RCB):
9°43.588´S, 151°34.526´E; 3245.8 mbsl
0–22.7 mbsf drilled; 22.7–28.7 mbsf cored; 0.10 m recovered (2%)

Site 1111

Hole 1111A (RCB):
9°43.059´S, 151°34.533´E; 3200.7 mbsl
0–173.70 mbsf cored; 15.19 m recovered (9%)

Site 1112

Hole 1112A (RCB):
9°44.749´S, 151°36.721´E; 3046.7 mbsl
0–122.4 mbsf cored; 5.85 m recovered (5%)

Hole 1112B (RCB):
9°44.746´S, 151°36.714´E; 3046.6 mbsl
0–126.1 mbsf drilled without coring; 126.1–164.6 mbsf cored; 1.19 m recovered (3%)

Site 1113

Hole 1113A (RCB):
9°45.449´S, 151°36.737´E; 2915.6 mbsl
0–25.20 mbsf cored; 0.44 m recovered (2%)

Sites 1110 through 1113 were drilled in various locations near the foot of Moresby Seamount in an attempt to find a viable alternate location to our primary Site 1108. With the hydrocarbon safety restriction of 485 mbsf, the depth reached at Site 1108, we sought to intercept the Moresby low-angle normal fault in other locations or at shallower depths. We first tried two locations ~6 km west-northwest of Site 1108, near the rift basin depocenter located due north of Moresby Seamount. We then tried two other locations updip of Site 1108, all without success.

At Site 1110, where the fault may be 400–450 mbsf, multiple holes were unable to penetrate below ~29 mbsf because of talus beneath ~9 m of surficial calcareous clay, late Pleistocene in age (<0.22 Ma). The pebbles and cobbles of the talus include micaschists, amphibolites, and rare granite porphyry.

Moving 1 km north, at Site 1111, we cored a single hole through ~154 m of Pleistocene deposits (<1.02 Ma): talus pebbles and cobbles in calcareous ooze, clay, and silty clay with lesser nannofossil-rich silt, sand, and gravel. The talus includes metasediments (micaschist and gneiss) and variably metamorphosed igneous rocks, both basic (diabase, metadiabase, and lamprophyre) and acidic (granite porphyry). Coring was stopped at 174 mbsf in large metamorphic cobbles. Based on temperatures measured at the mudline and at 135 mbsf, the thermal gradient is 95°C/km, similar to that encountered at Site 1108, and the heat flow is 86 mW/m^2.

Site 1112 is located.1.5 km west of, and updip from, Site 1108, where the depth to the fault is ~450 mbsf. Another thick pile of talus deposits in Pleistocene (<1.75 Ma) sediments, including silty clay with occasional ash, required two RCB holes to reach 165 mbsf. The recovery consisted of pebbles only, mostly of metadiabase and epidosite, but also minor andesite, granite porphyry, micaschist, and sandstones.

After offsetting 1.3 km south, we attempted a “bare rock” spud at the base of the slope of Moresby Seamount where the fault crops out (Site 1113), but there was enough talus to make the hole unstable and repeatedly refill, and it was abandoned at 25 mbsf in micaschist and epidosite pebbles and cobbles.

Most of the metamorphic rocks recovered from the talus of Moresby Seamount have igneous protoliths. In addition, micaschists and gneisses record an early tectono-metamorphic stage characterized by the development of a foliation under epidote-amphibolite to amphibolite facies conditions. A later retrograde metamorphism in the greenschist facies affected all protoliths.

This later stage was coeval to brittle extensional deformation and extensive hydrothermal alteration, probably during the normal faulting of Moresby Seamount and the subsequent unroofing of its basement.

Site 1117

Hole 1117A (RCB):
9°46.526´S, 151°32.945´E; 1663.2 mbsl
0–111.10 mbsf cored; 6.42 m recovered (6%)

Hole 1117B (RCB):
9°46.527´S, 151°32.951´E; 1663.2 mbsl
0–9.50 mbsf cored; 0.05 m recovered (0.5%)

Hole 1117C (RCB):
9°46.520´S, 151°32.943´E; 1663.2 mbsl
0–9.50 mbsf cored; 0.10 m recovered (1%)

Site 1117 is located on the upper slope of the northern flank of Moresby Seamount, 3.5 km to the northwest of Site 1114. It was a successful attempt to bare-rock spud into, and drill through, the main detachment fault where it crops out.

The base of the cored section consists of a noncumulate, quartz-magnetite gabbro that passes upward into brecciated and then mylonitized equivalents, with a fault gouge at the surface. The upward- increasing shearing and alteration confirm that the northern flank of the seamount is an outcropping fault surface. The first undeformed gabbro occurs at 86 mbsf, but brecciated gabbro was found deeper in the section, at 96 mbsf. Therefore, the minimum thickness of the shear zone preserved within the footwall is about 100 m.

In the surficial core we recovered 4 m of soft, light-colored clayey material with a soapy feel, which we interpret as a fault gouge. This material contains talc, chlorite, calcite, ankerite, and serpentine, which is consistent with hydrothermal alteration of the underlying deformed gabbro. It has low porosity (~30%), bulk density of ~2.2 g/cm^3, unconfined compressive strength in the range of 65–90 kPa, thermal conductivities of 1.3–1.8 W/(m•K), and transverse sonic velocities of ~2 km/s. These physical properties strongly contrast with those common to near-seafloor deposits and to the gabbro protolith below (porosity 3%, bulk density 2.76 g/cm^3, thermal conductivity up to 3.8 W/(m•K), and sonic velocity 6.0–6.4 km/s). Although the fault gouge has been exposed at the seafloor, its characteristics still reflect its deformational origin. The shape parameter of the ellipsoid of magnetic susceptibility (T = 0.2–0.8) indicates an oblate magnetic fabric and the degree of anisotropy of the magnetic susceptibility is maximum in the fault gouge (Pj = 1.1–1.2), both indicative of flattening as a result of high shear strain.

The deformation textures in the gabbro range from brecciated to cataclastic, to mylonitic, almost totally obscuring the initial subautomorphic texture. Mylonite clasts recovered down to 57 mbsf show a well-developed foliation with S-C structures. Within the foliation, the association of epidote-rich and very fine grained layers of quartz, epidote, and chlorite reveals greenschist facies conditions during deformation. Asymmetrical fibrous quartz pressure shadows present around pyrite also attest to syntectonic metamorphism. The gabbro between 62 and 86 mbsf shows evidence of increasing brecciation upward, passing progressively to the mylonite. Quartz + epidote

veins, reoriented parallel to the foliation in the mylonite, suggest that the brecciation was assisted by silica-rich fluids. Late veins of epidote and calcite cut the rock, attesting to more carbonate-rich fluids in the late stage of shearing. Late alteration, associated with fluid flow within the shear zone, has produced chlorite, talc, and fibrous amphibole replacing primary plagioclase and clinopyroxene.

The mineralogy and texture of the gabbro are similar to those of high-level gabbros occurring in ophiolites. These gabbros, together with the presence of diabases reminiscent of a sheeted diabase complex at Site 1114, suggest that Moresby Seamount may be part of an ophiolitic complex exhumed by extension along the northward-dipping low-angle normal fault bounding the seamount to the north.

Site 1114

Hole 1114A (RCB):
9°47.613´S, 151°34.504´E; 406.5 mbsl
0–352.80 mbsf cored; 43.78 m recovered (12%)

Site 1114 is located just north of the crest of Moresby Seamount where seismic reflection data indicate that the basement beneath a south-southwest-dipping normal fault is shallowest. The primary objective was to determine the internal structure and composition of Moresby Seamount, particularly the nature of the basement (rock type, pressure-temperature history, structural fabric, and deformation history). A second objective was to determine the sedimentology, biostratigraphy, and vertical motion history of the ~300 m of local sedimentary cover, which may correspond to the uplifted and partly eroded synrift sequence.

In Hole 1114A, we drilled ~286 m of Pliocene–Pleistocene sediments separated by a 6-m-thick tectonic breccia from a metadiabase that forms the basement. The diabase was metamorphosed under low-grade greenschist facies conditions before its upper part, which contained a chilled margin, was reactivated by normal faulting, leading to its unroofing.

The sediments consist of rift-related, mostly volcaniclastic, turbidites deposited in middle bathyal water depths (500–2000 m). The benthic foraminiferal assemblage is characteristic of a suboxic environment of deposition, which may correspond either to a basinal situation with restricted circulation or to the oceanographic oxygen minimum situated at middle to upper bathyal water depths. From bottom to top, the deposition changed from mostly coarse-grained sandstones, about 100 m thick, to a finer grained intercalation of sandstones, siltstones, and claystones. The mineralogy of the sandstones suggests that most of the turbidites were derived from calc-alkaline extrusive rocks, but minerals and clasts from ultramafics and metamorphics (serpentinite and calcschists) are also present, as well as ubiquitous bioclasts.

Only the uppermost sediments are Pleistocene. The indurated sediments below 35 cm in Core 1114A-2R are all late and middle Pliocene (from >1.67 Ma to 3.09–3.25 Ma) and were deposited at rates of at least 176 m/m.y. The offset of the porosity vs. depth curve suggests that from 220 to >400 m of the Pleistocene section has been removed, which we tentatively relate to the uplift of Moresby Seamount in the footwall of bounding normal fault systems.

The deformation in the recovered sedimentary rocks preferentially occurs in the fine-grained strata, where it is expressed as a scaly fabric with numerous striated surfaces. It increases in intensity approaching the tectonic breccia. The bedding dips in the upper ~110 m range from 0% to 30%, then increase to 25%–60% below that. The FMS data reveal that (1) bedding dip directions

are dominantly northwest, but range from north to west; (2) the basement/sediment faulted contact outlined by the breccia dips ~60% toward the southwest, slightly oblique to the main normal fault that offsets basement by >2 km; and (3) in contrast, faults within the overlying sedimentary rocks mostly dip to the north, but a few dip to the south just above the breccia. The sense of motion on faults within the sedimentary rocks is dominantly normal, but reverse and oblique slip faults also exist. These observations suggest that a component of left-lateral motion exists on the bounding, south-southwest-dipping normal fault, in agreement with regional evidence for north-south extension.

The brecciated fault contact is also marked by an abrupt increase in the degree of hydrothermal alteration. The alteration in the breccia and metadiabase is characterized by massive clay and calcite veins that crosscut numerous quartz and epidote veins. In the breccia, the latter veins are restricted to the clasts. The hydrothermal alteration tends to decrease downward in the metadiabase, suggesting that fluids were channeled into the tectonic breccia.

Site 1116

Hole 1116A (RCB):
9°51.934´S, 151°34.508´E; 1851.3 mbsl
0–158.90 mbsf cored; 32.61 m recovered (21%)

Site 1116 is located on the southern flank of Moresby Seamount, 8 km south of Site 1114, within a tilted block bounded by two normal faults that each offset the basement by >1 km to the south-southwest. The objectives for this site were to characterize the early rift sediments and the seamount basement (which was not reached).

Very low surface porosity (~30%), and high bulk density (~2.15 g/cm^3), sonic velocity (2.2–2.8 km/s), and thermal conductivity (1.0–2.2 W/(m•K) values, suggest that 700–1000 m of the section has been removed by faulting and/or erosion. This is consistent with the lack of a Quaternary and uppermost Pliocene section, as well as the seismic stratigraphy.

The recovered section is dominated by Pliocene indurated sandstones alternating with siltstones/claystones. The sandstones are fine to medium, occasionally coarse grained, and display parallel, wavy, and convolute laminations, which indicate they originated from turbidity currents in a near-source slope setting. A paraconglomerate is at 34–63 mbsf. The sandstones below this are subarkosic with a calcareous matrix. Measured $CaCO_3$ contents are <5%. Some thick-bedded, reverse-graded sandstones with occasional intraformational rip-up clasts were deposited from high-density turbidity currents. However, normal grading and lamination in some siltstones/sandstones also indicate deposition by low-concentration turbidity or bottom currents. The matrix-supported conglomerates, interbedded with sandstones and siltstones, comprise relatively unaltered, mainly angular clasts and are interpreted as debris-flow deposits.

Benthic foraminifers indicate middle bathyal paleowater depths (500–2000 m), with inner neritic (<50 m) benthic foraminifers redeposited within turbidite beds. The N20/N21 boundary (3.35 Ma) occurs between 104 and 128 mbsf, and the minimum age of 1.95 Ma at the surface yields a minimum sedimentation rate of 70 m/m.y. Burrows are either abundant or relatively depleted, suggesting alternating poorly and well oxygenated subseafloor conditions; within both cases abundant detrital organic matter input and a mostly terrigeneous source are indicated by C/N ratios.

The orientations of the subhorizontal maximum axes of the ellipsoids of magnetic susceptibility (corrected for bedding dip and core orientation) below 100 mbsf indicate northeast-southwest or northwest-southeast–directed paleocurrents during sedimentation.

The sources of clastics are little-altered basic extrusive rocks of mainly calc-alkaline affinities, probably derived from the Miocene Tobriand Arc, but also include silicic extrusives, shallow-water bioclasts, metamorphics, and serpentinite. The serpentinite, rare chromite, and some of the gabbro and diabase grains probably have an ophiolitic origin (Paleocene–Eocene Papuan Ultramafic Belt?).

The upper 100 m of the section shows abundant evidence of synsedimentary deformations, including folding and low-angle extensional faulting typical of gravity-driven processes. The bedding dips <10%, except for fold limbs where it is up to 50%. Common dewatering and fluidization features were possibly seismically triggered. Faults and scaly fabrics are within a narrow zone between 100 and 120 mbsf. They include steep strike-slip and 25%- to 55%-dipping pure normal faults. Below the fault zone, beds dip ~15%, consistent with the dip of seismic reflectors.

THEMATIC OVERVIEW

Depositional History

Discussion of depositional history of the sites drilled during Leg 180 can be conveniently divided into, first, those on the hanging wall and northern margin of the active rift basin (Sites 1108, l109, 1110–1113, 1115, and 1118) and, secondly, those on the footwall (Sites 1114 and 1116). The hanging wall sites are relatively little deformed, well dated, and can be correlated accurately using seismic reflection data. By contrast, the footwall sites are more highly deformed, less well dated, and difficult to correlate using seismic stratigraphy. In addition, owing to faulting, differential sedimentation, and erosion, the footwall and hanging wall sites cannot be correlated with confidence across the rift basin.

Hanging Wall and Northern Margin Sites

Middle to Late Miocene Forearc Succession and Emergence

The oldest well-dated sedimentary rocks recovered during Leg 180 were from Site 1115, the most northerly location of the south-north transect (Fig. 9), and are of middle Miocene to late Miocene age. They are interpreted as part of a forearc basin, located north of the calc-alkaline Trobriand Arc and south of the Trobriand Trough subduction zone. These sediments are mainly turbidites deposited in upper bathyal water depths (150–500 m) and mainly derived from basic extrusive rocks. Upward in the middle Miocene succession, there is an incoming of redeposited shallow-water carbonate and minor pebbly sandstone. Above this, the late Miocene interval records shallowing up to a major unconformity.

The latest Miocene succession above the unconformity at Sites 1115 and 1109 is emergent to lagoonal. At Site 1115, the recovery and FMS logging record the presence of ~3 m of conglomerate composed of well-rounded clasts of basalt, together with fine-grained sediments, including possible root traces. At Site 1109, drilling terminated in massive diabase. This could alternatively (1) form part of a regional Paleogene arc/forearc (part of the Papuan ophiolite belt), (2) record part of the Neogene Trobriand forearc, or (3) relate to rifting of the Woodlark Basin. The diabase is overlain by conglomerate, as confirmed by interpretation of FMS data. The conglomerates at both sites were apparently deposited in a fluvial to swamplike setting. At Site 1109 the nonmarine sediments are thicker and include goethite concretions and altered basaltic material. The overlying lagoonal facies is brackish (alternating fresh and hypersaline) at Site 1109 to initially relatively enclosed and then more open marine at Site 1115. A similar facies (Ruaba unit) is developed at the Nubiam-1 well ~100 km to the northwest where the underlying unconformity is dated as younger than 9.63 Ma (Francis et al., 1987). At this time Site 1118 was subaerial. An early Pliocene or older conglomerate, at least 50 m thick, was deposited at Site 1118 (Fig. 10), with clasts up to 0.5 m thick, again composed of basalt and diabase. Lateritic paleosol and breccia are present there in the interstices between clasts.

Rift-Related Subsidence

Each of the three Sites 1115, 1109, and 1118 show evidence of subsidence from paralic to shallow-marine to deeper (bathyal) water conditions. This transition was diachronous, taking place initially in latest Miocene to early Pliocene time (Fig. 11). The transition from inner to outer neritic and then to upper bathyal water depths occurred first at Site 1109 where shallow-marine carbonates of early Pliocene age accumulated on an open-shelf setting, influenced by traction currents. Similar transitions occurred shortly thereafter at the most northerly site, 1115. At Site 1118, situated on a paleotopographic high, a slightly younger transgression was marked by

deposition of early Pliocene or older shallow-marine conglomerates and then lagoonal carbonate with abundant calcareous algae. Then the sediments pass disconformably into upper bathyal calcareous sands in the latest early Pliocene.

Site 1115 exhibits deepening and rapid deposition (344 m/m.y.) mainly by turbidity currents during early Pliocene time (3.9–3.6 Ma). Calcium carbonate increases generally upward in the Pliocene–Pleistocene interval, which correlates with a general increase in the pelagic carbonate component through time (Fig. 12). At Site 1109, ~250 m of hemipelagic mud and fine-grained turbidites accumulated during middle to late Pliocene time. At Site 1118 sediments above the shallow-water succession (sandstone, siltstone, and volcaniclastic sandstone) accumulated in deeper water (150–500 m) at very high sedimentation rates (435–485 m/m.y.; Fig. 11) during latest early to late Pliocene time.

Pliocene–Pleistocene Deposition

At each of Sites 1118, 1109, and 1115 the Pliocene–Pleistocene successions are dominated by deep-marine turbiditic and pelagic successions, although with subtle differences in the facies and age at each location. The Pliocene–Pleistocene successions are thickest, and show the highest sedimentation rates in the south (Site 1118), decreasing northward through Sites 1109 and 1115 (Fig. 11).

At Site 1118 around 500 m of turbidites and hemipelagic sediments accumulated from upper bathyal depths to middle bathyal depths during middle Pliocene to late Pliocene–Pleistocene? time. Ash-rich interbeds are common (Fig. 13). Reddish, finely laminated, less bioturbated sediments are interspersed with darker colored mainly turbiditic sediments. The interval of reddish sediments can be traced northward on a seismic profile until it disappears before Site 1109 (Fig. 40). Geophysical logs suggest that the noncored interval at Site 1118 (above 205 mbsf) records turbiditic and hemipelagic deposition of mainly Pleistocene age.

At Site 1109 very rapid, thick (~250 m) deposition of hemipelagic sediments and turbiditic mud, silt, and minor sand occurred during middle to late Pliocene time at initially upper bathyal then middle to lower bathyal depths. Volcaniclastic sand and silt, mud and silt turbidites became more abundant at middle bathyal depths. Finally, during the Pleistocene, calcareous nannofossil-rich pelagic ooze and calcareous clay were interstratified with volcaniclastic silt, sand turbidites, volcanic ash, and rare calciturbidites.

At Site 1115 early Pliocene time (3.9–3.6 Ma) saw a transition to a deeper water succession (150–500 m) with rapid deposition (284 m/m.y.) of muds and volcaniclastic sands, mainly by turbidity currents. Deposition continued in an upper bathyal setting at a very rapid depositional rate during middle Pliocene time (3.6–2.5 Ma). Volcanic glass-rich beds, including rare pumice (Fig. 14, are interpreted as ash fallout layers. Further deepening took place during late Pliocene–Pleistocene time to upper middle bathyal depths, and the overall sedimentation rate decreased to 63 m/m.y. Pleistocene deposition was dominated by nannofossil ooze with volcanic ash (see below), and sedimentation slowed further (34 m./m.y.) after 0.5 Ma.

A counterpart of the Pliocene–Pleistocene successions at Sites 1109, 1115, and 1118 is found at Site 1108, located very close to the depocenter of the rift basin. The deeper part of the recovered succession is dominantly turbiditic, whereas the upper part is dominated by talus derived from the Moresby Seamount. The recorded sedimentation began in the middle to late Pliocene with rapid deposition (400 m/m.y.) of fine-, medium-, and coarse-grained sandstones, and minor conglomerate, interpreted mainly as deposits from turbidity currents and debris flows. Clasts and mineral grains were derived from basic and acid volcanic rocks, and to a minor extent from

plutonic rocks (including ultrabasic rocks), metamorphic rocks, and neritic carbonate (Figs. 15, 16). During the late Pliocene (1.95–2.58 Ma) there was an interval of fine-grained turbidity current deposition, affected by faulting. The turbiditic sediments were followed by emplacement of talus, up to ~50 m thick, comprised of angular clasts of mainly metadiabase of possible ophiolitic provenance, for which the obvious source is the Moresby detachment fault system. Finally, during the late Pleistocene deposition was relatively slow (15 m/m.y.) with accumulation of calcareous, nannofossil-rich clay with minor silt and sand, including volcanic ash.

A small amount of Pleistocene sediments were also recovered at Sites 1111, 1112, and 1113. Data from Site 1110 records deep-water Quaternary sedimentation in a setting of extreme sediment instability, as shown by the presence of turbidites and other inferred mass-flow deposits. Metamorphic clasts are most likely to be talus deposits derived from the nearby Moresby Seamount. At Site 1111 individual clasts of igneous, metamorphic, and rare sedimentary rocks were recovered, and at Site 1112 there was minor recovery of talus of mainly metamorphic rocks intercalated with clay and silty clay, silt and sand, and several ash beds.

Footwall Sites

Sedimentary evidence from the footwall sites (Sites 1114 and 1116) on the Moresby Seamount was limited by poor recovery, incomplete log data, and imprecise dating (Fig. 17).

At Site 1114 the recovered section comprises classical turbidites, mud turbidites, and paraconglomerates possibly deposited by high-density turbidity currents, or debris-flow deposits, that accumulated at middle bathyal depths (500–2000 m) during middle to late Pliocene time at an average sedimentation rate of >176 m/m.y. for the entire succession. The sediment was apparently derived from calc-alkaline, metamorphic, and possibly ophiolitic sources.

At Site 1116 Pleistocene sediments are absent, and the deep-water succession is dominated by coarse-grained turbidites, debris flows, and fine-grained deposits, with a minor input of shallow-water carbonate. The whole of the recovered succession accumulated during middle late Pliocene time at middle bathyal depths (500–2000 m) at an average sedimentation rate of >70 m/m.y. The provenance at Site 1116 was again mainly from a calc-alkaline arc terrain, with a minor metamorphic (Fig. 18) and possibly an ophiolitic contribution.

In summary, the overall sedimentary regime at Sites 1114 and 1116 is consistent with a relatively proximal rift setting. By contrast, sediments in the hanging wall sites were more distally derived, with a variable volcanogenic input, as summarized below.

History of Volcanism

The occurrence of volcanogenic ash layers in the sediments at Sites 1118, 1109, and 1115 is displayed in terms of thickness and number of volcanogenic ash layers per million years for the Pliocene–Pleistocene time (Fig. 19). Only one volcaniclastic ash layer was recovered in the middle Miocene section and none from the latest middle Miocene to earliest Pliocene time interval.

Several prominent episodes of volcanogenic input are recorded during Pliocene–Pleistocene time. Beginning at the end of early Pliocene and extending through the middle Pliocene, the western Woodlark Basin received large amounts of volcaniclastic ash and silicic ash fallout, defining a major volcanic/tectonic episode that may relate to continental rifting or arc splitting. During the early to middle Pliocene transition (3.5–3.6 Ma) volcaniclastic ash layers are particularly abundant at the southernmost site, 1118, with 100 layers and a thickness of 8.7 m per 0.1 m.y. By comparison, the frequency at Site 1115 peaks at 10 layers per 0.1 m.y. and at Site 1109 at 15 layers per 0.1 m.y. A few volcanic ash layers occurred during the middle Pliocene, but

these are volumetrically minor compared to the supply of volcaniclastic turbidites. However, the presence of as many as 25 volcanic ash layers at Site 1118 indicates that explosive volcanism possibly related to rifting did take place during middle Pliocene time. These volcanic ash interbeds, interpreted as primary fallout layers, are composed of rhyodacitic to rhyolitic bubble wall shards and highly vesicular and pipe vesicular shards with minor phenocrysts. By contrast, the volcaniclastic component consists of brown and colorless glass shards, crystals of plagioclase, quartz, biotite, amphibole, pyroxene, and opaque minerals. Phenocrysts may reach up to 50% by volume of the sediment.

Middle to late Pliocene abundant volcanogenic material (mainly volcaniclastic) was recovered at Site 1118, in contrast to Site 1109 and Site 1115, where only minor input was dominated by airfall silicic ash. Furthermore, a prominent episode of mainly volcaniclastic sediment took place at Site 1109 in early Pleistocene time, but this was not recorded at Site 1115 further north. Finally, the Pleistocene at both Sites 1109 and 1115 was marked by abundant, dominantly silicic, airfall ash of platy and bubble wall type indicating a phase of explosive volcanism. The probable source was adjacent volcanoes, located in the vicinity of the D'Entrecasteaux Islands and the Trobriand forearc (e.g., Amphlett Islands and Egum Atoll).

Erosion Estimates

Porosity profiles reflect a combination of loading history, lithologic effects (e.g., differences in grain size, grain shape, mineralogy, strength, etc.), and chemical effects (e.g., degree of pore filling by cementation, permeability differences that affect dewatering rates, etc.). Typically, seafloor porosities of marine oozes are high (70%–80%). For homogeneous sediments that are not overpressured, porosity loss follows an exponential relationship (e.g., Terzaghi, 1925; Athy, 1930).

As shown in Figure 20, porosity data from Sites 1109, 1111, 1115, and 1118 show a widely scattered, but consistent downhole trend, which starts at ~70% to 80% seafloor porosity and then decreases exponentially to values between ~30% to ~55% at ~700 mbsf. Other than ~120 k.y. of missing sediment at the top of Site 1115, no obvious hiatuses have been noted above the regional unconformity for the sedimentary record recovered from these sites. In contrast, porosity data from Sites 1108, 1114, and 1116 differ remarkably from the above trend, ranging from ~15% to ~45%, although the boreholes were rather shallow (~150 to ~485 mbsf). These anomalously low porosities may reflect erosion of overlying material, although other factors such as cementation may also contribute.

The thickness of eroded material was estimated at these sites using a regression least-squares exponential fit to the data from each site (e.g., Athy, 1930). The estimates regarding the thickness of removed deposits are ~400 m at Site 1108, ~220 to >400 mbsf at Site 1114, and ~960 m at Site 1116 (see Table 2). However, the limited amount of data and poor curve fits reduces the reliability of these estimates.

In a second approach presented here, porosity profiles from Sites 1108, 1114, and 1116 are compared to the range shown by data from the non- (or minor-) erosion sites (Fig. 20). This approach assumes that the lithologies and compaction histories of these sites allow them to be used as references for Site 1108 in the graben and for Sites 1114 and 1116, now uplifted on the Moresby Seamount. This comparison indicates that porosities at Sites 1108, 1114, and 1116 correlate to much deeper sections of the low-erosion sites (Fig. 20), and the data were shifted in depth to obtain a reasonable visual fit. Site 1108 porosity data were shifted 500 m above 165 mbsf, and 700 m below 165 mbsf. The additional 200 m of removal is due to faulting. Similarly, 750 m

of erosion was applied to the upper part of the sedimentary succession at Site 1114, resulting in a broad agreement of the data with that from the "reference" sites. Finally, porosities from Site 1116 were shifted down 1000 m (Table 2).

In summary, consistent results were obtained for Sites 1108 and 1116 using the two methods, but at Site 1114, the application of an exponential relationship yielded a significantly lower amount of sediment removed relative to that estimated by the comparison of these sites to the "reference" sites. One possible explanation is that the second approach overestimates erosion where fluid-enhanced cementation, as suggested from filled veins at Sites 1108 or 1114, contributes to the low porosities observed. Proximity to active fluid flow along fault zones may cause these sites to be preferentially cemented.

Magnetic Susceptibility Intersite Correlation

Magnetic susceptibility reflects changes in magnetic mineralogy (e.g., lithologic variations) and was obtained routinely as part of the multisensor track (MST) measurement of sediment cores from Sites 1108, 1109, 1114, 1115, 1116, and 1118. The quality of magnetic susceptibility data commonly degrades from A.C.- to XCB- to RCB-cored sections because of a combination of reduced core diameter and core fracturing. For these reasons, Leg 180 magnetic susceptibility data show considerable scatter.

Intersite correlations are based on recognizing characteristic features in the magnetic susceptibility data sets. For Leg 180 Sites 1118, 1109, and 1115, a first-order difference exists between a consistently high-amplitude susceptibility zone within the upper part of the stratigraphic section and a lower zone identified by a dramatic decrease in susceptibility amplitude (Fig. 21). This high-/low-amplitude combination occurs within the turbidite units that characterize much of the basin infill. The magnetic susceptibility profiles shown in Figure 21 have been aligned relative to the Top Mammoth datum, a datum recognized at both Sites 1115 and 1118. In general, the high-amplitude susceptibility zone correlates with the presence of high-frequency, clayey silt/silty clay turbidites. In contrast, the low-amplitude magnetic susceptibility zone relates to high-frequency, silty, and, on occasion, sandy turbidites. Lithologically, these differing clay- and silt-dominated turbidite units have been termed distal and proximal, respectively. By using the paleontologic- and paleomagnetic-determined sedimentation rates for each site, it is possible to display the magnetic susceptibility as a function of time (Fig. 22). This format removes the effects of varying sedimentation rate between sites. Within the accuracy of the age determinations (viz., 100–200 ka), it would seem that the transition between the first-order low- and high-amplitude magnetic susceptibility variation is coeval between the sites. Second-order trends are represented by the relatively high-amplitude magnetic susceptibility variations that occur at the base of each stratigraphic succession.

Explaining the origin of the magnetic susceptibility variations within, and between, the Leg 180 sites remains enigmatic. Although the magnetic susceptibility generally correlates with the remnant magnetization intensity, there is no simple relationship with either grain size, main lithologic boundaries, and/or gamma-ray count. A general correspondence does exist between magnetic susceptibility and remanent magnetic intensity, indicating a common magnetic mineralogy. However, X-ray diffraction failed to identify this mineralogy although the high remanent intensities suggest that magnetite is the dominant mineral with respect to the remanence. Ferromagnesium-rich clays such as smectite and, less frequently, chlorite, are likely important contributors to the magnetic susceptibility.

The mixing between magnetic and nonmagnetic clays and sands, in addition to the approximately synchronous change in magnetic susceptibility character across the sites, implies sediment input and mixing from multiple provenances.

Petrology of the Diabases and Gabbros

Apart from clasts and crystals in volcanogenic sandstones and a few clasts of hornblende basalt at Site 1116, diabases, metadiabases, and quartz gabbros were recovered at Sites 1108, 1109, 1110–1114, 1117, and 1118. Several conclusions have been drawn from preliminary analyses of these rocks:

1. Ubiquitous diabase and some gabbro (Fig. 23) were recovered on both the footwall and the hanging wall of the detachment. Diabase is the major rock type in the upper levels of the basement of Moresby Seamount.

2. Preliminary chemical comparison shows similar major and trace element compositions in the diabase and gabbro from the seamount sites (1114 and 1117) and the diabase from Site 1118. All of these differ from the Site 1109 diabase, which is generally fresher. The relationship between these units is not yet clear, but further chemical evidence may provide clarification to provenance, as may dating the time(s) of their formation.
3. The rocks underwent a similar history of metamorphism and alteration. Metamorphism of these rocks has progressed from the formation of foliation and veining. Subsequently, these structures were refolded and subjected to greenschist facies conditions and hydrothermal alteration. A final phase of brittle deformation is shown by fractures filled with quartz and calcite.

Figure 24 shows average values of major and trace elements from Sites 1114, 1117, and 1118 normalized to the average for Site 1109, which, on petrographic evidence, is the freshest of the sites. The patterns are remarkably consistent, showing very little variation except for K_2O, Rb, and Ba. Because these are all well-known mobile elements, it is tempting to ascribe this variation to the effects of alteration, either by weathering or hydrothermal activity. The rocks from Site 1118 are the most affected by weathering, on the basis of the core descriptions, which record extensive formation of red iron oxides, but may also have suffered some hydrothermal alteration too. As this site diverges least from the values from Site 1109, we conclude that the variations shown are most likely caused by metamorphism and hydrothermal alteration, especially as these variations are most marked at Site 1114. Small variations, especially in Ni, Cr, and V can probably be ascribed to different amounts of igneous fractionation, as seen at Site 1118.

Figure 25 shows the variation in altered rocks at Sites 1108, 1111, and 1114 normalized to values for Site 1109. The samples plotted here are specifically chosen to reflect varying degrees of alteration. These samples were arranged in order of decreasing loss on ignition, as a first-order index of alteration. Encouragingly, Site 1109, judged to be the least altered, had also the lowest loss on ignition. This method of plotting the results shows unequivocally that these samples have gained K_2O, Rb, and Ba relative to Site 1109. Also, the order of increase for all these elements is consistent. Thus, the foliated metadiabase from Site 1114 is the most enriched, followed by the foliated epidote-rich schist, then by the nonfoliated diabase and the nonfoliated metadiabase, and finally by the metadiabase pebble from Site 1108. This is not the order of loss on ignition, but this may not be too significant. Petrographic evidence shows that the metadiabase from Site 1108 has

suffered low-temperature alteration, which has altered the feldspars, while other samples show epidote growth indicative of more drastic changes. As an increasing degree of enrichment is related to increasing signs of metamorphism on the basis of, among other things, epidote growth, we conclude that the enrichments shown in Figures 24 and 25 are caused by hydrothermal effects associated with greenschist facies metamorphism. On the evidence from Site 1117, we propose that this metamorphism and chemical alteration have taken place adjacent to fault zones in the presence of fluids channeled by these faults, which have facilitated the metamorphism and hydrothermal alteration.

Data shown in Figure 26 suggest that the Leg 180 diabases and gabbros are remarkably similar to enriched mid-ocean ridge basalt (E-MORB), with the exception of the elements noted as deviating in the two previous figures, and Ba and Ce are rather surprisingly below the values for E-MORB at all localities. The easiest explanation for this is that Ba is intrinsically low in these samples, as is Ce, suggesting that a better comparison may be with normal- (N-) MORB. This is especially true for Site 1109, which is the least altered of the Leg 180 sites. The other sites have higher Ba because of alteration, as noted above, but never quite reaching E-MORB levels. Barium is strongly enriched over N-MORB levels in island arc related lavas and is one of the elements that distinguishes the two, e.g., in the Lau Basin (Hergt and Farley, 1994). Because the Leg 180 diabases and gabbros have been subjected to varying degrees of Ba enrichment, but have still not reached E-MORB levels, the shipboard geochemical data do not show evidence of a subduction-related signature.

Faulting at Moresby Seamount and on the Flexured Margin

The most spectacular tectonic structure encountered during Leg 180 is the Moresby detachment fault, dipping at 25%–30% toward the north-northeast (Fig. 4). At Site 1117, where the fault plane crops out on the northern flank of Moresby Seamount (Fig. 6), we drilled an ~100-m-thick succession of deformed rocks above a basement of undeformed gabbro (Fig. 17). From bottom to top, the gabbro ranges from undeformed (Fig. 23) to brecciated to mylonitic, with a well-developed foliation with S-C structures (Fig. 27). Epidote and quartz dominate the secondary minerals, indicating syntectonic greenschist facies conditions. Above this, a fault gouge (Fig. 28) several meters thick, crops out on the seafloor and represents the most advanced stage of deformation, with evidence for fluid-assisted alteration to produce serpentinite, chlorite, talc, calcite, ankerite, and fibrous amphibole.

By contrast, at Site 1114, a south-southwest-facing normal fault offsets the basement by about 2 km near the crest of the seamount. At Site 1114, a 6-m-thick tectonic breccia occurs above a basement of metadiabase. We thus infer a much larger displacement and more extreme P-T conditions along the Moresby detachment fault. One other large normal fault was penetrated at 165 mbsf at Site 1108 within the rift basin. This fault, of which the dip direction could not be determined, is revealed mainly by well-developed scaly fabric. It has a vertical offset of ~200 m, which is based on offsets in sediment age, porosity, pore-water chemistry, and temperature curves vs. depth. Otherwise, the observed normal faults have minor offsets and correspond to high level brittle faulting.

At all sites, dip-slip normal faults are predominant, but usually coexist with both oblique and strike-slip faults. The proportion of strike-slip faults markedly increases from the northern sites toward the Moresby Seamount (Fig. 29), in agreement with probable oblique motion on west-northwest-trending normal faults that affect the seamount. This oblique motion, inferred to be left lateral, is in agreement with the north-south extension deduced from earthquake fault plane solutions and GPS measurements.

Thermal Gradients

Estimates of thermal gradient were obtained at five sites during Leg 180 (Fig. 30). The most reliable estimates were from Sites 1109 and 1115 (31°and 28°C/km, respectively), where in situ data were collected from multiple Adara temperature tool (Adara) and Davis-Villinger temperature probe (DVTP) deployments. At Site 1111, two in situ DVTP deployments were made, which were supplemented by an open-hole measurement that was used to extrapolate in situ temperature. Results suggested natural or drilling-induced influx of seawater at shallow depths, with a large-scale thermal gradient of 95°C/km, based on the mudline temperature and a reliable DVTP estimate at 136.5 mbsf.

Thermal estimates from Sites 1108 and 1118 were obtained solely from open-hole temperature surveys in which data were collected at several depth stations. Measurements from Site 1108 used the Adara tool on the wireline, whereas Site 1118 data were collected with the temperature tool (TLT) on the logging string. Results from Site 1108 suggest a thermal gradient of 100°C/km, but the profile suggests possible disruption due to recent faulting or fault-related fluid flow. Results from Site 1118 yield an approximate thermal gradient of 60°C/km. However, this estimate was based on only the mudline temperature and one extrapolation at 835 mbsf, and evidence suggests influx of warm fluid at ~700 mbsf. Overall, temperature measurements indicate a trend of increasing thermal gradients toward the graben to the north of Moresby Seamount.

Interstitial Pore-Water Geochemistry and Sediment Diagenesis

The inorganic geochemistry sampling program during Leg 180 focused in large part on the acquisition of high-resolution pore-water profiles at Sites 1109, 1115, and 1118. Data from these three northern sites provide a basis for evaluating sediment diagenesis in the Woodlark Rise on a regional basis.

Although notable differences exist between the three sites, similar trends in various portions of the profiles of interstitial water (IW) constituents at Sites 1109, 1115, and 1118 indicate that many of the same diagenetic processes mediate the pore-water composition throughout sediments of the Woodlark Rise. The IW chemistry is most similar at Sites 1109 and 1115, with these two sites displaying greater differences with respect to the southernmost Site 1118.

Concentrations of IW constituents in the upper portions of all holes reflect the oxidation of organic matter mediated by microbial activity and the concomitant early diagenesis of biogenic carbonates. This is reflected in extensive SO_4^{2-} depletion and NH_4^+ production (see below) in the younger sedimentary sequences section of each site. The upper 500 m at Site 1109 is most similar to the upper 700 m at Site 1118 in this regard, as the sediments of the thick onlap sequence at Site 1118 represent an expanded version of part of the section cored at Site 1109. Specific reactions thought to occur include dissolution of aragonite and recrystallization into low-magnesian calcite. The dominant lithologies and mineralogies at all three sites support this inference. The alteration of volcanic matter and clay-mineral diagenesis also occurs at all three sites, albeit to a varying extent. The profiles of dissolved Ca^{2+}, Mg^{2+}, and SiO_2 shown in Figure 31 reflect a combination of carbonate diagenesis and alteration of volcanic matter. Volcanic alteration and clay-mineral authigenesis typically increase in importance deeper in the sedimentary sequences of each hole. At each site, volcanic ash layers as well as volcaniclastic sands disseminated in carbonates are altered leading to enrichment of SiO_2 and Ca^{2+} in the pore fluids, whereas the precipitation of various authigenic minerals (e.g., chlorite, smectite, and zeolites) leads to a decrease in the concentration of Mg^{2+} and other pore-water constituents such as K^+ and Na^+. Conversion of pre-existing detrital clays, such as illite interlayering into smectite, also contributes to depletion of K^+ downhole.

The differences between the three sites are often attributable to differences in the thickness and/or the presence of different lithologies at one site relative to the other. Paramount among these are the existence of a lagoonal/brackish water to freshwater transitional sediment sequence overlying diabase at the bottom of Site 1109, a connectivity between the forearc sediment sequence and the synrift sediments at Site 1115, and the absence of this transitional lagoonal/brackish water to freshwater sequence at Site 1118. A marked limestone/coarse sandstone neritic sediment sequence at Site 1118 imposes important constraints on changes in the pore-water chemistry at this site. The elevated dissolved SiO_2 (and also Li^+ and Sr^{2+}) concentrations deep at this site likely reflect the alteration of the volcanic matter under a higher temperature regime than exists at Sites 1109 and 1115.

The chemical composition of the IW in the sediments of the Woodlark Rise is influenced by a series of sedimentary diagenesis reactions. The alteration of volcanic matter whether as ash layers or dispersed throughout the sediments, carbonate recrystallization reactions mediated by the microbially driven oxidation of organic matter, as well as silicification reactions, all contribute to the observed profiles of pore-water constituents.

Bacterial Activity and Hydrocarbon Generation

Biogeochemical Cycling in the Northern Sites, 1109, 1115, and 1118

Bacteria play a dominant role in the degradation of organic matter in sediments and, as a consequence, drive chemical changes and diagenesis. Although the existence of a deep bacterial biosphere in marine sediments has only recently been established (Parkes et al., 1994), the activity of bacteria at depths to 750 mbsf and their direct involvement in geochemical changes have been demonstrated.

Bacteria were present in all samples analyzed at all three of the deep “northern” sites drilled during Leg 180 (Sites 1109, 1115, and 1118 [Fig. 32]). Near-surface bacterial populations are similar to those at other sites with similar overlying water depths and near-surface organic carbon concentrations. Population numbers decrease rapidly with increasing depth and conform to the general model for bacterial distributions in marine sediments of Parkes et al. (1994), although in the deeper, more indurated sediments from Leg 180 there is an indication that numbers are decreasing more rapidly than the model predicts, resulting in a sigmoid depth distribution (Fig. 32A).

The activity of deep subsurface microbial populations is evident in geochemical data from these sites (Fig. 32B–D). Pore-water sulfate concentrations are depleted in the uppermost sediments, below which methane concentrations increase rapidly as methanogenic bacteria gain a competitive advantage over sulfate-reducing bacteria for common organic substrates. Biological decomposition of organic matter is also evident from the accumulation of ammonia in pore waters.

At Site 1118, below ~700 mbsf, an increase in pore-water sulfate concentrations, probably associated with lateral fluid flow, is associated with a rapid drop in methane concentrations (two orders of magnitude in one core; Fig. 32B). This constitutes compelling evidence for continuing microbiological activity in the deep subseafloor environment.

In contrast, at Site 1109, sulfate concentrations were depleted to 0 by 107 mbsf, and remained very low throughout the rest of the depth profile (Fig. 32C). The pore-water ammonia profile shows two distinct peaks, the uppermost of which is associated with a peak in bacterial numbers (Fig. 32A) and is clear evidence of bacterial organic matter degradation. The second peak in ammonia was associated with an increase in alkalinity (data not shown), reflecting continued microbiological activity at depth.

At Site 1115, there are distinct minima in both methane and ammonia depth profiles around ~520–580 mbsf (Fig. 32D). These suggest two separate zones of peak bacterial activity, which are separated by the regional unconformity at 572 mbsf.

Hydrocarbon Generation at Site 1108

At Sites 1109, 1115, and 1118, C_1/C_2 ratios remain between 10^3 and 10^4 throughout the holes, reflecting the biological origin of methane (Fig. 32E). At Site 1108, methanogenesis was biological in origin in the uppermost sediments, with a dramatic increase in methane concentrations occurring below the depth of pore-water sulfate depletion. However, increasing quantities of ethane with increasing depth cause a decrease in the C_1/C_2 ratio (Fig. 32E). Below ~100 mbsf small quantities of ethane and propane were present in the headspace gas samples; their concentrations increased with depth. Furthermore, below ~400 mbsf traces of branched and straight-chain C_4 and C_5 components were also detected. The accumulation of $>C_1$ hydrocarbons and the concomitant decrease in C_1/C_2 ratio confirm a thermogenic gas input to the sediments. The presence of thermogenic gas at shallow depths is consistent with the high thermal gradient at Site 1108 (~100°C /km) and the thick sedimentary section in the rift basin. Pollution and safety concerns, therefore, prevented us from deepening this site.

Implications for a Deep Bacterial Biosphere in Marine Sediments

The continued presence of bacterial populations at more than 800 mbsf is of fundamental significance. The persistance of microbial life into indurated sedimentary rock adds to a steadily growing body of evidence for a more extensive biosphere than previously imagined. Microbes live in high-temperature regions of the lithosphere (e.g., oil reservoirs, aquifers, iron-rich ores, ocean rifts, and hot springs; Brock, 1985) and even into basalt (Furnes et al., 1996; Giovannoni et al., 1996), and granites (Pedersen and Ekendahl, 1990). Bacteria are known to grow at as much as to ~120°C (Stetter et al., 1993) with indirect evidence for the existence of cells approaching 400°C at abyssal depths (Deming and Baross, 1993) and at pressures of over 1000 atmospheres. The bacterial biosphere in deep-marine sediments may be conservatively equivalent to about 10% of the surface biosphere (Parkes et al., 1994). Recent advances have made significant inroads into understanding both energy sources (e.g., Wellsbury et al., 1997) and electron acceptors (Lovley et al., 1996; Raiswell and Canfield, 1996) for life at “extremes,” along with significant improvements in understanding the diversity and physiology of microbial life in deep-sea sediments. The discovery of the deep bacterial biosphere has extended our perception of life from merely a surface phenomenon, and has profound implications for the biodiversity of our planet, fossil fuel formation, the origins of life on Earth, and the potential for life on other planets.

The limits of life on Earth remain unknown: ODP Leg 180 has provided samples and data that considerably extend our knowledge of the deep-marine component of our biosphere.

Downhole Logging

During Leg 180, four holes were logged by the triple-combo geophysics and the FMS-sonic tool strings, and among these, three were logged for more than 750 m (Table 3). This yields around 2.4 km of FMS and classical logs.

Downhole Measurements

Despite rather uniform lithologies for most of the holes, the log response shows significant variability and will therefore provide a significant lever in the effort to correlate the different drilled sequences (Figs. 33, 34, 35, 36). For instance, the 200–250 mbsf interval in Hole 1118A shows low gamma ray (Fig. 33), low porosity (Fig. 34), and high sonic velocities (Fig. 36). The same features are observed in Hole 1109D in a narrower interval around 230 mbsf. In both cases, this interval can be correlated with a prominent seismic reflector. However, the closer convergence of the two porosity estimates in Hole 1109D indicates that the corresponding sedimentary unit contains less clay than in Hole 1118A. The brackish environment encountered above the major regional unconformity at 572 mbsf in Hole 1115C and at 773 mbsf in Hole 1109D also displays a characteristic log response in both holes. The sonic velocity logs will be used to interpolate the regional velocity structure and better migrate existing multichannel seismic data.

Formation MicroScanner Images

The FMS images acquired during Leg 180 provided critical information about the detailed stratigraphy and structure of both the hanging wall and footwall drill sites around Moresby Seamount (Figs. 37, 38). Excellent quality FMS images were acquired at the three sites on the northern margin (Sites 1109, 1115, and 1118), and at one site near the crest of Moresby Seamount, which penetrated an antithetic normal fault (Site 1114). The FMS images from the northern sites reveal conductive clay and resistive sandy or carbonate-rich interbedded units; centimeter-scale depositional features such as parallel laminae, foresets, and bioturbation; and post-depositional faults and fractures. In particular, FMS images were instrumental in determining the precise depths of important stratigraphic boundaries and the structural orientations of beds and fractures, which could not be precisely determined from core samples alone. Analysis of bed and fracture dips in the FMS images from Site 1114 revealed two distinct dip populations that vary vertically with distance from the south-southwest-dipping antithetic normal fault (Fig. 38). Histogram plots of the dip directions and stereonet plots of the strikes were particularly useful in determining the major bed and fracture dip distributions (Fig. 39).

Vertical Seismic Profiling, Depth Conversion, and Site Correlation

The VSP experiments were carried out at Sites 1109, 1115, and 1118. The depth range of the recording locations were limited at Sites 1109 and 1115 (effectively to “check shots”) but covered 565 m at Site 1118. In conjunction with the VSP experiments, we compiled data of velocity variation with depth, using laboratory measurements when sonic velocity data from logging were absent, erroneous (because of washouts), or failed to characterize very thin, high-velocity horizons. The resultant velocity-depth functions were used to depth convert the multichannel seismic (MCS) data immediately adjacent to the boreholes. Check shot information derived from the VSP experiment was used to refine these depth conversions to errors within about 10 m. This will be further refined postcruise.

Depth conversion of the seismic data allows direct correlation of the Site 1109, 1115, and 1118 results with the regional stratigraphy. Figure 40 shows the depth conversions at Sites 1109 and 1118, along with the lithostratigraphic columns. The MCS data in time, correlated with depth, are shown linking the two sites, which are 8.7 km apart. The limestones and calcareous sandstones close to the base of Site 1118 are thin in comparison to those at Site 1109. These two units, both formed in a neritic environment, fall within a continuous seismic horizon, except that Site 1118 contains only the upper part of the sequence. The interval between 430 and 715 mbsf at Site 1118, corresponding to claystones, siltstones, and sandstones, rapidly thins between common midpoint

(CMP) 4075 and 4200, maintaining a conformable relationship with the underlying beds. This interval corresponds to 305 to 390 mbsf at Site 1109. Volcaniclastic layers are found toward the bottom of the interval at both sites. The reddish claystone and siltstone found between 380 and 430 mbsf at Site 1118 was not seen at Site 1109. Following the corresponding reflectors from Site 1118 toward Site 1109 reveals that this unit pinches out northward between CMP 3950 and 4100, and does not reach Site 1109. The overlying reflectors indicate the possibility of local channel fill above this horizon. Above 385 mbsf at Site 1118 and ~300 mbsf at Site 1109, the lithostratigraphy is dominated by monotonous silty clays and clayey silts with a middle bathyal origin. However, these horizons correlate well between the two sites.

REFERENCES

Abers, G.A., 1991. Possible seismogenic shallow-dipping normal faults in the Woodlark-D'Entrecasteaux extensional province, Papua New Guinea. *Geology,* 19:1205–1208.

Abers, G.A., Mutter, C.Z., and Fang, J., 1997. Earthquakes and normal faults in the Woodlark-D'Entrecasteaux rift system, Papua New Guinea. *J. Geophys. Res.,* 102:15301–15317.

Athy, L.F., 1930, Density, porosity, and compaction of sedimentary rocks, *AAPG Bull.,* 14:1–23.

Baldwin, S.L., Lister, G.S., Hill, E.J., Foster, D.A., and McDougall, I., 1993. Thermochronologic constraints on the tectonic evolution of active metamorphic core complexes, D'Entrecasteaux Islands, Papua New Guinea. *Tectonics,* 12:611–628.

Brock, T.D., 1985. Life at high temperatures. *Science,* 29: 132–138.

Davies, H.L., 1980. Folded thrust and associated metamorphics in the Suckling-Dayman massif, Papua New Guinea. *Am. J. Sci.,* 280:171–191.

Davies, H.L., and Warren, R.G., 1992. Eclogites of the D'Entrecasteaux Islands. *Contrib. Mineral. Petrol.,* 112:463–474.

Deming, J. W. and Baross, J. A., 1993. Deep-sea smokers: windows to a sub-surface biosphere. *Geochim. Cosmochim. Acta,* 57: 3219–3230.

Francis, G., Lock, J., and Okuda, Y., 1987. Seismic stratigraphy and structure of the area to the southeast of the Trobriand Platform. *Geo-Marine Lett.,* 7:121–128.

Furnes, H., Thorseth, I. H., Tumyr, O., Torsvik, T., and Fisk, M.R, 1996. Microbial activity in the alteration of glass from pillow lavas from Hole 896A. *In* Alt, J.C., Kinoshita, H., Stokking, L.B., and Michael, P. J. (Eds.), *Proc. ODP, Sci. Results,* 148: College Station, TX (Ocean Drilling Program), 191–206.

Giovannoni, S.J., Fisk, M.R., Mullins, T.D., and Furnes, H., 1996. Genetic evidence for endolithic microbial life colonizing basaltic glass/seawater interfaces. *In* Alt, J.C., Kinoshita, H., Stokking, L. B., and Michael, P. J. (Eds.), *Proc. ODP, Sci. Results,* 148: College Station, TX (Ocean Drilling Program), 207–214.

Goodliffe, A., Taylor, B., Martinez, F., Hey, R., Maeda, K., and Ohno, K., 1997. Synchronous reorientation of the Woodlark Basin spreading center. *Earth Planet. Sci. Lett.,* 146:233–242.

Goodliffe, A., 1998. The rifting of continental and oceanic lithosphere: observations from the Woodlark Basin [Ph.D. thesis]. Univ. Hawaii, Honolulu, HI.

Hegner, E., and Smith, I´E.M., 1992. Isotopic compositions of late Cenozoic volcanics from southeast Papua New Guinea: evidence for multi-component sources in arc and rift environments. *Chem. Geol.,* 97:233–249.

Hergt, J.M., and Farley, K.N., 1994. Major element, trace element, and isotope (Pb, Sr, and Nd) variations in site 834 basal: implications for the initiation of backarc opening. *In* Hawkins, J., Parson, L., Allan, J., et al., *Proc. ODP, Sci. Results,* 135: College Station, TX (Ocean Drilling Program), 471–485.

Hill, E.J., 1994. Geometry and kinematics of shear zones formed during continental extension in eastern Papua New Guinea. *J. Structural Geol.,* 16:1093–1105.

Hill, E.J., and Baldwin, S.L, 1993. Exhumation of high-pressure metamorphic rocks during crustal extension in the D'Entrecasteaux region: Papua New Guinea. *J. Metamorphic Geol.,* 11:261–277.

Hill, E.J., Baldwin, S.L., and Lister, G.S., 1992. Unroofing of active metamorphic core complexes in the D'Entrecasteaux Islands, Papua New Guinea. *Geology,* 20:907–910.

Hill, E.J., Baldwin, S.L., and Lister, G.S., 1995. Magmatism as an essential driving force for formation of active metamorphic core complexes in eastern Papua New Guinea. *J. Geophys. Res.,* 100:10,441–10,451.

Lister, G.S., and Baldwin, S.L., 1993. Plutonism and the origin of metamorphic core complexes. *Geology,* 21:607–610.

Lovley, D.R., Coates, J.D., Blunt-Harris, E.L., Phillips, E.J.P., Woodward, J.C., 1996. Humic substances as electron acceptors for microbial respiration. *Nature,* 382, 445–448.

Mutter, J.C., Mutter, C.Z., and Fang, J., 1996. Analogies to oceanic behavior in the continental breakup of the western Woodlark Basin. *Nature,* 380:333–336.

Parkes, R.J., Cragg, B.A., Bale, S.J., Getliff, J.M., Goodman, K., Rochelle, P.A., Fry, J.C., Weightman, A.J., and Harvey, S.M., 1994. A deep bacterial biosphere in Pacific Ocean sediments. *Nature,* 371:410–413.

Pedersen, K., and Ekendahl, S., 1990. Distribution and activity of bacteria in deep granitic groundwaters of South East Sweden. *Microbial Ecology,* 20: 37–52.

Raiswell, R., and Canfield, D.E., 1996. Rates of reaction between silicate iron and dissolved sulfide in Peru Margin sediments. *Geochim. Cosmochim. Acta,* 60: 2777–2787.

Smith, I.E., and Simpson, C.J., 1972. Late Cenozoic uplift in the Milne Bay area, eastern Papua New Guinea. *Bur. Min. Resour. Aust. Bull.,* 125:29–35.

Smith, I.E.M., 1976. Peralkaline rhyolites from the D'Entrecasteaux Islands, Papua New Guinea, *In* Johnson, R.W. (Ed.), *Volcanism in Australasia:* Amsterdam (Elsevier), 275–285.

Stetter, K.O., Huber, R., Blöchl, E., Kurr, M., Eden, R.E., Fielder, M., Cash, H. and Vance, I., 1993. Hyperthermophilic Archaea are thriving in deep North Sea and Alaskan oil reservoirs. *Nature,* 365: 743–745.

Stolz, A.J., Davies, G.R., Crawford, A.J., and Smith, I.E.M., 1993. Sr, Nd and Pb isotopic compositions of calc-alkaline and peralkaline silicic volcanics from the D'Entrecasteaux Islands, Papua New Guinea, and their tectonic significance. *Mineral. and Petrol,* 47:103–126.

Sun, S.-S., and McDonough, W.F., 1989. Chemical and isotope systematics of oceanic basalts: implications for mantle composition and processes. *In* Saunders, A.D., and Norry, M.J. (Eds.), *Magmatism in the Ocean Basins.* Geol. Soc. Spec. Publ. London, 42:313–345.

Taylor, B., Goodliffe, A., Martinez, F., and Hey, R., 1995. A new view of continental rifting and initial seafloor spreading. *Nature,* 374:534–537.

Taylor, B., Mutter, C., Goodliffe, A., and Fang, J., 1996. Active continental extension: the Woodlark Basin, *JOI/USSAC Newsletter,* 9:1–4.

Terzaghi, K., 1925. Erdbaumechanik auf bodenphysikalischer Grundlage. Leipzig (Deuticke), 399p.

Tregoning, P., Lambeck, K., Stolz, A., Morgan, P., McClusky, S., van der Beek, P., McQueen, H., Jackson, R., Little, R., Laing, A., and Murphy, B., 1998, Estimation of current plate motions in Papua New Guinea from Global Positioning System observations. *J. Geophys. Res.,* 103:12,181–12,203.

Weissel, J.K., Taylor, B., and Karner, G.D., 1982. The opening of the Woodlark Basin, subduction of the Woodlark spreading system and the evolution of northern Melanesia since mid-Pliocene time. *Tectonophysics,* 87:253–277.

Wellsbury, P., Goodman, K., Barth, T., Cragg, B.A., Barnes, S.P., and Parkes, R.J., 1997. Deep marine biosphere fueled by increasing organic matter availability during burial and heating. *Nature,* 388: 573–576

TABLE CAPTIONS

Table 1. Leg 180 drill site locations and coring totals.

Table 2. Thickness of removed sediment at Sites 1108, 1114, and 1116, as estimated from exponential curves (Athy, 1930) and use of porosity data from Sites 1109, 1111, 1115, and 1118 for reference.

Table 3. Intervals logged during Leg 180.

FIGURE CAPTIONS

Figure 1. Major physiographic features and active plate boundaries of the Woodlark Basin region. The stippled area encloses oceanic crust formed during the Brunhes Chron at spreading rates (labeled in mm/yr). MT and ST = Moresby and Simbo transform faults, respectively; DE = D'Entrecasteaux Islands. Inset, geographical location of the Woodlark Basin.

Figure 2. Topography of the Papuan Peninsula and bathymetry of the western Woodlark Basin showing relocated epicenters (black circles) and earthquake focal mechanisms from Abers et al. (1997). G = Goodenough Island, F = Fergusson Island, N = Normanby Island, R = Rossel Island, T = Tagula Island, MS = Moresby Seamount, MT = Moresby transform fault, M = Misima Island, W = Woodlark Island. Exploration wells Goodenough-1 and Nubiam-1 are labeled G-1 and N-1. The solid line is the landward boundary of oceanic crust and the thin double lines locate the spreading axes (Taylor et al., 1995).

Figure 3. Nested meridional sections at 151°34.5´E showing the (**A**) regional bathymetry and (**B**) local structures across the incipient conjugate margins (modified after Taylor et al., 1996). Leg 180 drill sites are depicted on the B section. VE = vertical exaggeration; M.S. = Moresby Seamount.

Figure 4. Stacked, migrated, and depth-converted 196-channel (EW95-1369) and 148-channel (EW95-1374) seismic sections collected with a 5-km streamer across the rift basin north of Moresby Seamount that is the locus of current deformation ahead of the Woodlark spreading center (the western tip of the neovolcanic zone is hatched in the inset). There is no vertical exaggeration. The bounding low-angle normal detachment wraps around Moresby Seamount and has a true dip of 27°± 3° toward 015°. Structure contours from 3 to 9 km depth are shown in the inset, with bathymetric contours labeled in hundreds of meters. The antithetic hanging wall normal fault dips south at 45°. On line EW95-1369 the planar detachment (curvi-planar in three dimensions) is imaged over the full depth extent of the seismogenic zone (3–9 km) determined from earthquake waveform inversion results (Abers et al., 1997). Miocene strata on the southern flank of the pre-rift forearc basin dip north at ~10% beneath the northern margin. Figure modified from Taylor et al., (unpubl. data**)** to show the location of Sites 1108, 1112, and 1113.

Figure 5. Stacked and migrated time section of 148-channel seismic line EW95-1366, located in Figure 7, on which Sites 1109–1111, 1114–1116, and 1118 were drilled. Common depth points (CDPs) are labeled 1–7 (in thousands). The top and bottom parts overlap by 100 CDPs (1.25 km). North is to the right.

Figure 6. Stacked and migrated time section of 196-channel seismic line EW95-1371, located in Figure 7, on which Site 1117 was drilled. CDPs are labeled 1–4 (in thousands). Four hundred CDPs equals 5 km. North is to the right.

Figure 7. Shaded relief map showing the locations of the Leg 180 drill sites and multichannel seismic tracks, plotted on a base map with 200-m bathymetric contours (thicker contours labeled every kilometer).

Figure 8. Multibeam bathymetry map (with 100-m contours and thicker contours labeled every kilometer) showing the locations of the Leg 180 drill sites in the vicinity of Moresby Seamount. Multichannel seismic tracks are plotted and labeled every 100 CDPs.

Figure 9. Lithology and correlation of Sites 1108, 1109, 1115, and 1118 from the footwall of the Woodlark rift basin.

Figure 10. Core photograph illustrating the transition facies from diabase, interpreted as a clast in conglomerate, overlain by shallow-marine conglomerates and limestone.

Figure 11. Sedimentation curves at Sites 1115 (solid line), 1109 (dashed line), 1118 (dotted line), 1108 (solid line upper right), 1114 (dashed line upper right), and 1116 (dotted line upper right), based on nannofossil (square) and planktonic foraminifer (circle) datum events, magnetic chron and subchron boundaries (triangle), and lithostratigraphic correlation (star). Symbols with arrows denote actual datum point can be above or below and older or younger than indicated by the symbols. Shown below are average sedimentation rates, calculated for intervals separated by vertical lines, and paleobathymetry, based on benthic foraminifers, at Sites 1115, 1109, and 1118. Broken lines indicate uncertainty in the placement of paleodepth boundaries. Unconformity represented by wavy line.

Figure 12. Calcium carbonate content plotted vs. depth at Site 1115. Note the downward decrease in carbonate content to 400 mbsf.

Figure 13. Digital photomicrograph. Plane-polarized light. Crystal vitric tuff, with abundant angular, fresh pipe vesicle glass shards in a glassy matrix (Sample 180-1118A-38R-3, 128–130 cm).

Figure 14. Digital photomicrograph. Plane-polarized light. A pumiceous rock containing phenocrysts of hornblende within a glassy groundmass. Occurs as a granule-size clast within a sandy silty claystone (Sample 180-1108B-12R-5, 50–53 cm).

Figure 15. Digital photomicrograph. Viewed under crossed nicols. A well-rounded clast of fresh glassy basalt with plagioclase and biotite microphenocrysts, set in a calcitic matrix including volcanic and metamorphic grains (Sample 180-1115C-12R-4, 144–148 cm).

Figure 16. Digital photomicrograph. Viewed under crossed nicols . A subrounded clast of basalt with plagioclase microphenocrysts (right); an acidic clast (left), and a clast of serpentinite (lower). The matrix is calcareous, with quartz and feldspar grains (Sample 180-1108B-3R-CC, 0–4 cm).

Figure 17. Correlated lithologic logs of Sites 1114, 1116, and 1117 from the footwall of the Woodlark rift basin. See site summaries for discussion.

Figure 18. Digital photomicrograph. Angular fragment of calc-schist, surrounded by glassy basalt and silicic fragments, set in a sparry calcite cement (Sample 180-1116A-13R-2, 25–27 cm).

Figure 19. Occurrence of volcanogenic ash layers at Sites 1118, 1109, and 1115 shown in terms of thickness (gray pattern) and number of volcanogenic ash layers (black pattern) for Pliocene–Pleistocene time. Note: the spiky nature of the peaks of volcaniclastic input are in part artifacts of variable core recovery. Refer to the visual core descriptions on the CD-ROM for details of recovery.

Figure 20. Physical properties data for Sites 1108, 1109, 1111, 1114, 1115, 1116, and 1118. **A.** Porosity data, as measured from discrete index property samples. Dashed lines show the depth of the regional unconformity at the northern sites. **B.** Porosity data, with depth shifts as follows: Site 1108: 500 m added to mbsf depths above 165 mbsf (the location of a fault zone), 700 m added below 165 mbsf; 750 m added to Site 1114 data; and 1000 m added to Site 1116 data. Data below the unconformities at Sites 1109, 1115, and 1118 are not shown because of the unknown hiatus. See text for discussion.

Figure 21. Magnetic susceptibility for Sites 1118, 1109, and 1115 aligned with respect to the location of the Top Mammoth datum (interpolated from biostratigraphy at Site 1109).

Figure 22. Magnetic susceptibility for Sites 1118, 1109, and 1115 plotted as a function of time. Given the accuracy of the age data, the transition from low-amplitude to high-amplitude magnetic susceptibility is approximately coeval across the sites.

Figure 23. Photograph of hand specimen of gabbro fragment showing coarse-grained, nonlaminated nature. No layering was apparent at the scale of the recovered material (Sample 180-1117A-13R-1, 19–23 cm).

Figure 24. Plots of diabases and metadiabases from Sites 1109, 1114, 1117 and 1118 where they were recovered in situ. Samples from the other holes are normalized to values from Site 1109 (presumed closest to pristine diabase). av. = average.

Figure 25. Plot of diabase and metadiabase samples from talus samples at Sites 1108, 1111, and 1114 normalized to the average values for unaltered diabase from Site 1109. Key: 1 = foliated, epidote-rich schist in Hole 1111A (Sample 180-1111A-16R-CC, 8–15 cm); 2 = metadiabase pebble in sediments of Hole 1108B (Sample 180-1108B-47R-CC, 1–3 cm); 3 = nonfoliated metadiabase in Hole 1114A (Sample 180-1114A-36R-2, 40–42 cm); 4 = foliated metadiabase pebble in Hole 1114A (Sample 180-1114A-36R-1, 70–72 cm).

Figure 26. Plot of major and trace elements of diabases and metadiabases from Sites 1108, 1109, 1111, 1114, 1117, and 1118 normalized to E-MORB using the values of Sun and McDonough (1989).

Figure 27. Close-up photograph of highly sheared gabbro with a well developed foliation plane and shear bands (Sample 180-1117A-9R-1, 24–32 cm).

Figure 28. Core photograph of the fault gouge recovered at Site 1117. This shows soft, light-colored clayey material that contains talc, chlorite, calcite, ankerite, and serpentine. This material is consistent with intense shearing and hydrothermal alteration of underlying deformed gabbro.

Figure 29. Schematic cross section showing the increasing proportion (circles) of strike-slip and oblique-slip faults toward the Moresby Seamount. Note that oblique- and strike-slip faults at Sites 1109 and 1115 occur in the pre-rift sequence.

Figure 30. Estimated thermal gradients (in °C/km) from Leg 180. Confidence in data is discussed in the text.

Figure 31. Plot of dissolved Ca, Mg, and SiO_2 at northern Woodlark Rise sites. The shapes of the Ca and Mg profiles reflect the effects of carbonate diagenesis and a variable extent of alteration of volcanic matter in the upper portion of the sedimentary column of each site. Deeper downhole, alteration of volcanics exerts a more dominant control on pore-water profiles. Large increases in dissolved Ca result primarily from alteration of plagioclase whereas depletion of Mg reflects its uptake during authigenic smectite formation. The dissolved SiO_2 profiles depict a downhole progression including dissolution of volcanic ash in the upper sedimentary column, and WST reactions deeper downhole. Particularly elevated SiO_2 concentrations deep in Site 1118 are attributable to an abundance of fresh to slightly altered volcanic matter in higher porosity sediments.

Figure 32. Biogeochemical profiles in sediments from the Woodlark Basin, Leg 180: **A.** Total bacterial populations at Sites 1109, 1115, and 1118. The solid curve represents a general regression line of bacterial numbers vs. depth in deep-sea sediments (Parkes et al., 1994), with 95% upper and lower prediction limits shown by dashed curves. Sulfate, ammonia, and methane depth profiles at Sites (**B**) 1118, (**C**) 1109, and (**D**) 1115. Unconformity at each site represented by wavy line. **E.** C_1/C_2 ratios at Sites 1108, 1109, 1115, and 1118.

Figure 33. Natural gamma ray from the triple-combo runs in Holes 1114A, 1118A, 1109D, and 1115C.

Figure 34. Neutron porosity and density porosity from the triple-combo runs in Holes 1114A, 1118A, 1109D, and 1115C.

Figure 35. Photoelectric effect (PEFL) from the triple-combo runs in Holes 1114A, 1118A, 1109D, and 1115C.

Figure 36. Sonic velocity *(V_p)* from the array sonic tool in Holes 1114A, 1118A, 1109D, and 1115C.

Figure 37. This dynamically normalized, double pass FMS image from Site 1115 shows well defined, flat-lying, conductive clayey layers interbedded with thin (~10 cm), resistive sandy or carbonate-rich beds, which are characteristic of the stratigraphy observed in FMS images from each of the three hanging wall drill sites (1109, 1115, and 1118). The dashed lines mark the Pad 1 azimuth trace of each FMS pass. The FMS images are oriented from 0° to 360° from geographic north.

Figure 38. Statically normalized FMS image (left) and tadpole plot (right) from Site 1114. Sinusoidal fit to dipping beds (dashed) and fractures (solid) are used to measure dips and dip directions, which are shown on the tadpole plot. Dominant bed dips are ~30° oriented northwest, while dominant fracture dips are ~50° to ~60° oriented north within the same interval.

Figure 39. Bed and fracture dip direction distributions from Site 1114. **A**, **B.** Histograms of bed and fracture dip directions. **C, D.** Rose diagrams of bed and fracture strikes. The two main populations consist of beds that strike northeast and fractures that strike just north of east.

Figure 40. Depth converted multichannel seismic (MCS) traces at Sites 1118 and 1109, displayed with the lithostratigraphic columns. The MCS data in time, spanning the two sites, is shown correlated with depth. CMP = common midpoint. TWT = two-way traveltime. Lithologic patterns as in Figure 9.

Hole	Latitude	Longitude	Water depth (mbsl)	Number of cores	Interval cored (m)	Core recovered (m)	Total recovered (%)	Drilled without coring (m)	Total penetration (mbsf)	Time on hole (days)
1108A	09°44.708 S	151°37.514 E	3162.7	n/a	n/a	n/a	n/a	16.3	16.3	0.59
1108B	09°44.724 S	151°37.543 E	3177.2	51	485.2	148.58	30.6%	0.0	485.2	5.73
		SITE 1108 TOTALS:		**51**	**485.2**	**148.58**	**30.6%**	**16.3**	**501.5**	**6.32**
1109A	09°30.390 S	151°34.388 E	2210.9	1	9.5	9.96	104.8%	0.0	9.5	0.25
1109B	09°30.396 S	151°34.391 E	2211.1	2	14.8	15.14	102.3%	0.0	14.8	0.08
1109C	09°30.392 S	151°34.390 E	2211.0	41	375.7	323.11	86.0%	0.0	375.7	2.56
1109D	09°30.380 S	151°34.355 E	2211.0	51	449.2	299.87	66.8%	352.8	802.0	6.68
		SITE 1109 TOTALS:		**95**	**849.2**	**648.08**	**76.3%**	**352.8**	**1202.0**	**9.57**
1110A	09°43.599 S	151°34.511 E	3246.4	2	9.5	9.50	100.0%	0.0	9.5	0.36
1110B	09°43.609 S	151°34.508 E	3246.3	3	22.3	5.37	24.1%	0.0	22.3	0.52
1110C	09°43.599 S	151°34.498 E	3245.8	0	0.0	0.00	N/A	15.0	15.0	0.56
1110D	09°43.588 S	151°34.526 E	3245.8	1	6.0	0.16	2.7%	22.7	28.7	0.24
		SITE 1110 TOTALS:		**6**	**37.8**	**15.03**	**39.8%**	**37.7**	**75.5**	**1.68**
1111A	09°43.059 S	151°34.533 E	3200.7	18	173.7	15.19	8.7%	0.0	173.7	7.9
		SITE 1111 TOTALS:		**18**	**173.7**	**15.19**	**8.7%**	**0.0**	**173.7**	**7.9**
1112A	09°44.749 S	151°36.721 E	3046.7	14	122.4	5.85	4.8%	0.0	122.4	5.3
1112B	09°44.746 S	151°36.714 E	3046.6	4	38.5	1.49	3.9%	126.1	164.6	
		SITE 1112 TOTALS:		**18**	**160.9**	**7.34**	**4.6%**	**126.1**	**287.0**	**5.3**
1113A	09°45.449 S	151°36.737 E	2915.6	3	25.2	0.44	1.7%	0.0	25.2	1.3
		SITE 1113 TOTALS:		**3**	**25.2**	**0.44**	**1.7%**	**0.0**	**25.2**	**1.3**
1114A	09°47.613 S	151°34.504 E	406.5	37	352.8	43.78	12.4%	0.0	352.8	3.5
		SITE 1114 TOTALS:		**37**	**352.8**	**43.78**	**12.4%**	**0.0**	**352.8**	**3.5**
1115A	09°11.389 S	151°34.450 E	1149.6	1	4.4	4.43	100.7%	0.0	4.4	0.1
1115B	09°11.382 S	151°34.437 E	1148.8	31	293.1	286.84	97.9%	0.0	293.1	1
1115C	09°11.383 S	151°34.422 E	1148.7	54	519.3	291.63	56.2%	283.2	802.5	5.3
		SITE 1115 TOTALS:		**86**	**816.8**	**582.90**	**71.4%**	**283.2**	**1100.0**	**6.4**
1116A	09°51.934 S	151°34.508 E	1851.3	18	158.9	32.61	20.5%	0.0	158.9	3.3
		SITE 1116 TOTALS:		**18**	**158.9**	**32.61**	**20.5%**	**0.0**	**158.9**	**3.3**
1117A	09°46.526 S	151°32.945 E	1163.2	14	111.1	6.42	5.8%	0.0	111.1	1.7
1117B	09°46.527 S	151°32.951 E	1163.2	1.0	9.5	0.05	0.5%	0.0	9.5	0.2
1117C	09°46.520 S	151°32.943 E	1163.2	1.0	9.5	1.05	11.1%	0.0	9.5	0.3
		SITE 1117 TOTALS:		**16**	**130.1**	**7.52**	**5.8%**	**0.0**	**130.1**	**2.2**
1118A	09°35.110 S	151°34.421 E	2303.6	76	721.6	466.21	64.6%	205.0	926.6	7.6
		SITE 1118 TOTALS:		**76**	**721.6**	**466.21**	**64.6%**	**205.0**	**926.6**	**7.6**
		LEG 180 TOTALS:		**424**	**3912.2**	**1967.68**	**50.3%**	**1021.1**	**4933.3**	**55.1**

Table 1

	Site 1108	Site 1114	Site 1116
Thickness of removed sediment, as calculated from exponential least-squares function (m)	~400	~220 to >400	~960
Thickness of sediment removed, as estimated from Leg 180 "reference sites" (m)	500	750	1000

Table 2

Tool string			Hole 1108B	Hole 1109D	Hole 1114A	Hole 1115C	Hole 1118A
Triple combo	In pipe	Top	–20	–68	–27	–38	–67
		Bottom	98	82	75	80	100
	Open hole	Top	98	82	75	80	100
		Bottom	165	786	305	784	891
FMS-sonic	In pipe	Top			39	42	67
		Bottom			75	80	98
	Open hole	Top		82	75	80	98
		Bottom		351	298	787	892
	In pipe	Top		376			
		Bottom		385			
	Open hole	Top		385			
		Bottom		786			

Table 3

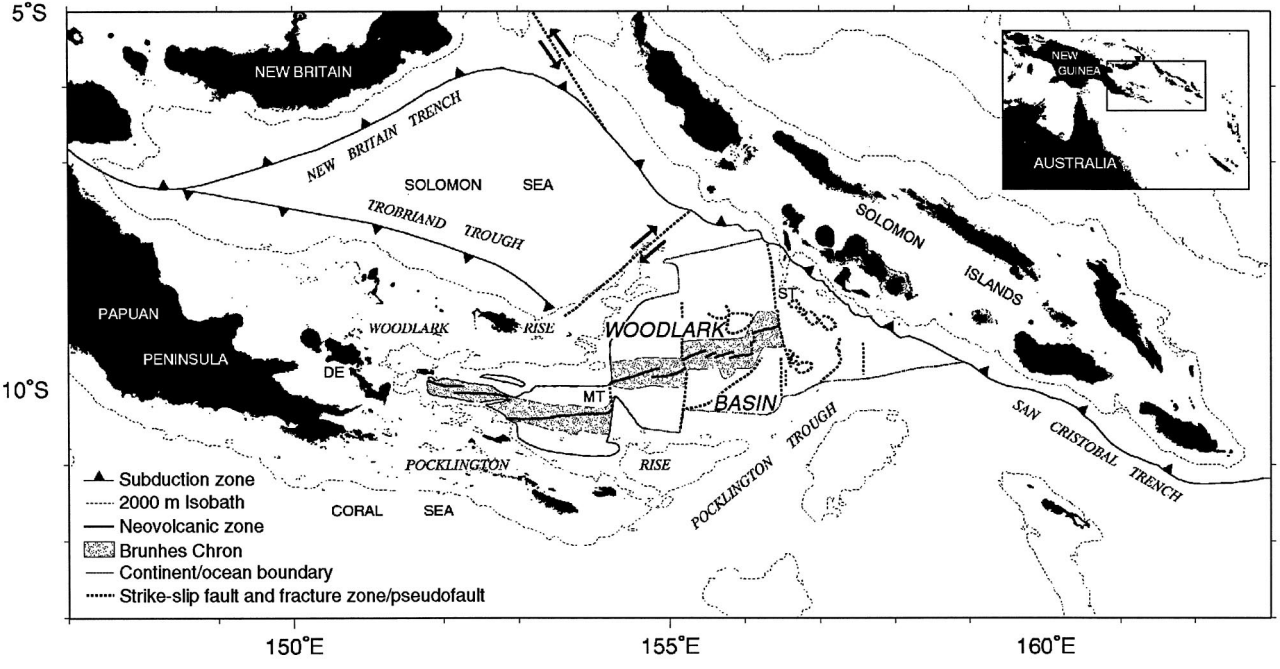
5°S
10°S
150°E
155°E
160°E
NEW BRITAIN
NEW BRITAIN TRENCH
SOLOMON SEA
TROBRIAND TROUGH
PAPUAN PENINSULA
WOODLARK RISE
WOODLARK BASIN
DE
MT
ST
SOLOMON ISLANDS
SAN CRISTOBAL TRENCH
POCKLINGTON RISE
POCKLINGTON TROUGH
CORAL SEA
NEW GUINEA
AUSTRALIA
Subduction zone
2000 m Isobath
Neovolcanic zone
Brunhes Chron
Continent/ocean boundary
Strike-slip fault and fracture zone/pseudofault

Figure 1

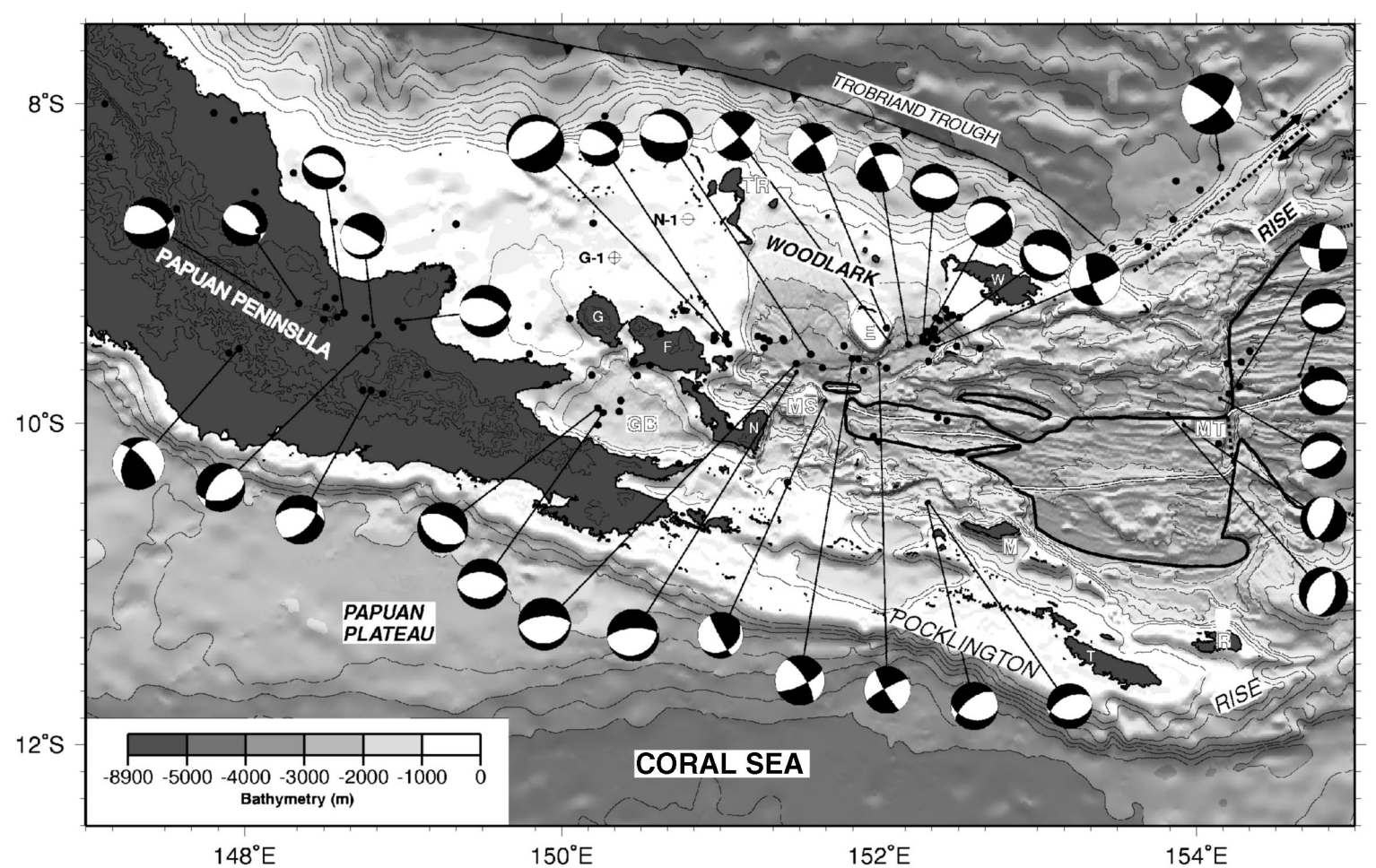
8°S
10°S
12°S
148°E
150°E
152°E
154°E
TROBRIAND TROUGH
RISE
WOODLARK
PAPUAN PENINSULA
PAPUAN PLATEAU
POCKLINGTON
RISE
CORAL SEA
N-1
G-1
TR
W
E
G
F
GB
N
MS
MT
M
R
-8900 -5000 -4000 -3000 -2000 -1000 0
Bathymetry (m)

Figure 2

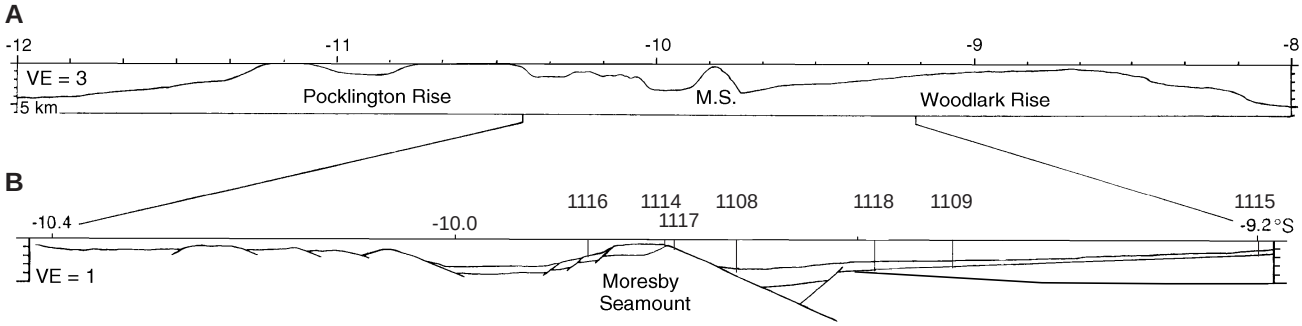
A
-12
-11
-10
-9
-8
VE = 3
5 km
Pocklington Rise
M.S.
Woodlark Rise
B
-10.4
-10.0
1116
1114
1117
1108
1118
1109
1115
-9.2°S
VE = 1
Moresby
Seamount

Figure 3

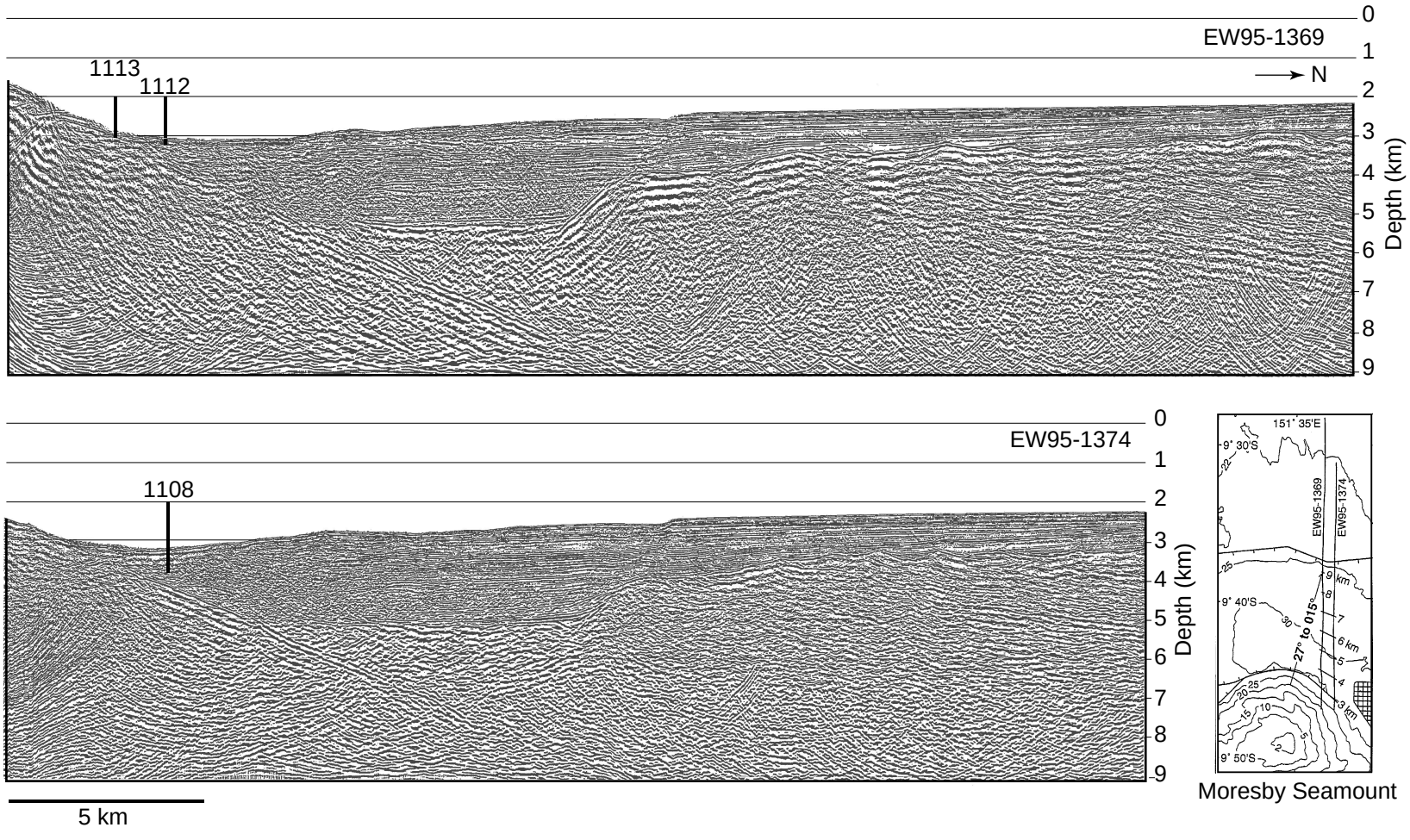
EW95-1369
N
1113
1112
0
1
2
3
4
5
6
7
8
9
Depth (km)
EW95-1374
1108
0
1
2
3
4
5
6
7
8
9
Depth (km)
5 km
151° 35'E
9° 30'S
9° 40'S
9° 50'S
EW95-1369
EW95-1374
9 km
7
6 km
5
4
3 km
27° to 015°
Moresby Seamount

Figure 4

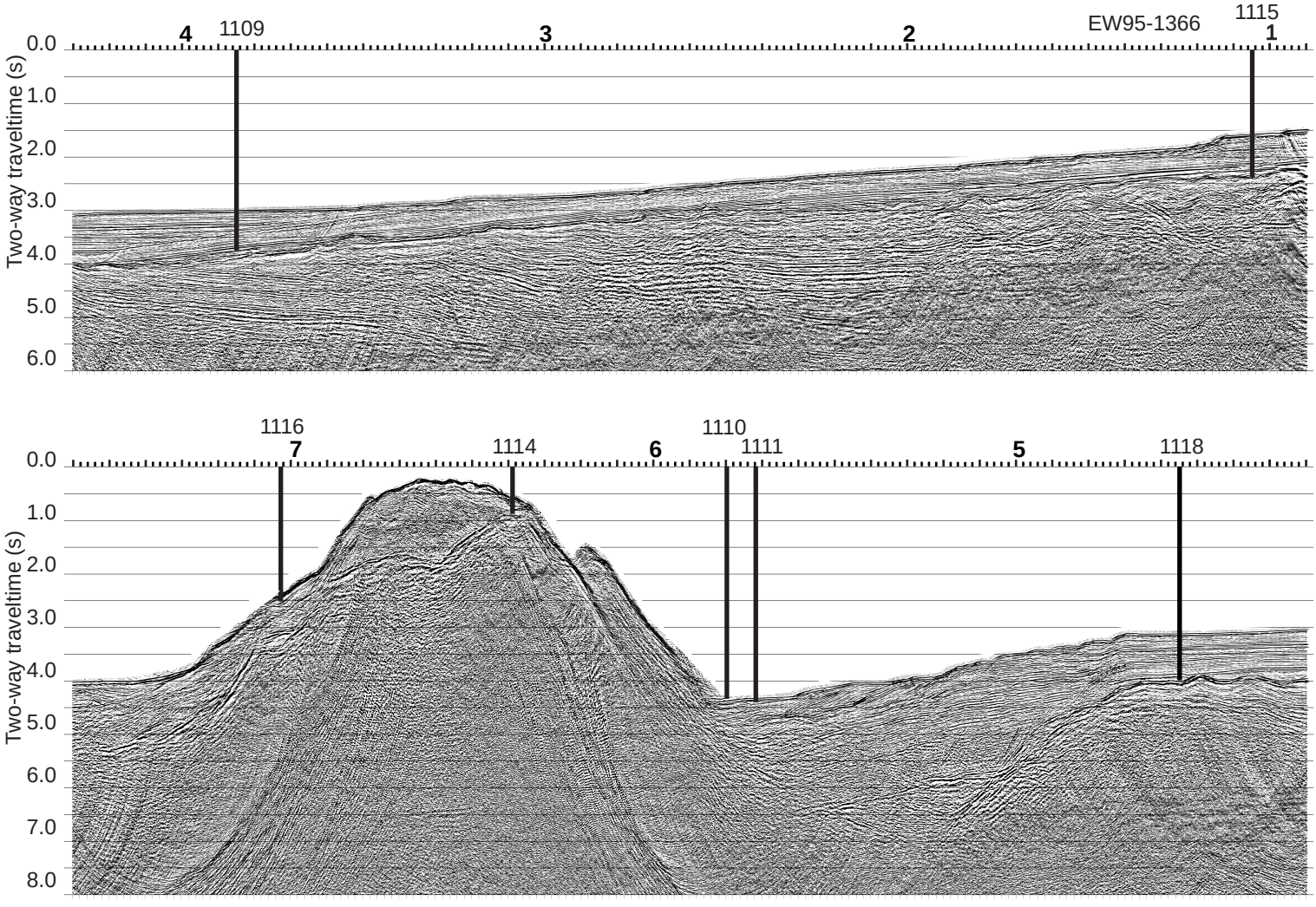
4
1109
3
2
EW95-1366
1115
1
Two-way traveltime (s)
0.0
1.0
2.0
3.0
4.0
5.0
6.0
1116
7
1114
6
1110
1111
5
1118
Two-way traveltime (s)
0.0
1.0
2.0
3.0
4.0
5.0
6.0
7.0
8.0

Figure 5

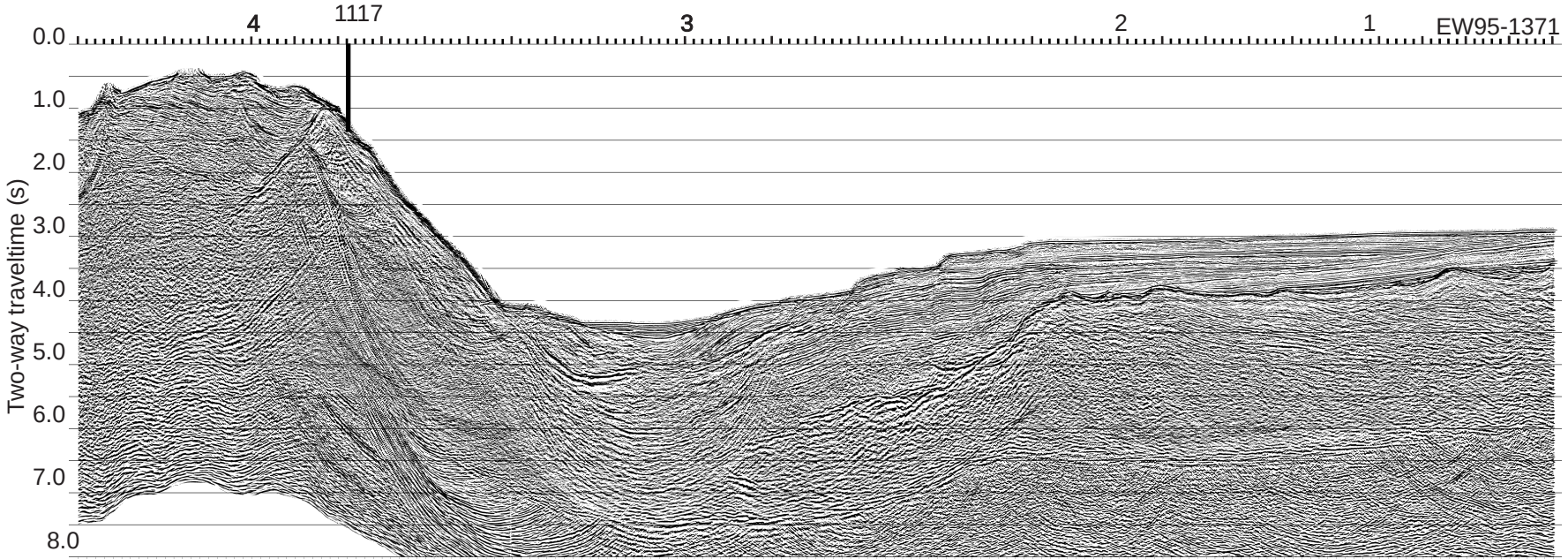
4
1117
3
2
1
EW95-1371
0.0
1.0
2.0
3.0
4.0
5.0
6.0
7.0
8.0
Two-way traveltime (s)

Figure 6

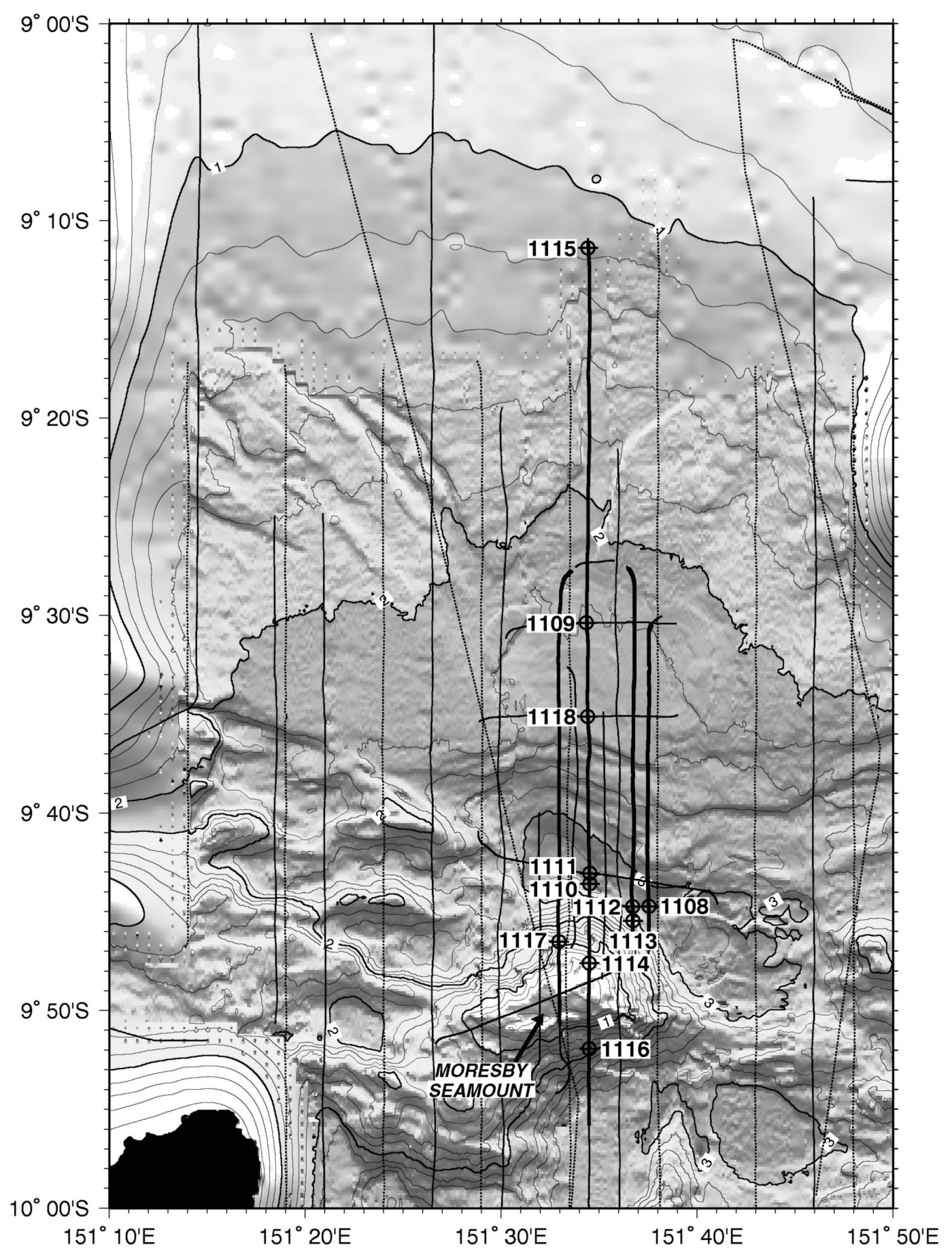
9° 00'S
9° 10'S
9° 20'S
9° 30'S
9° 40'S
9° 50'S
10° 00'S
151° 10'E
151° 20'E
151° 30'E
151° 40'E
151° 50'E
1115
1109
1118
1111
1110
1112
1108
1117
1113
1114
1116
MORESBY
SEAMOUNT

Figure 7

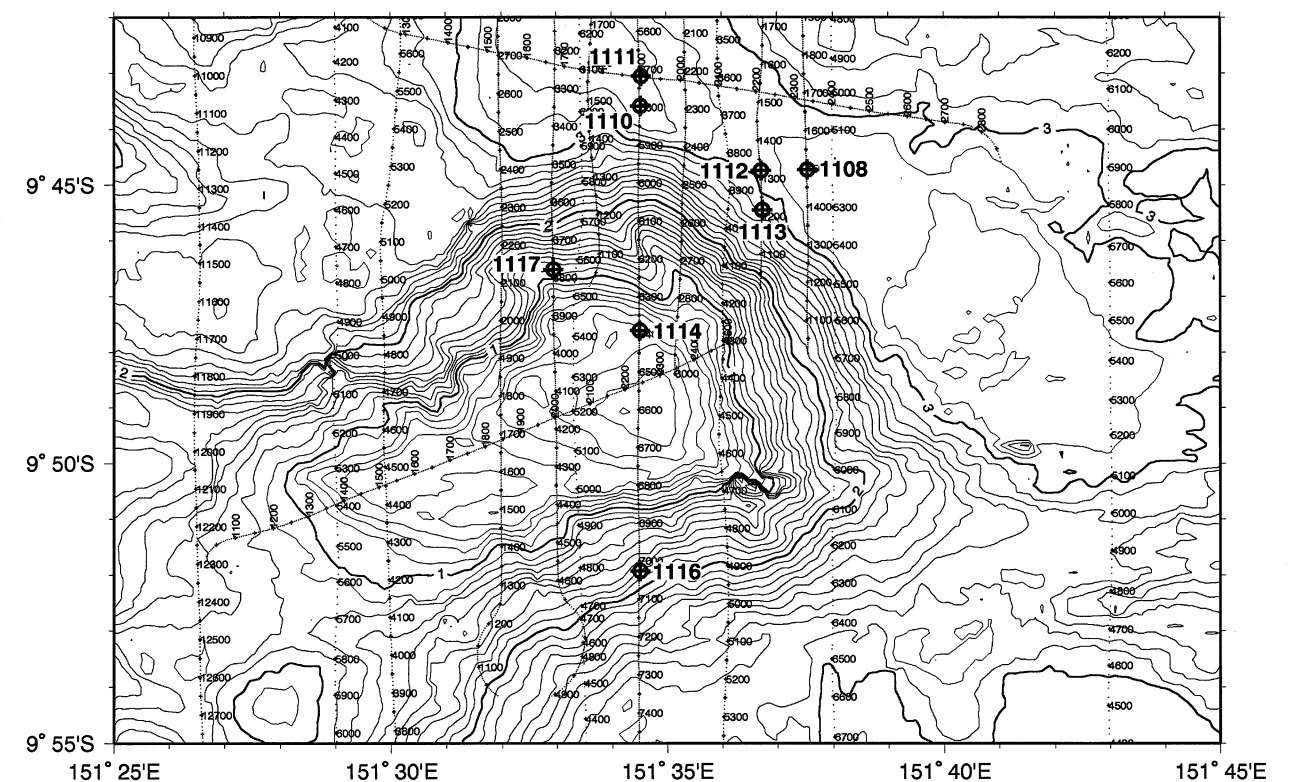
1111
1110
1112
1108
1113
1117
1114
1116
9° 45'S
9° 50'S
9° 55'S
151° 25'E
151° 30'E
151° 35'E
151° 40'E
151° 45'E

Figure 8

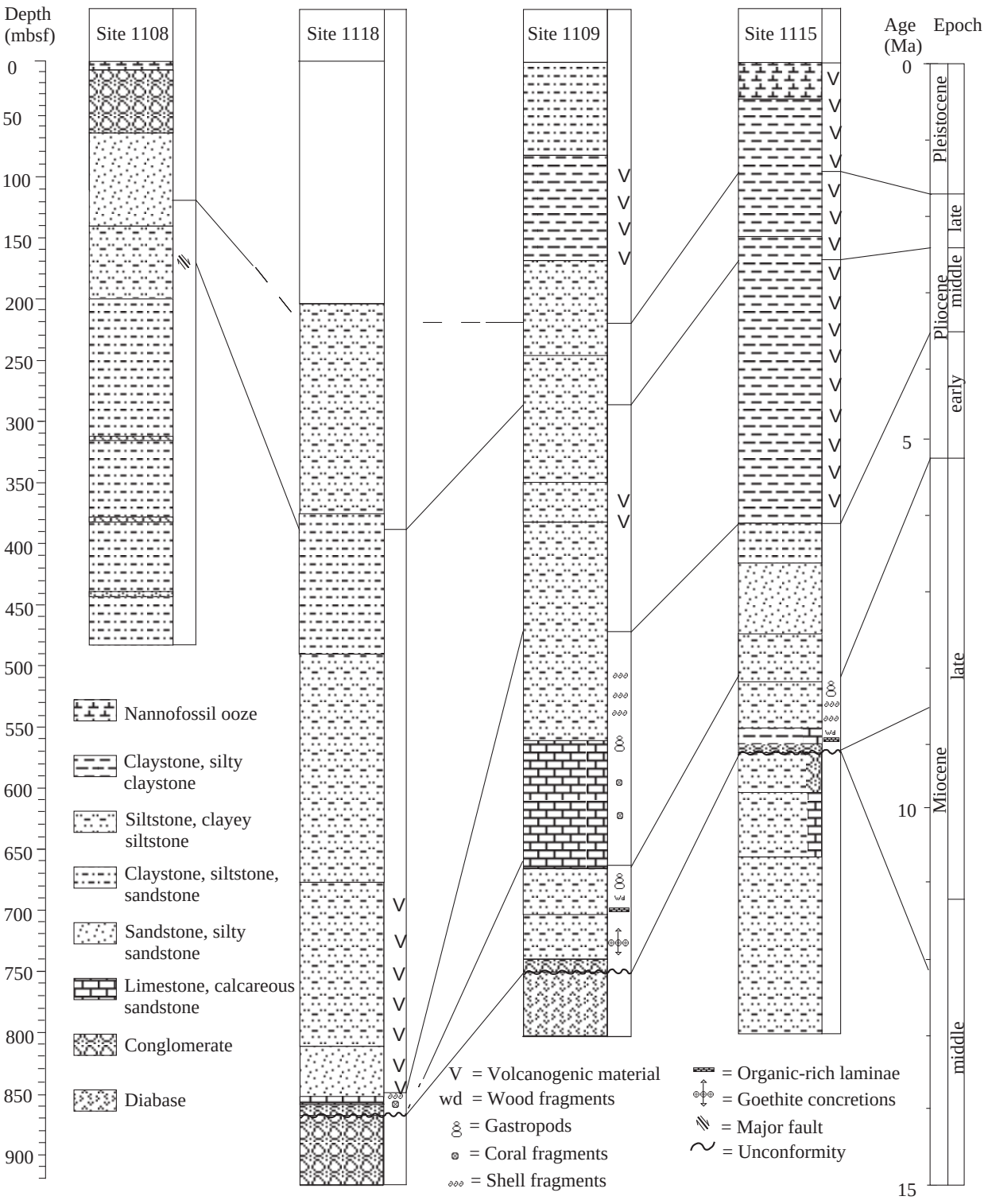
Depth (mbsf)
0
50
100
150
200
250
300
350
400
450
500
550
600
650
700
750
800
850
900
Site 1108
Site 1118
Site 1109
Site 1115
Age (Ma)
Epoch
0
5
10
15
Pleistocene
Pliocene
late
middle
early
Miocene
late
middle
Nannofossil ooze
Claystone, silty claystone
Siltstone, clayey siltstone
Claystone, siltstone, sandstone
Sandstone, silty sandstone
Limestone, calcareous sandstone
Conglomerate
Diabase
V = Volcanogenic material
wd = Wood fragments
= Gastropods
= Coral fragments
= Shell fragments
= Organic-rich laminae
= Goethite concretions
= Major fault
= Unconformity

Figure 9

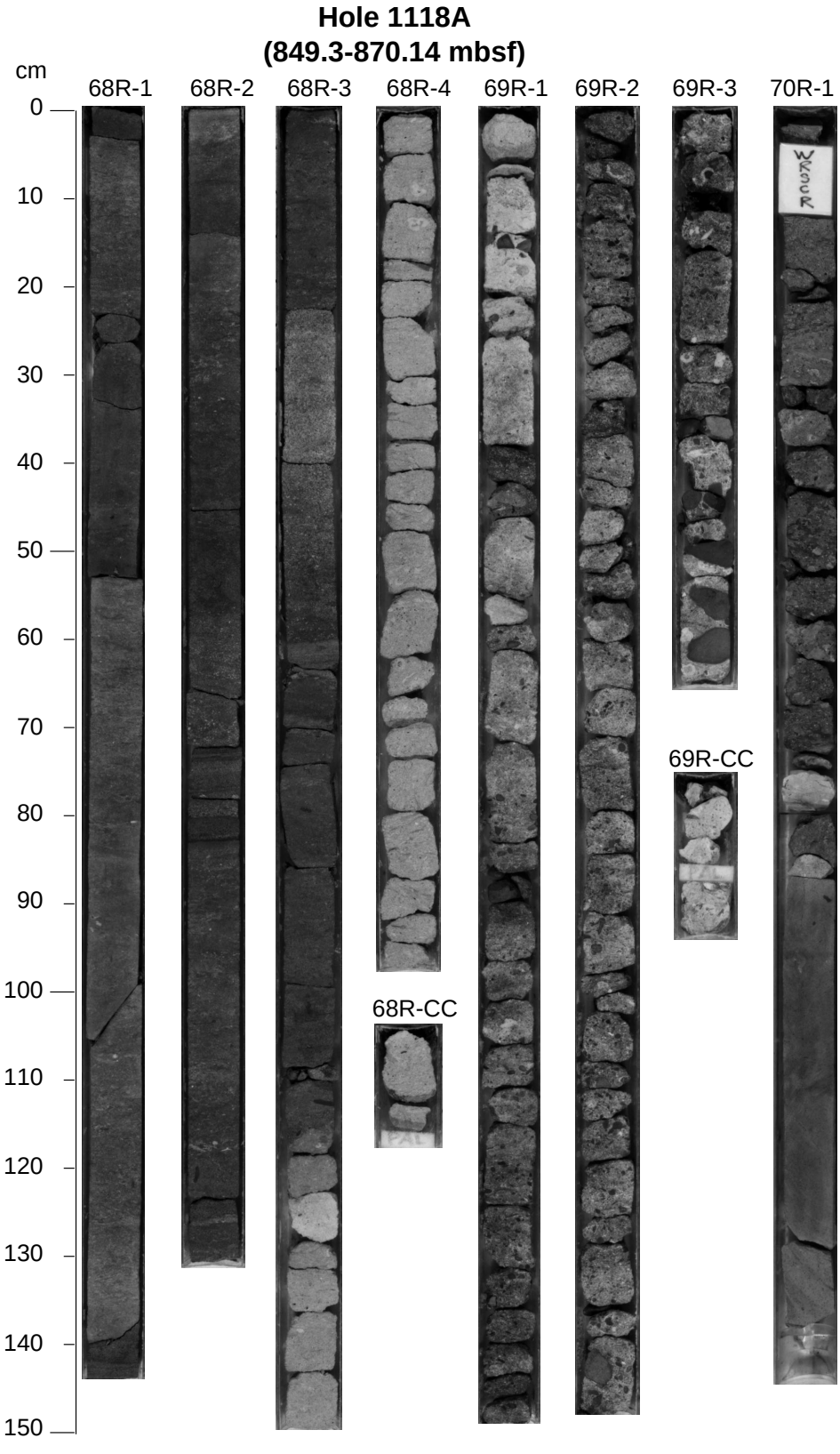
Hole 1118A
(849.3-870.14 mbsf)
cm
0
10
20
30
40
50
60
70
80
90
100
110
120
130
140
150
68R-1
68R-2
68R-3
68R-4
68R-CC
69R-1
69R-2
69R-3
69R-CC
70R-1

Figure 10

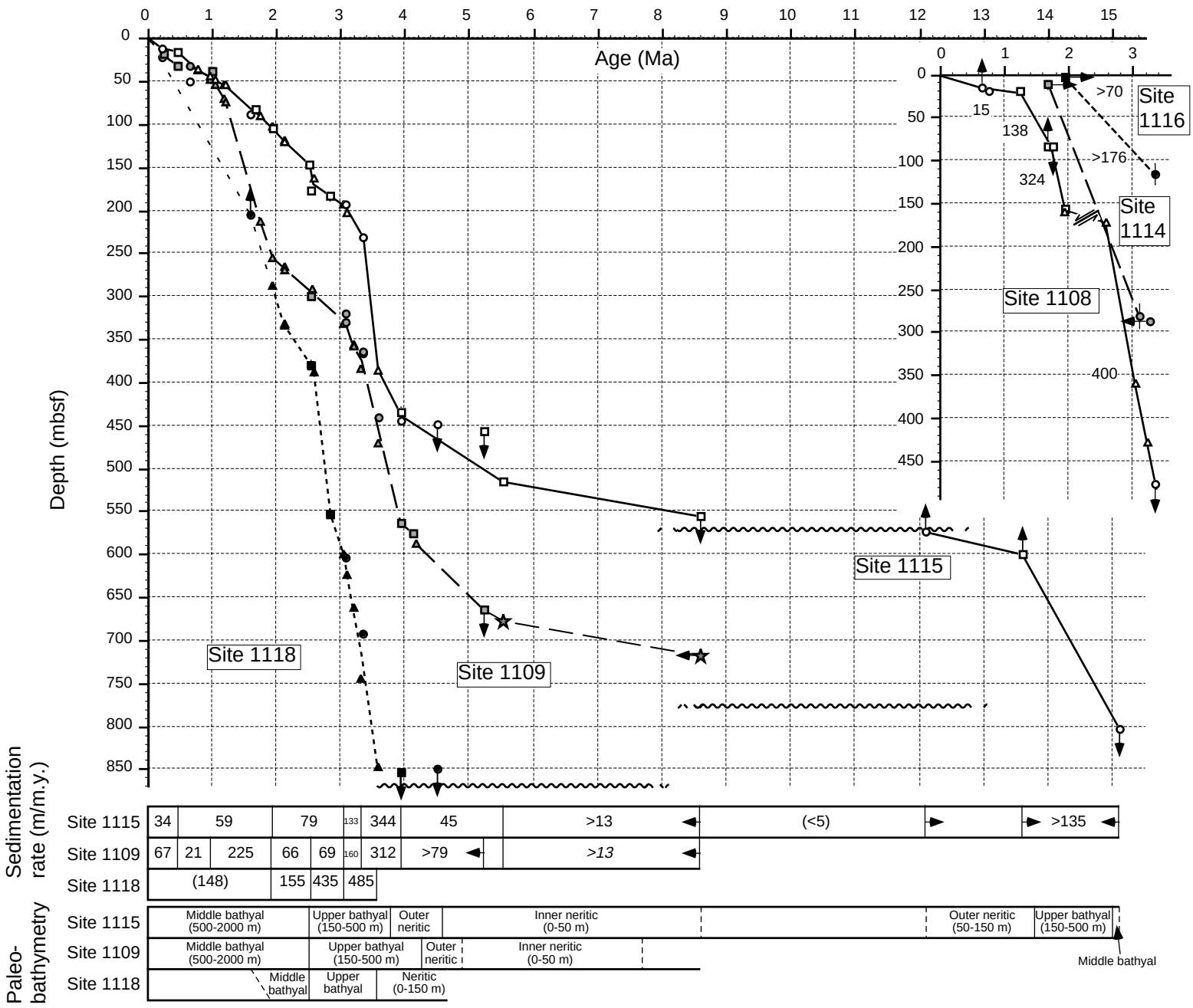
Age (Ma)
Depth (mbsf)
Site 1118
Site 1109
Site 1115
Site 1108
Site 1114
Site 1116
15
138
324
>70
>176
400
Sedimentation rate (m/m.y.)
Site 1115
34
59
79
133
344
45
>13
(<5)
>135
Site 1109
67
21
225
66
69
160
312
>79
>13
Site 1118
(148)
155
435
485
Paleo-bathymetry
Site 1115
Middle bathyal (500-2000 m)
Upper bathyal (150-500 m)
Outer neritic
Inner neritic (0-50 m)
Outer neritic (50-150 m)
Upper bathyal (150-500 m)
Site 1109
Middle bathyal (500-2000 m)
Upper bathyal (150-500 m)
Outer neritic
Inner neritic (0-50 m)
Middle bathyal
Site 1118
Middle bathyal
Upper bathyal
Neritic (0-150 m)

Figure 11

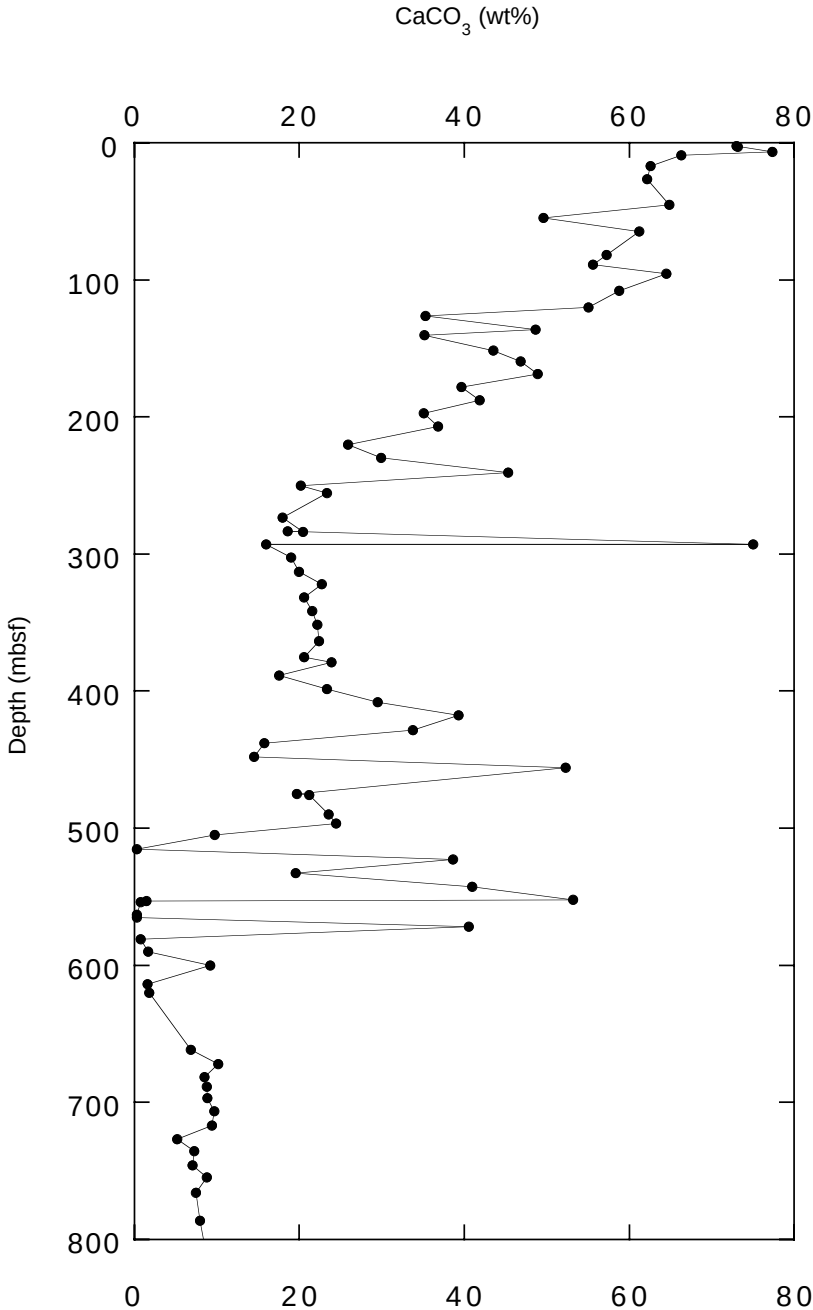
CaCO3 (wt%)
0
20
40
60
80
Depth (mbsf)
0
100
200
300
400
500
600
700
800

Figure 12

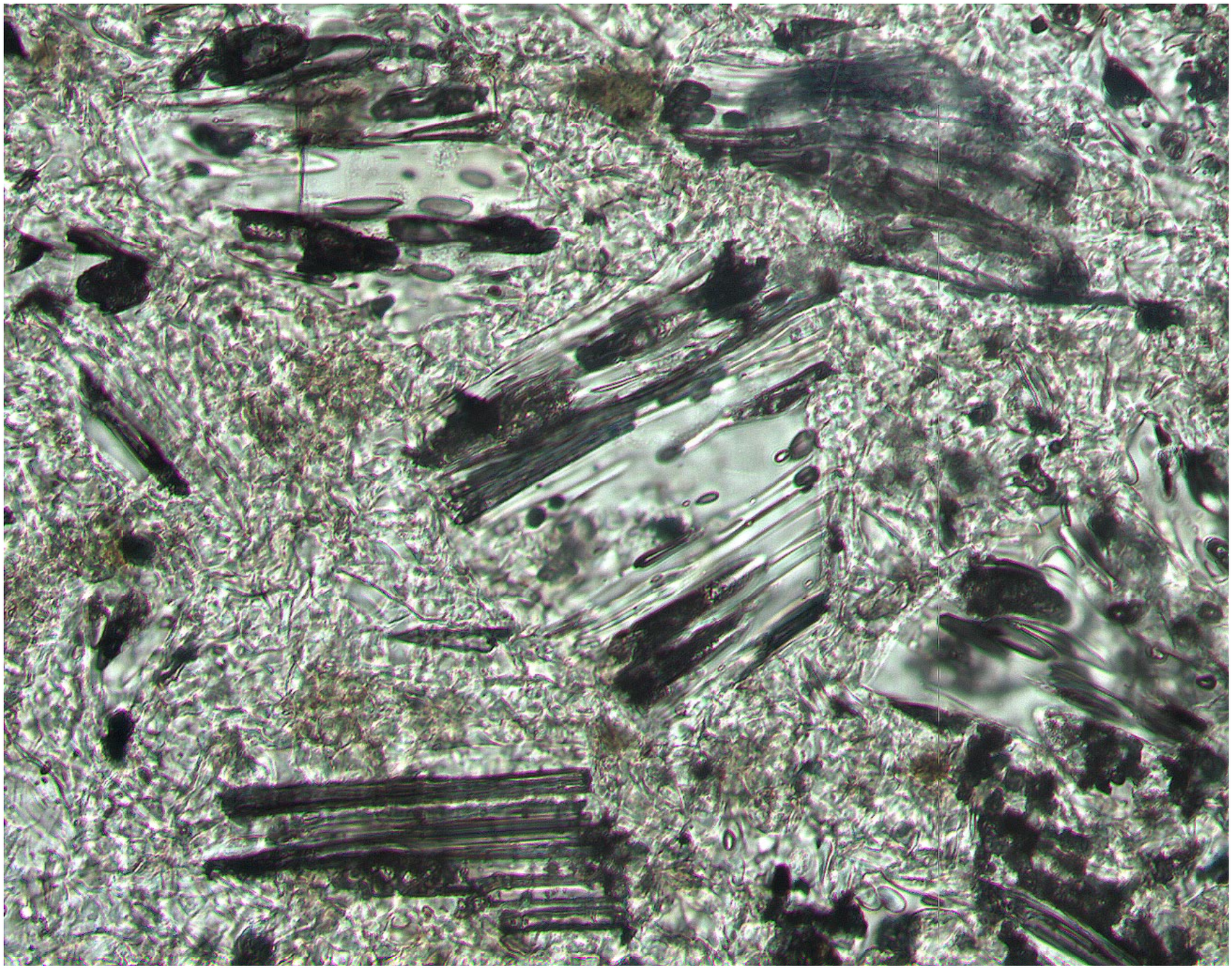

Figure 13

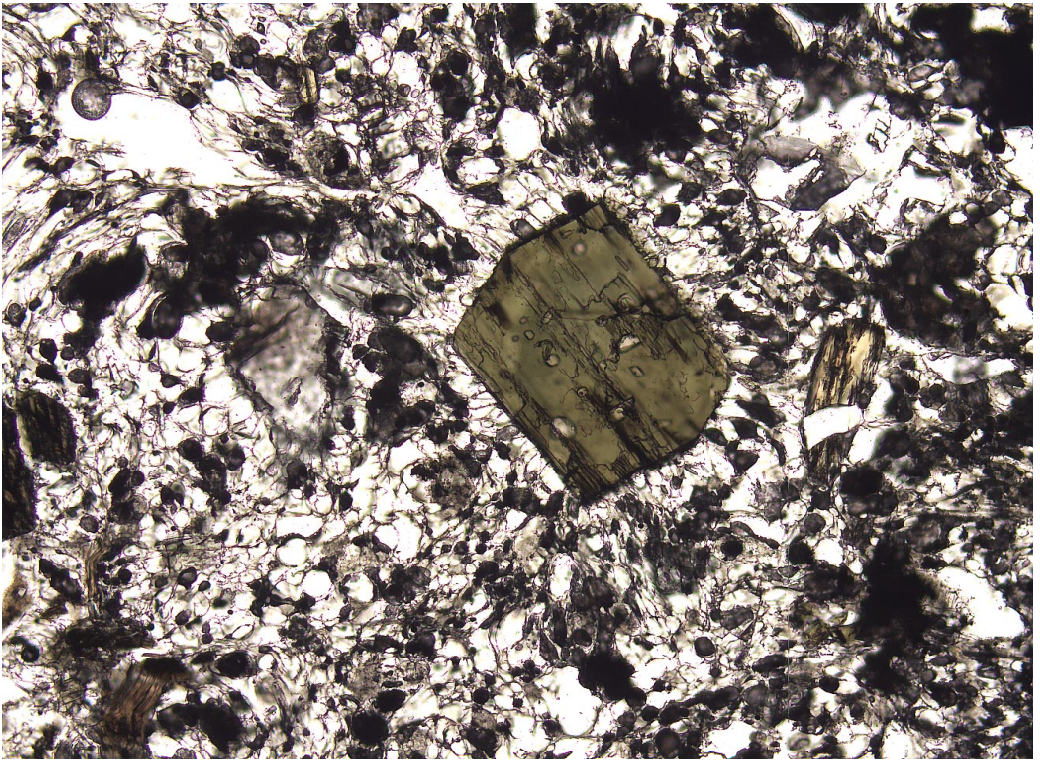

Figure 14

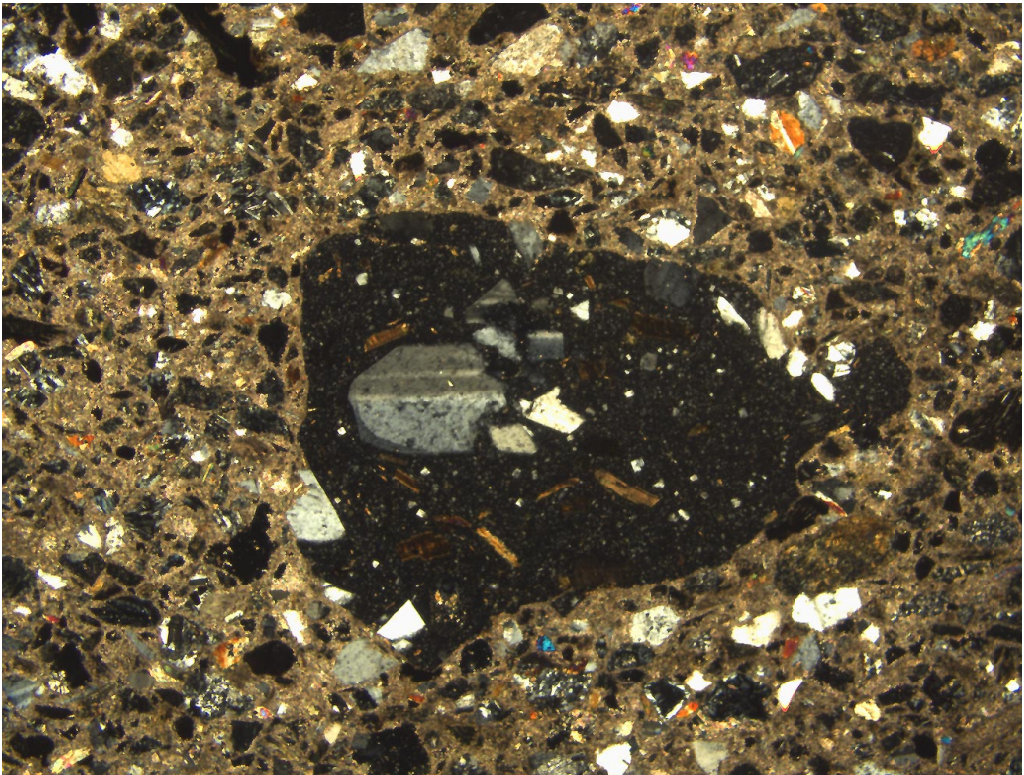

4 mm

Figure 15

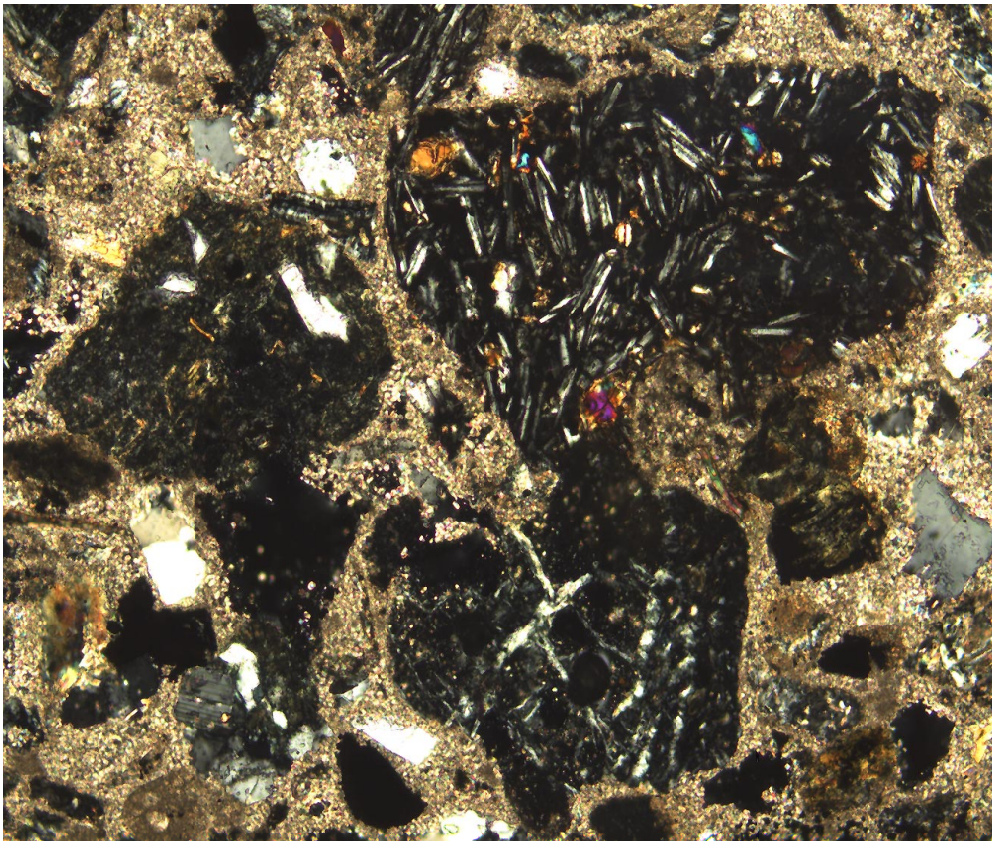

Figure 16

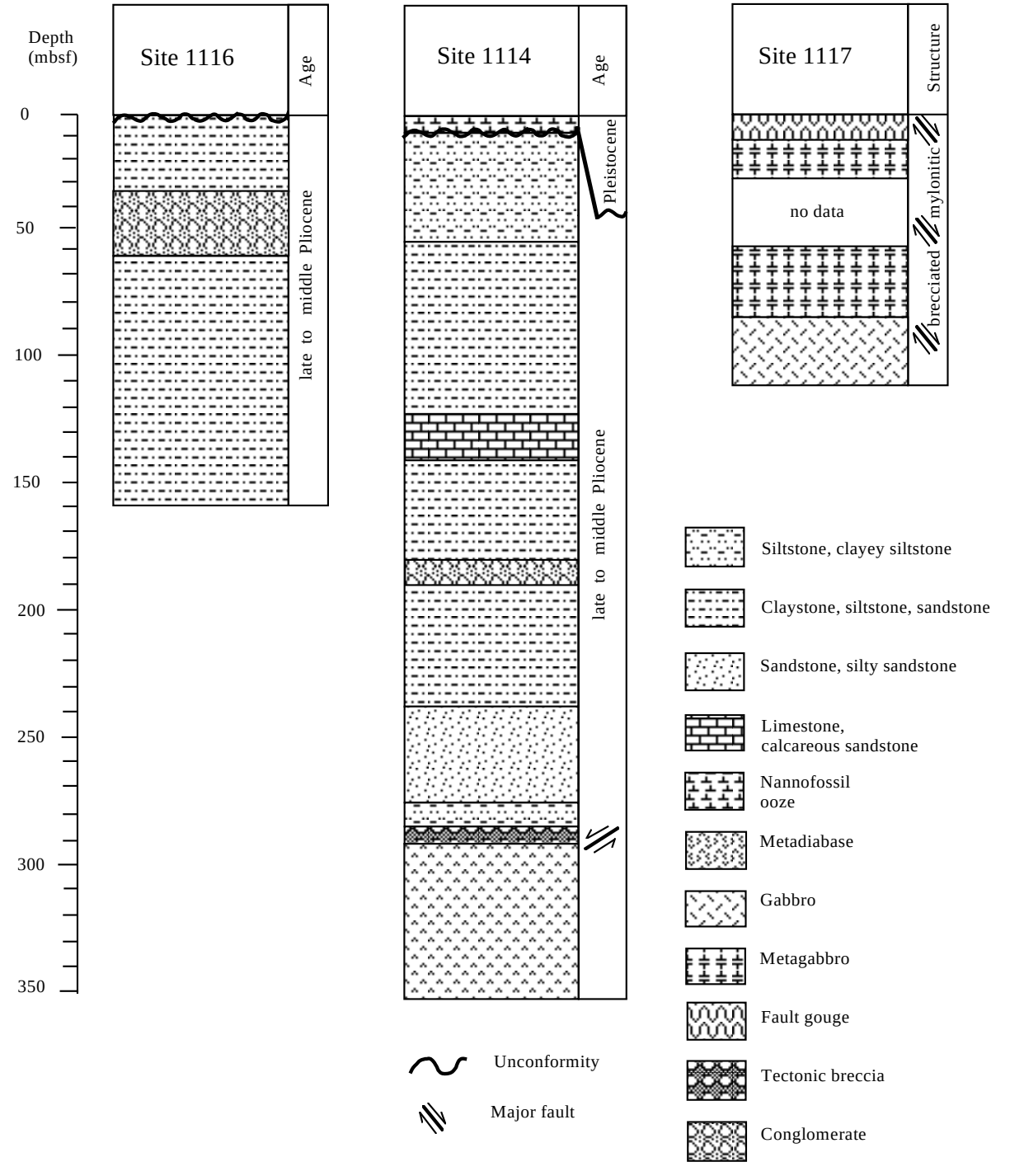
Depth
(mbsf)
0
50
100
150
200
250
300
350
Site 1116
Age
late to middle Pliocene
Site 1114
Age
Pleistocene
late to middle Pliocene
Site 1117
Structure
no data
mylonitic
brecciated
Siltstone, clayey siltstone
Claystone, siltstone, sandstone
Sandstone, silty sandstone
Limestone,
calcareous sandstone
Nannofossil
ooze
Metadiabase
Gabbro
Metagabbro
Fault gouge
Tectonic breccia
Conglomerate
Unconformity
Major fault

Figure 17

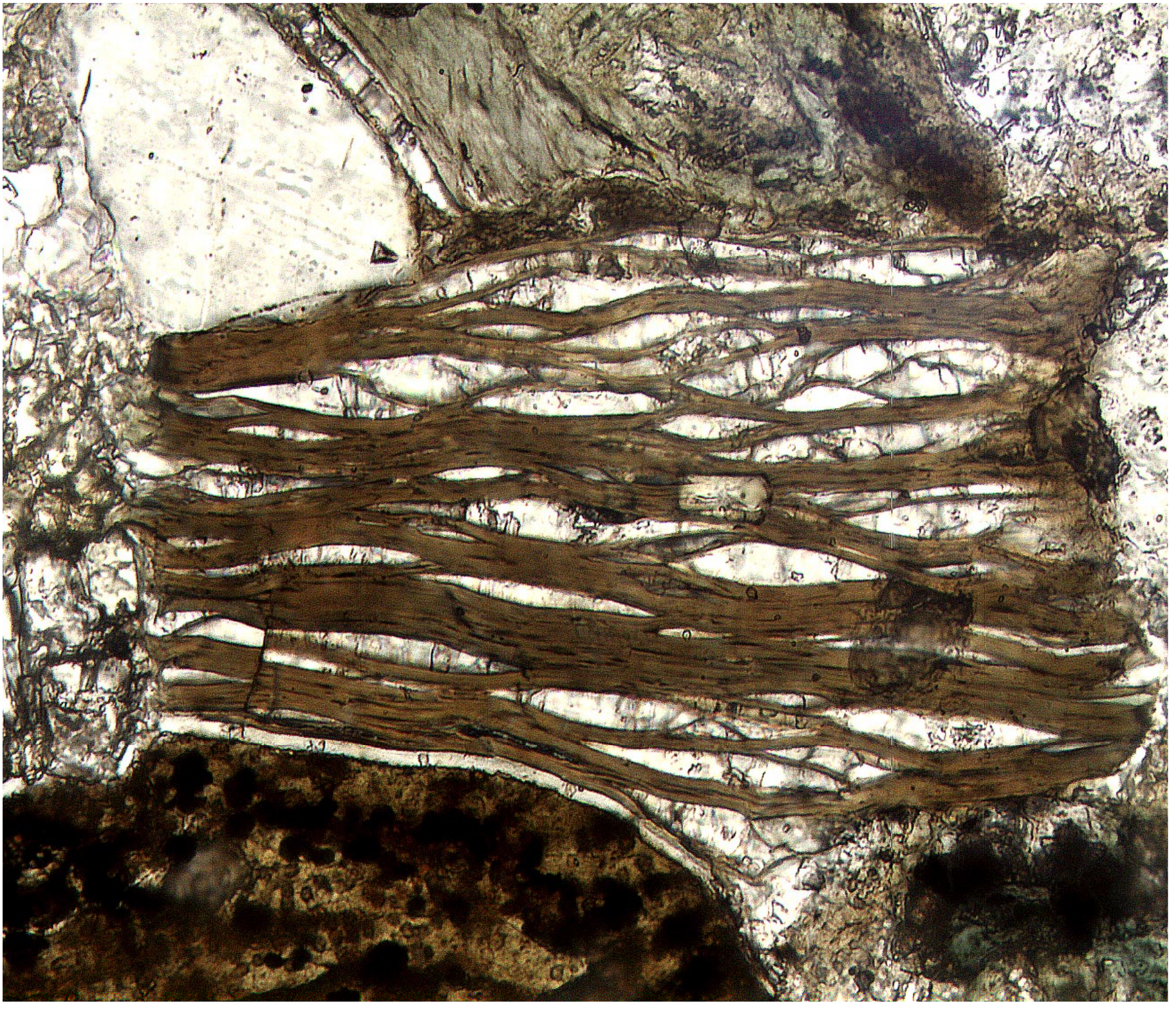

0.25 mm

Figure 18

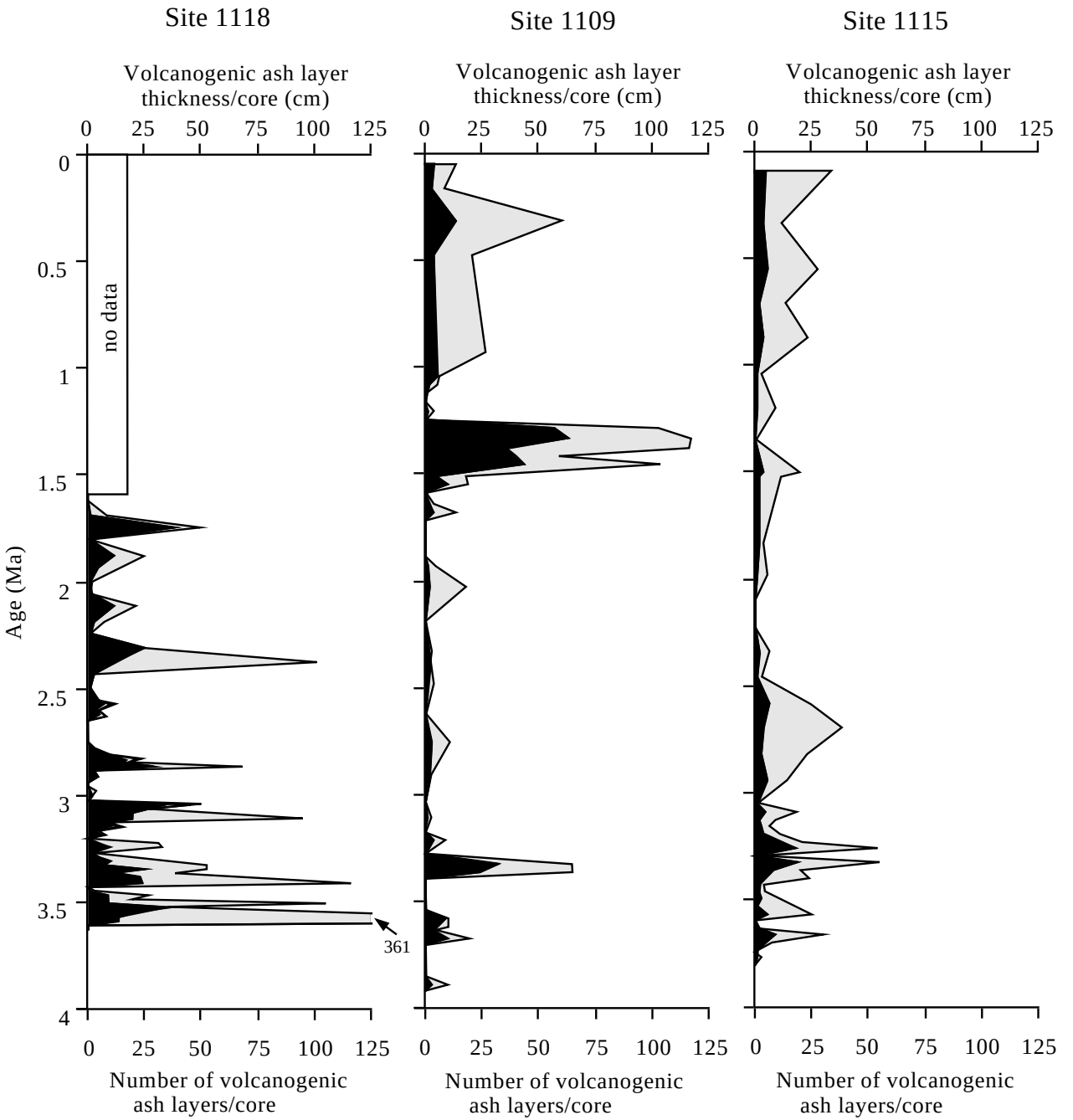
Site 1118
Site 1109
Site 1115
Volcanogenic ash layer thickness/core (cm)
0 25 50 75 100 125
no data
Age (Ma)
0
0.5
1
1.5
2
2.5
3
3.5
4
361
Number of volcanogenic ash layers/core

Figure 19

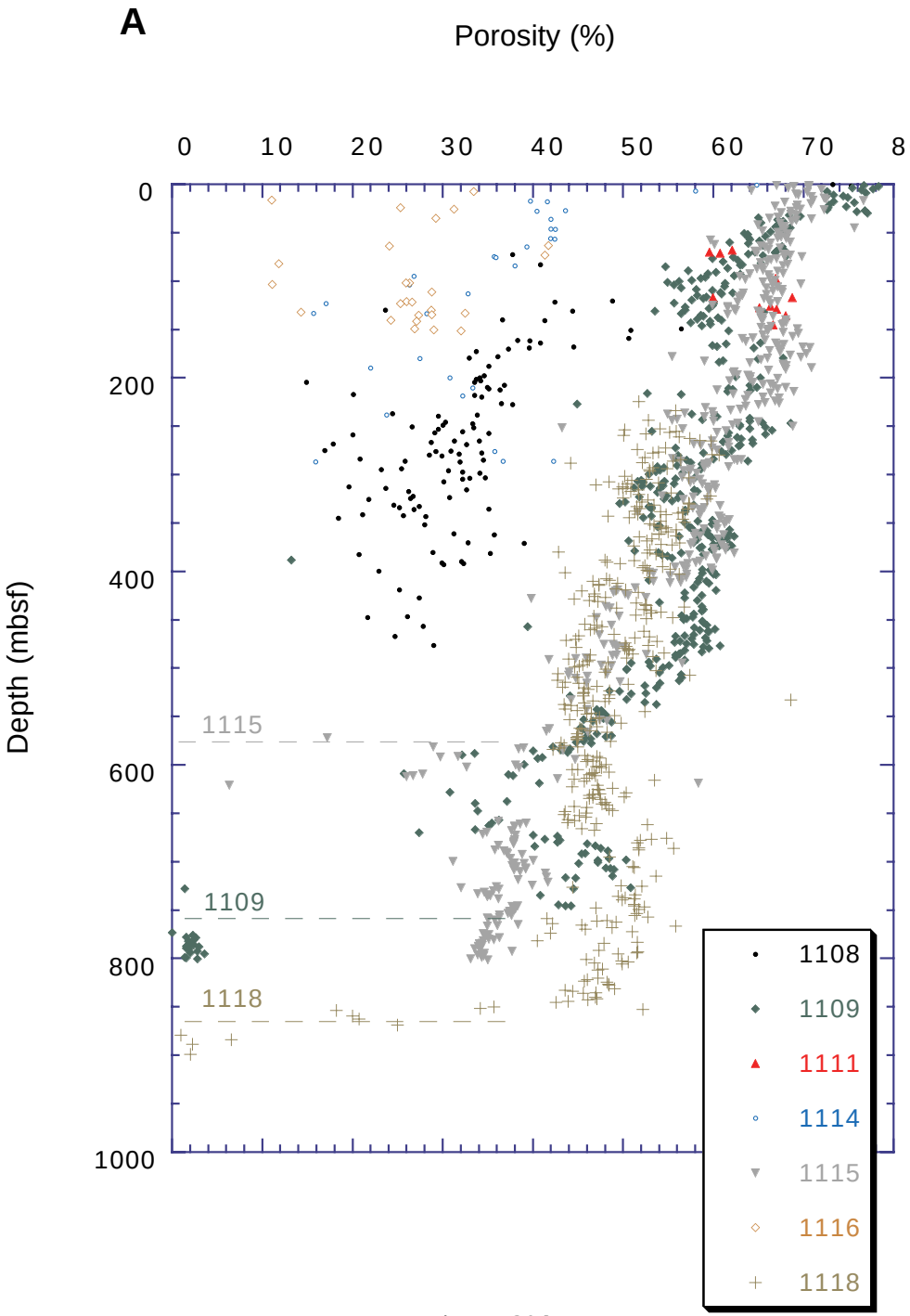
A
Porosity (%)
0
10
20
30
40
50
60
70
80
Depth (mbsf)
0
200
400
600
800
1000
1115
1109
1118
1108
1109
1111
1114
1115
1116
1118

Figure 20A

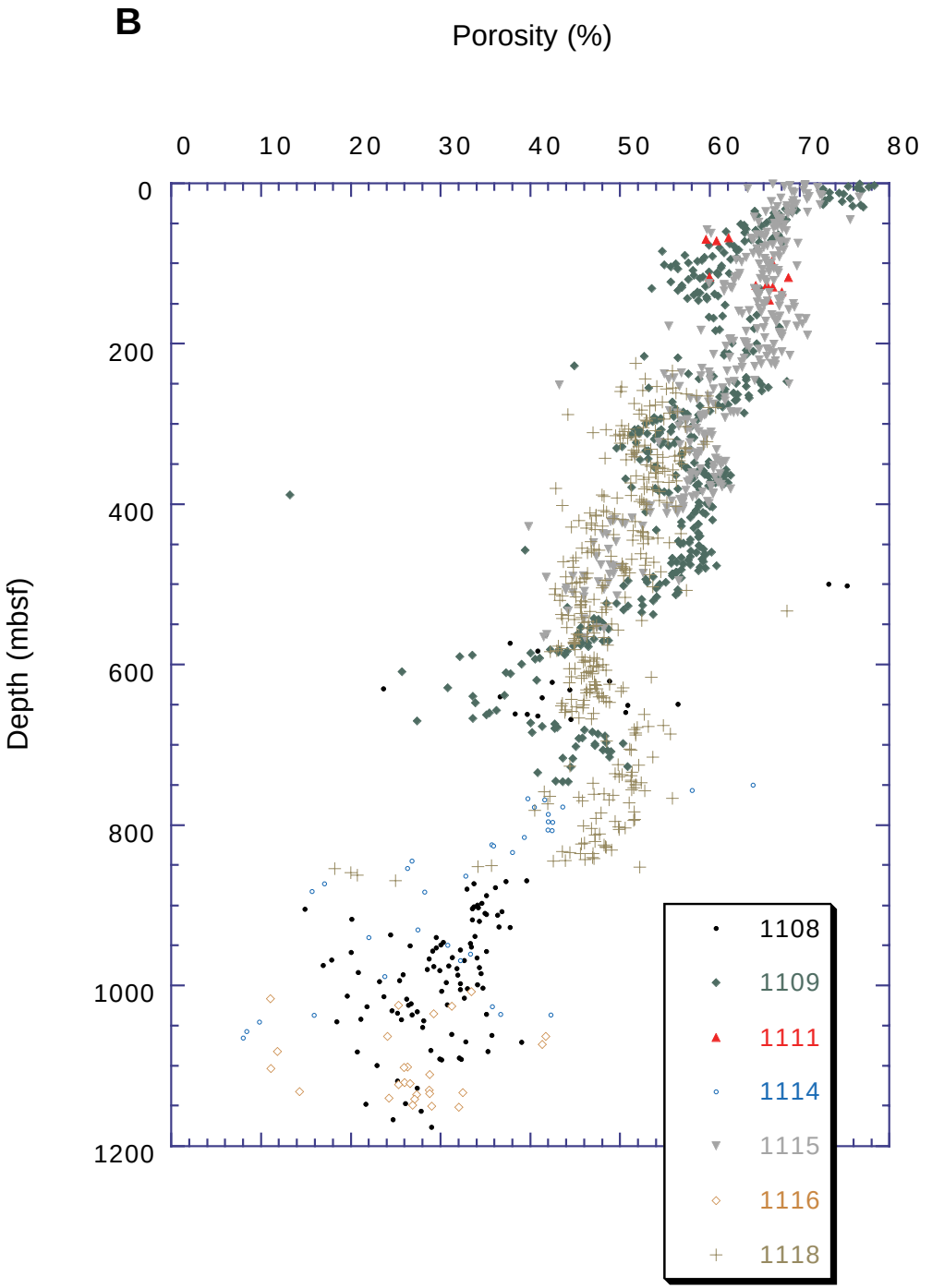
B
Porosity (%)
0
10
20
30
40
50
60
70
80
Depth (mbsf)
0
200
400
600
800
1000
1200
1108
1109
1111
1114
1115
1116
1118

Figure 20B

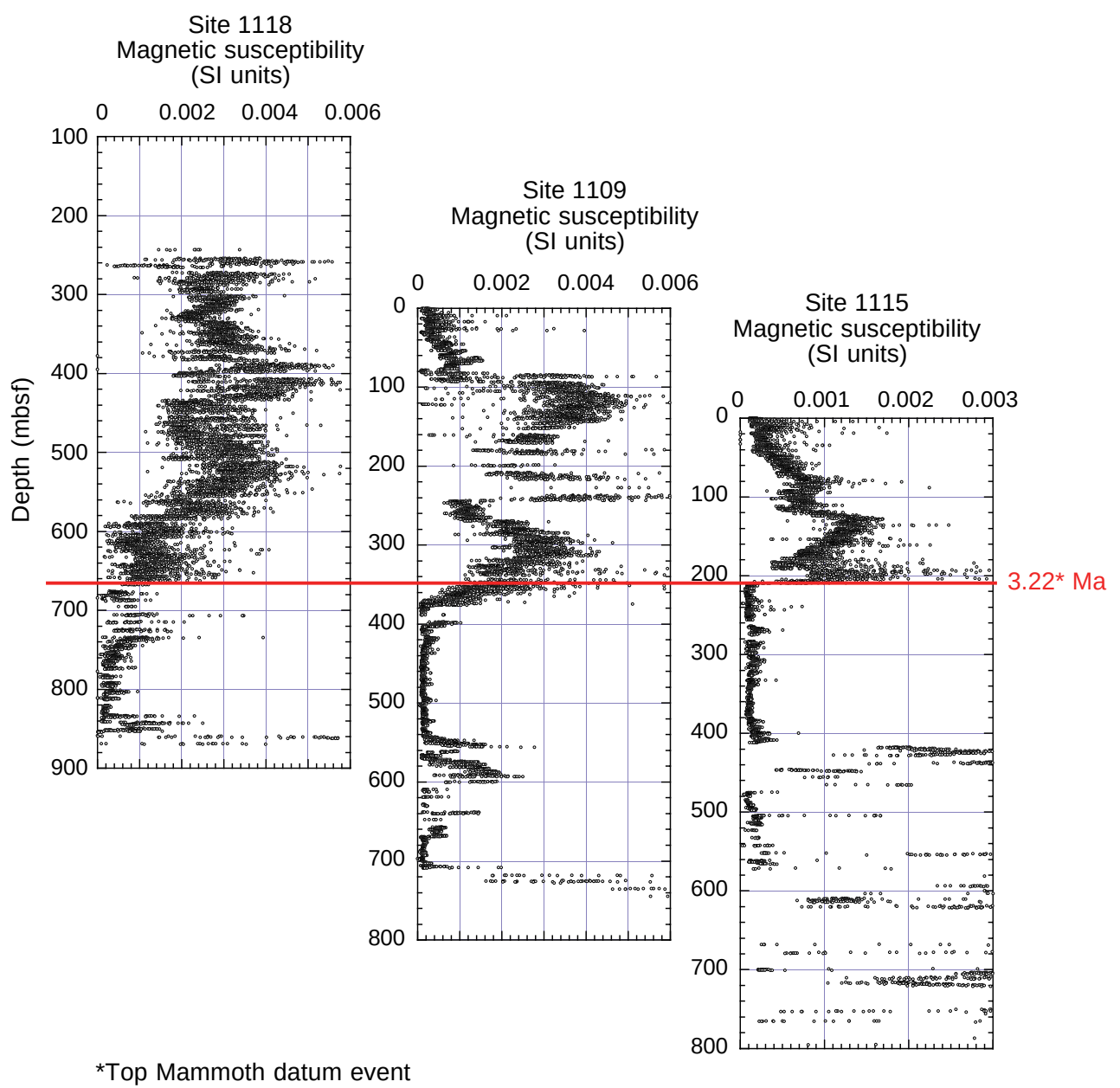

*Top Mammoth datum event

Figure 21

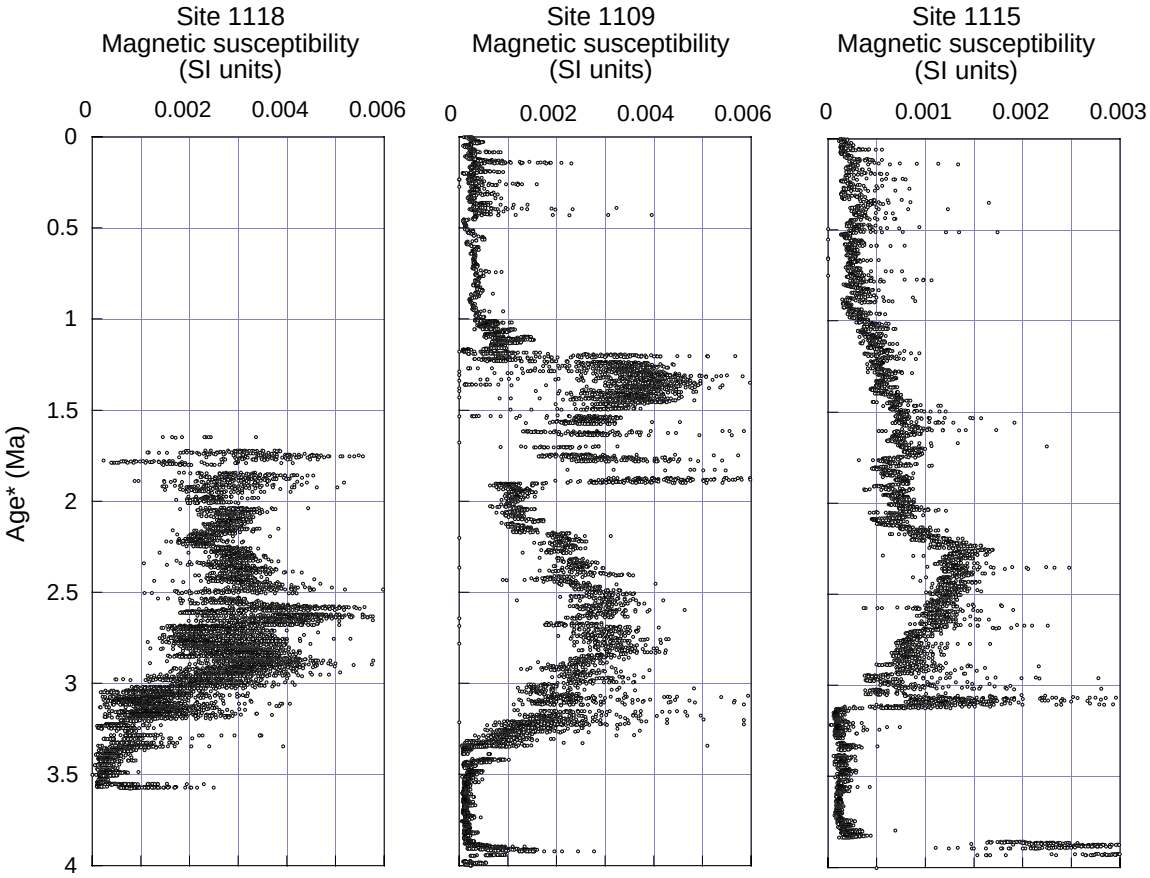

*Biostratigraphic/paleomagnetic estimates

Figure 22

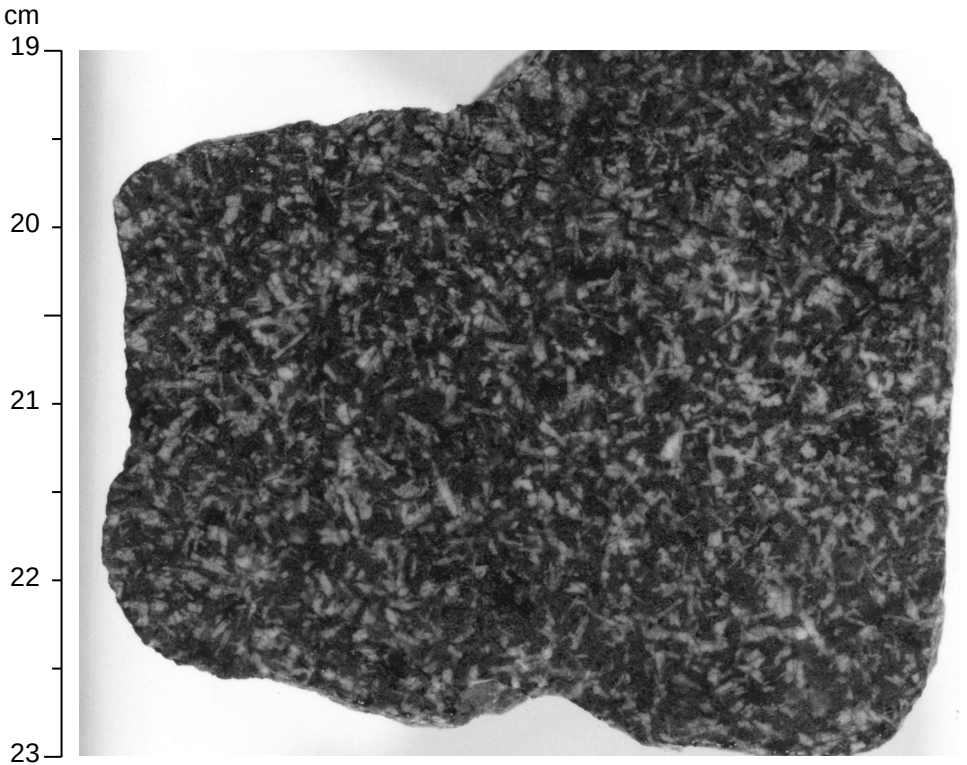

Figure 23

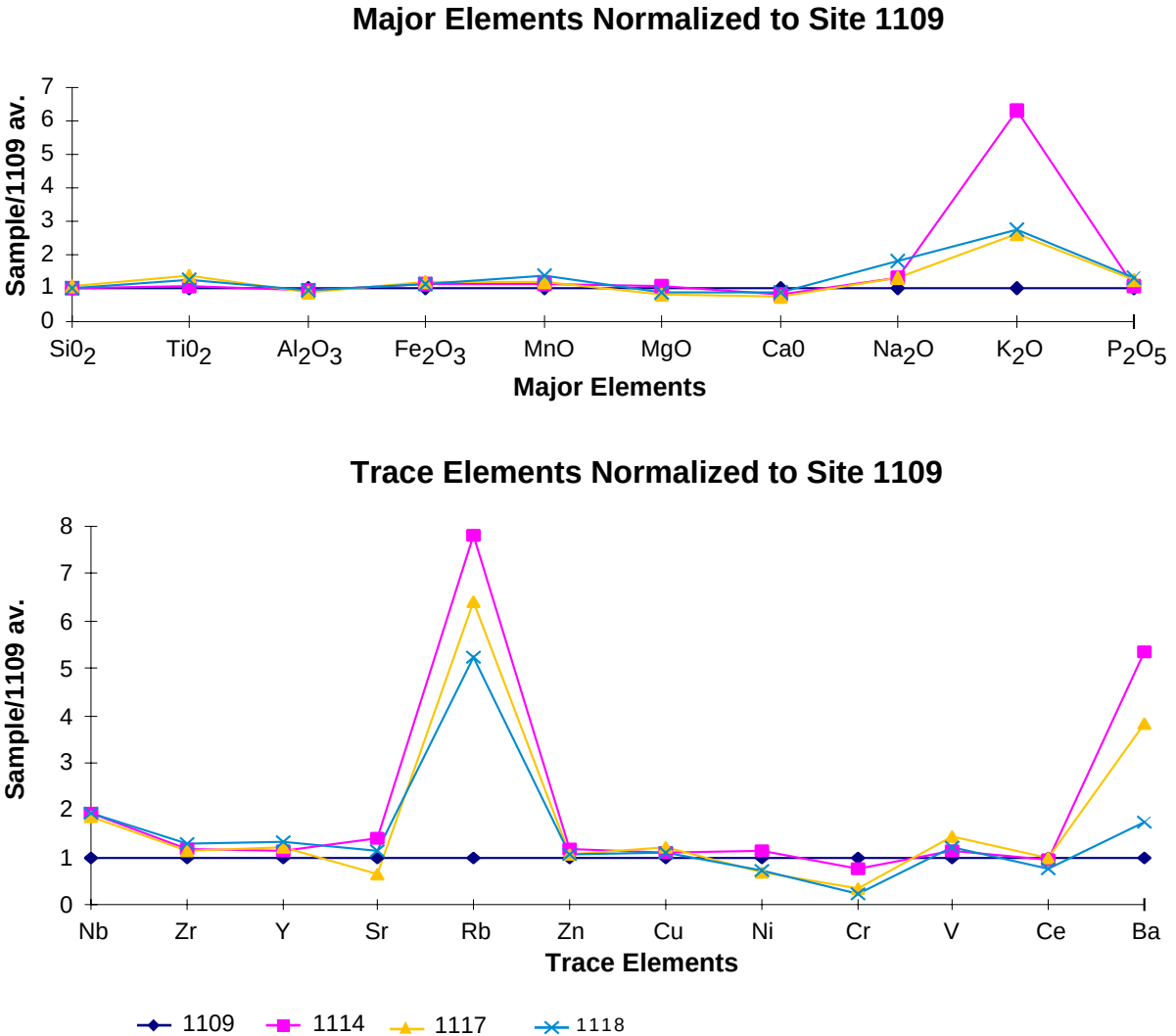
Major Elements Normalized to Site 1109
Sample/1109 av.
0
1
2
3
4
5
6
7
Si0$_2$
Ti0$_2$
Al$_2$O$_3$
Fe$_2$O$_3$
MnO
MgO
Ca0
Na$_2$O
K$_2$O
P$_2$O$_5$
Major Elements
Trace Elements Normalized to Site 1109
Sample/1109 av.
0
1
2
3
4
5
6
7
8
Nb
Zr
Y
Sr
Rb
Zn
Cu
Ni
Cr
V
Ce
Ba
Trace Elements
1109
1114
1117
1118

Figure 24

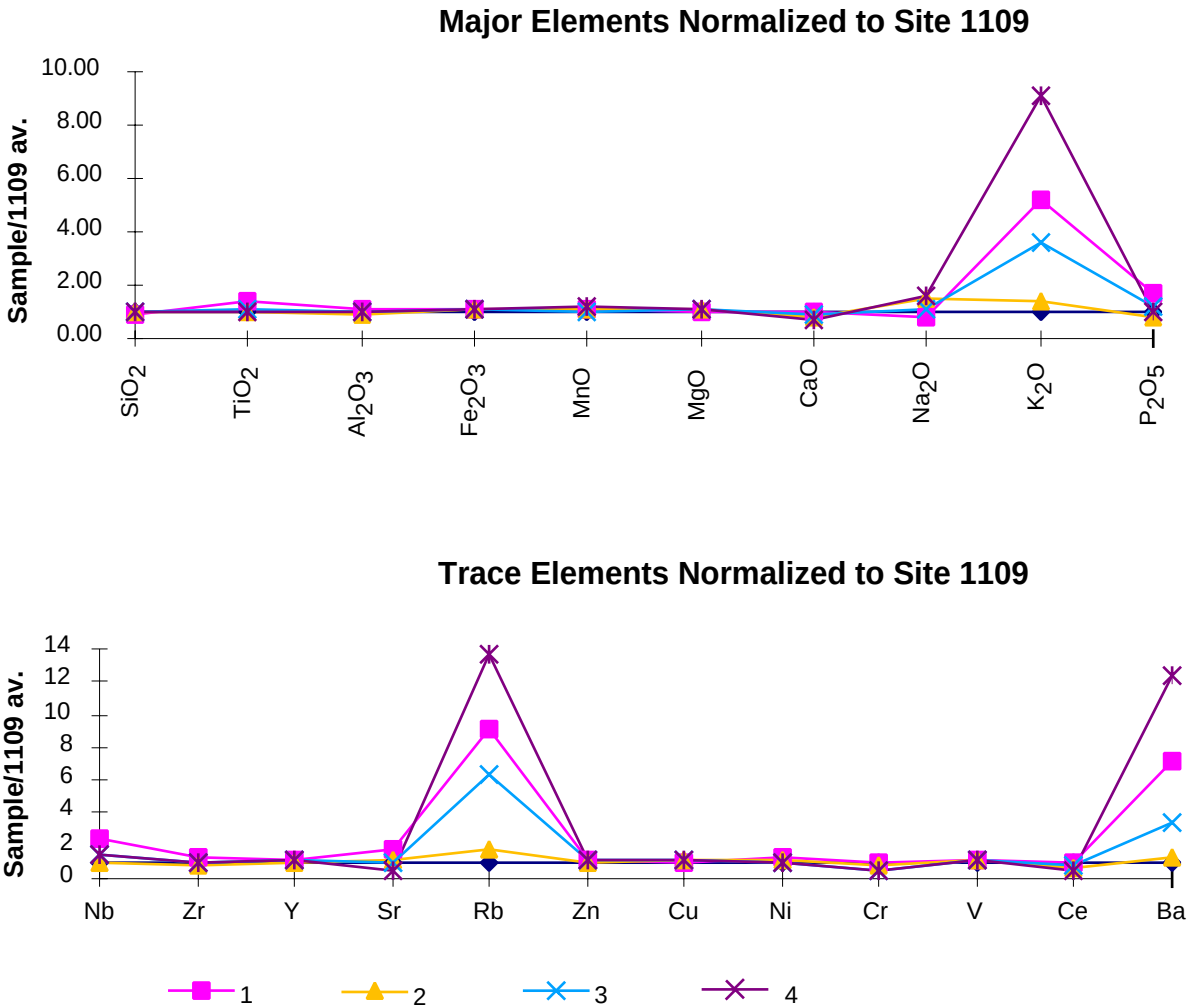
Major Elements Normalized to Site 1109
Sample/1109 av.
10.00
8.00
6.00
4.00
2.00
0.00
SiO2
TiO2
Al2O3
Fe2O3
MnO
MgO
CaO
Na2O
K2O
P2O5
Trace Elements Normalized to Site 1109
Sample/1109 av.
14
12
10
8
6
4
2
0
Nb
Zr
Y
Sr
Rb
Zn
Cu
Ni
Cr
V
Ce
Ba
1
2
3
4

Figure 25

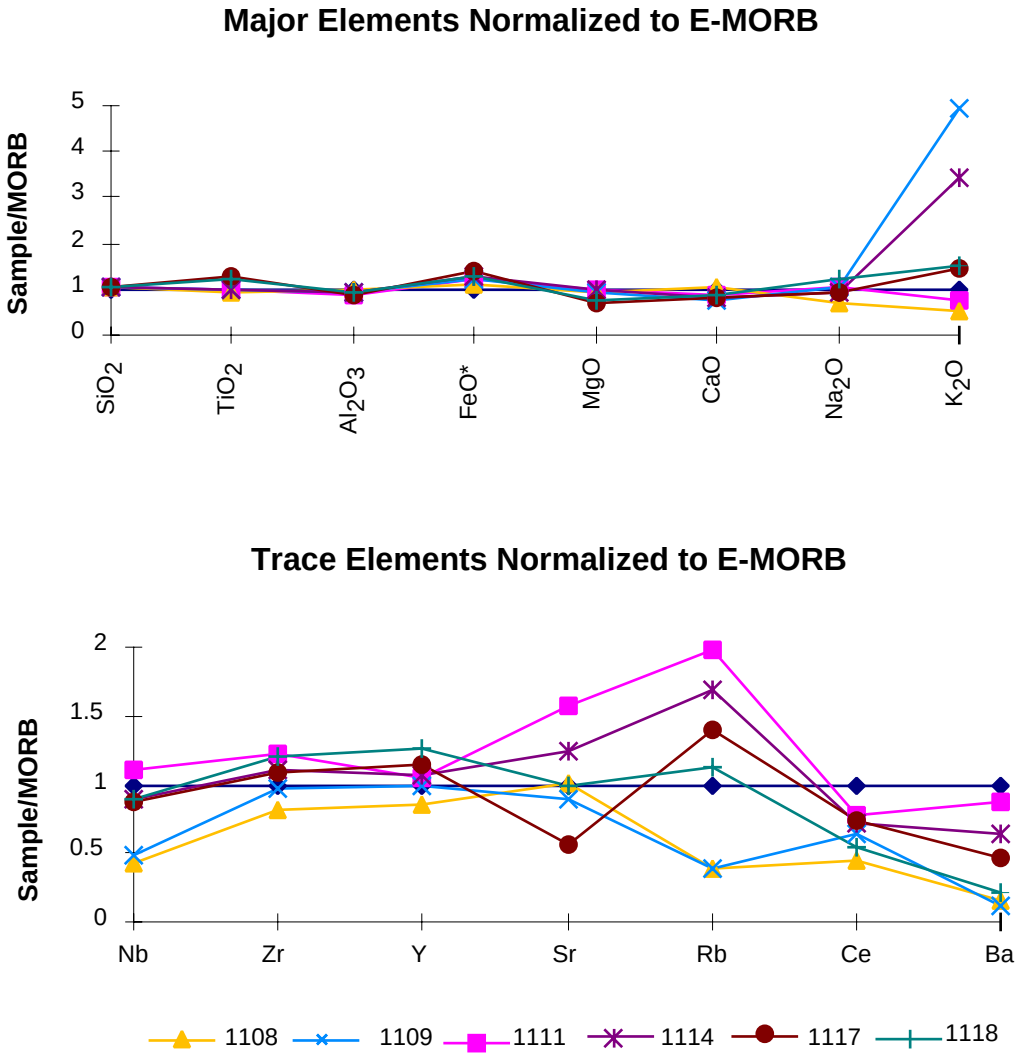
Major Elements Normalized to E-MORB
Sample/MORB
5
4
3
2
1
0
SiO2
TiO2
Al2O3
FeO*
MgO
CaO
Na2O
K2O
Trace Elements Normalized to E-MORB
Sample/MORB
2
1.5
1
0.5
0
Nb
Zr
Y
Sr
Rb
Ce
Ba
1108
1109
1111
1114
1117
1118

Figure 26

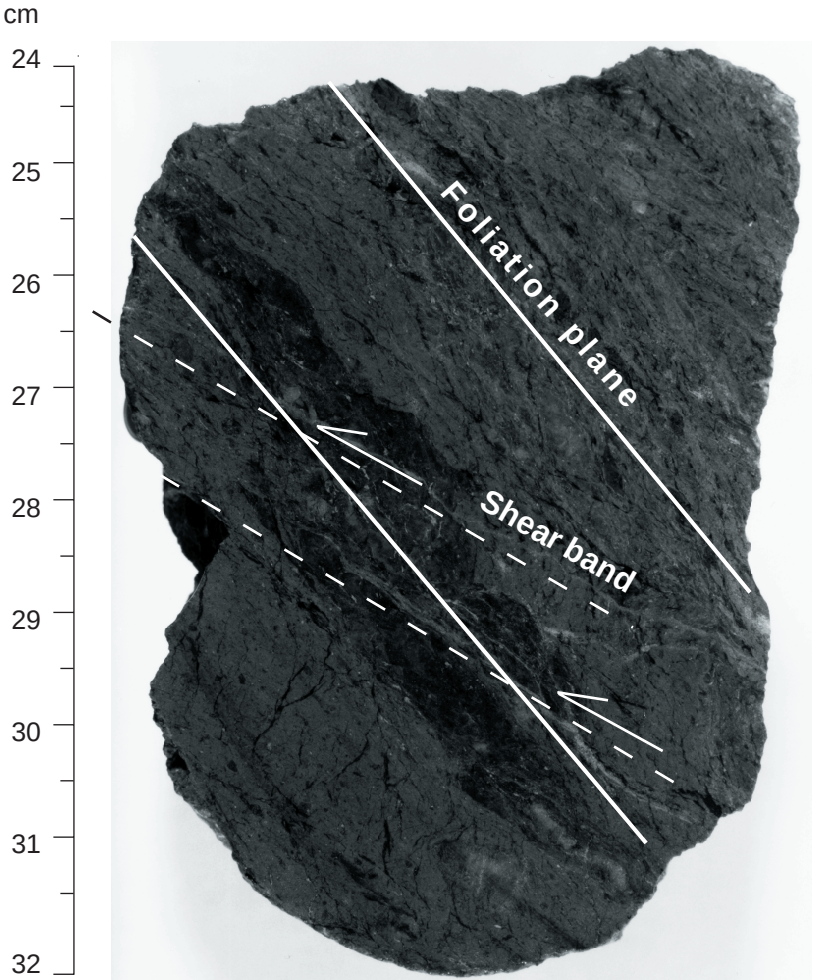

Figure 27

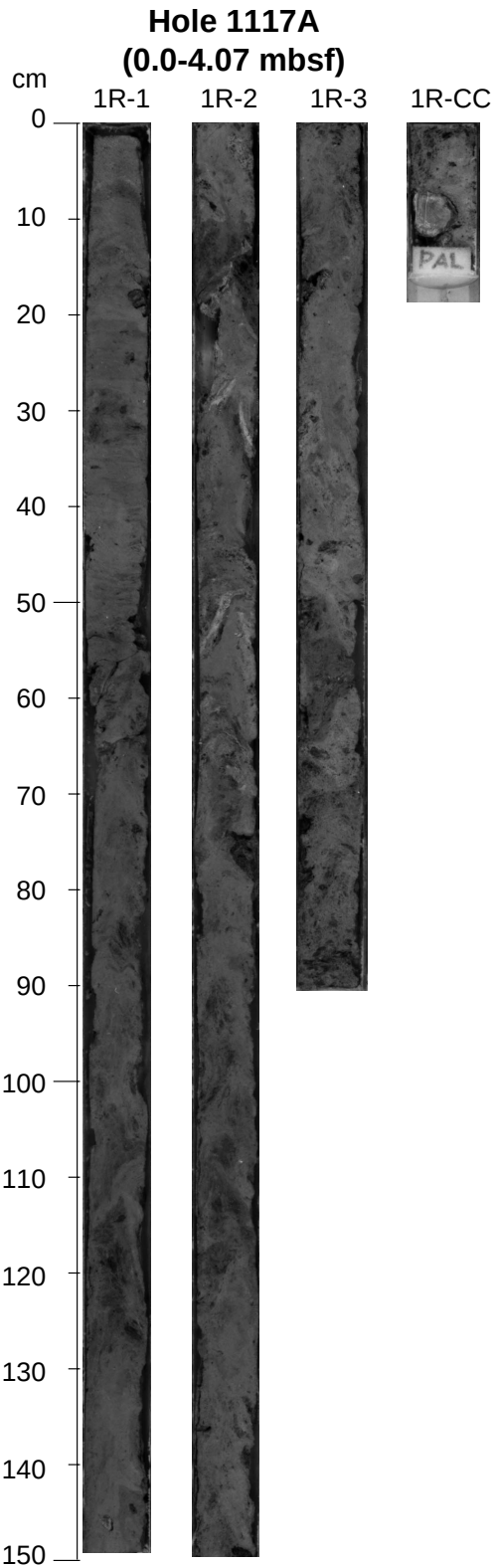
Hole 1117A
(0.0-4.07 mbsf)
cm
1R-1
1R-2
1R-3
1R-CC
0
10
20
30
40
50
60
70
80
90
100
110
120
130
140
150
PAL

Figure 28

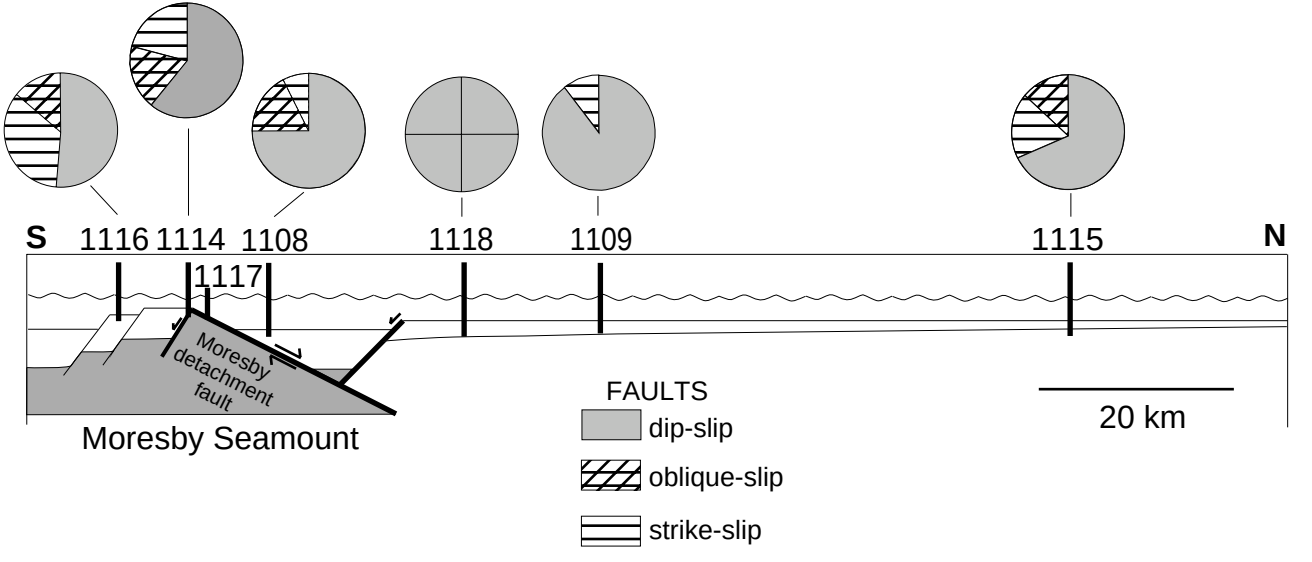
S
1116
1114
1108
1118
1109
1115
N
1117
Moresby detachment fault
Moresby Seamount
FAULTS
dip-slip
oblique-slip
strike-slip
20 km

Figure 29

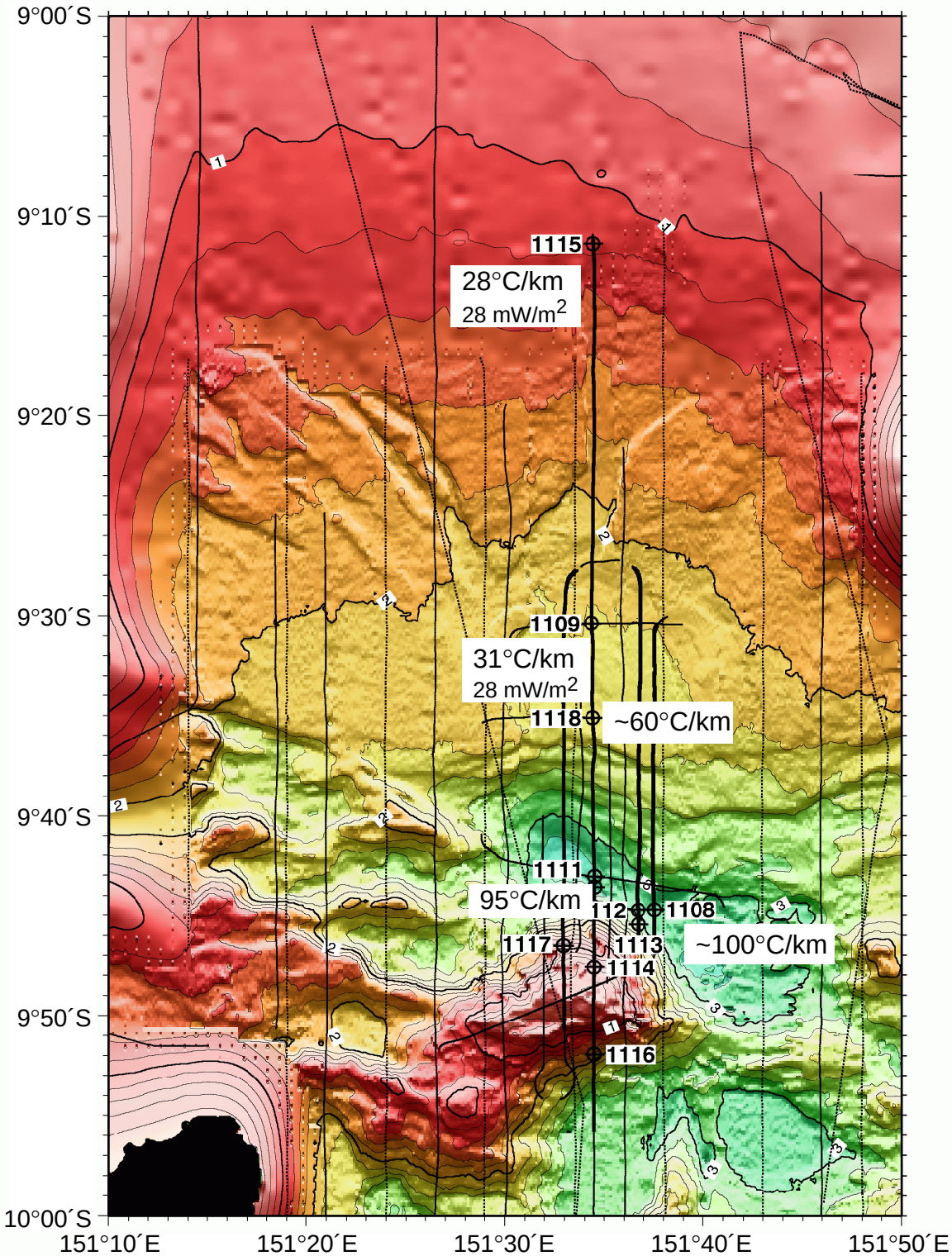
9°00´S
9°10´S
9°20´S
9°30´S
9°40´S
9°50´S
10°00´S
151°10´E
151°20´E
151°30´E
151°40´E
151°50´E
1115
28°C/km
28 mW/m2
1109
31°C/km
28 mW/m2
1118
~60°C/km
1111
95°C/km
112
1108
1117
1113
1114
~100°C/km
1116

Figure 30

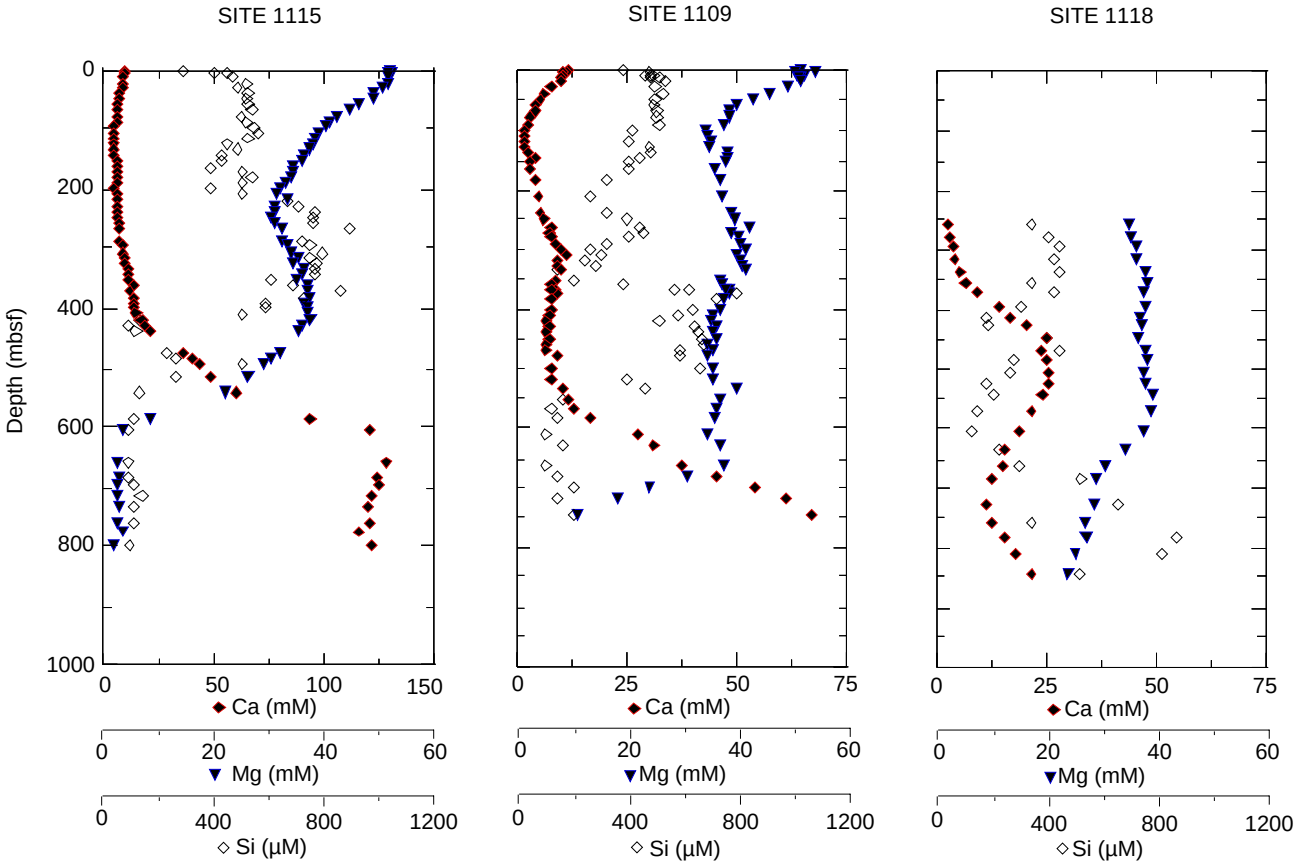
SITE 1115
SITE 1109
SITE 1118
Depth (mbsf)
0
200
400
600
800
1000
0
50
100
150
Ca (mM)
0
20
40
60
Mg (mM)
0
400
800
1200
Si (µM)
0
25
50
75
Ca (mM)
0
20
40
60
Mg (mM)
0
400
800
1200
Si (µM)
0
25
50
75
Ca (mM)
0
20
40
60
Mg (mM)
0
400
800
1200
Si (µM)

Figure 31

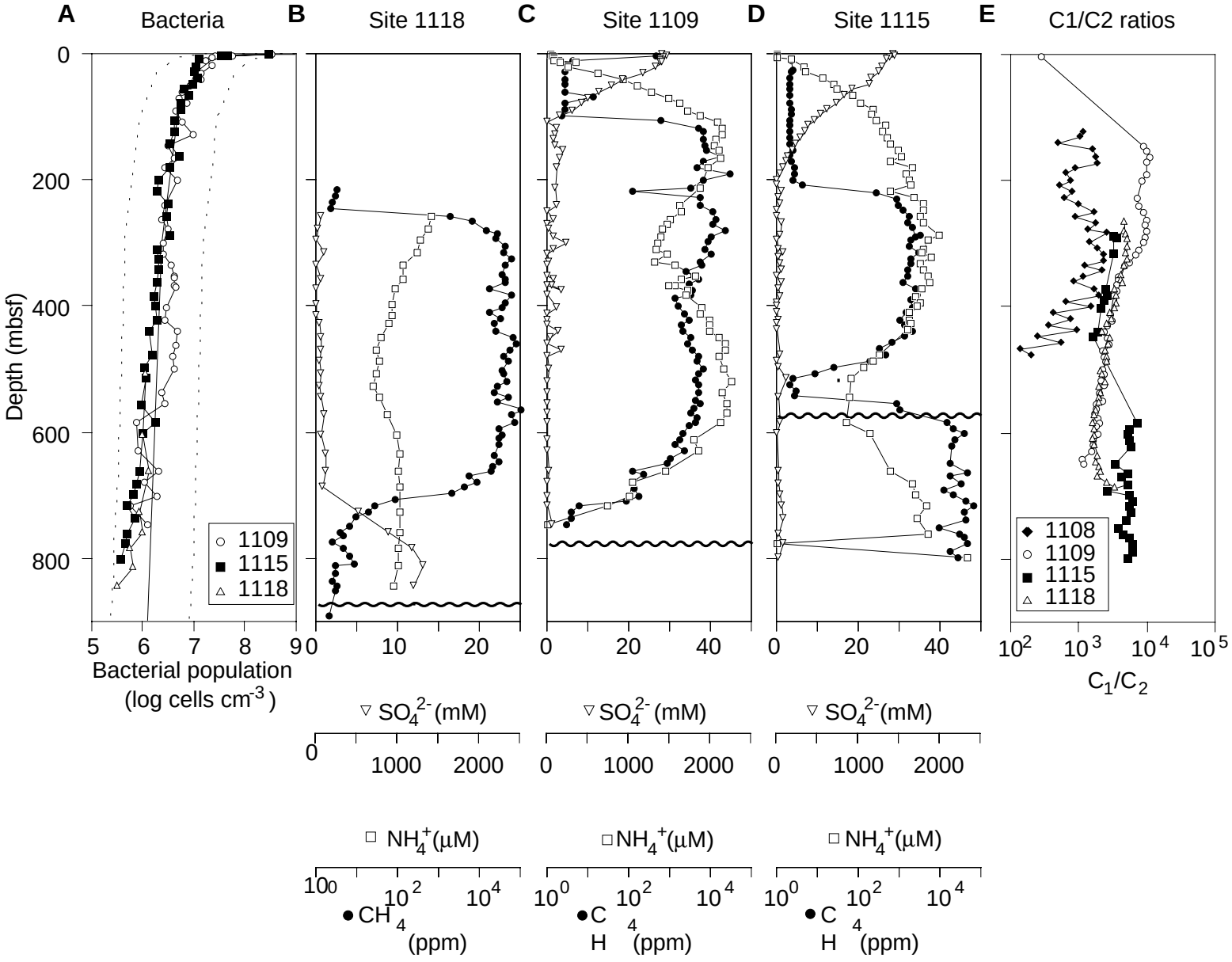
A
Bacteria
B
Site 1118
C
Site 1109
D
Site 1115
E
C1/C2 ratios
Depth (mbsf)
0
200
400
600
800
1109
1115
1118
5
6
7
8
9
Bacterial population
(log cells cm-3)
0
10
20
0
20
40
0
20
40
1108
1109
1115
1118
10^2
10^3
10^4
10^5
C1/C2
SO4 2- (mM)
0
1000
2000
NH4+(µM)
10^0
10^2
10^4
CH4 (ppm)

Figure 32

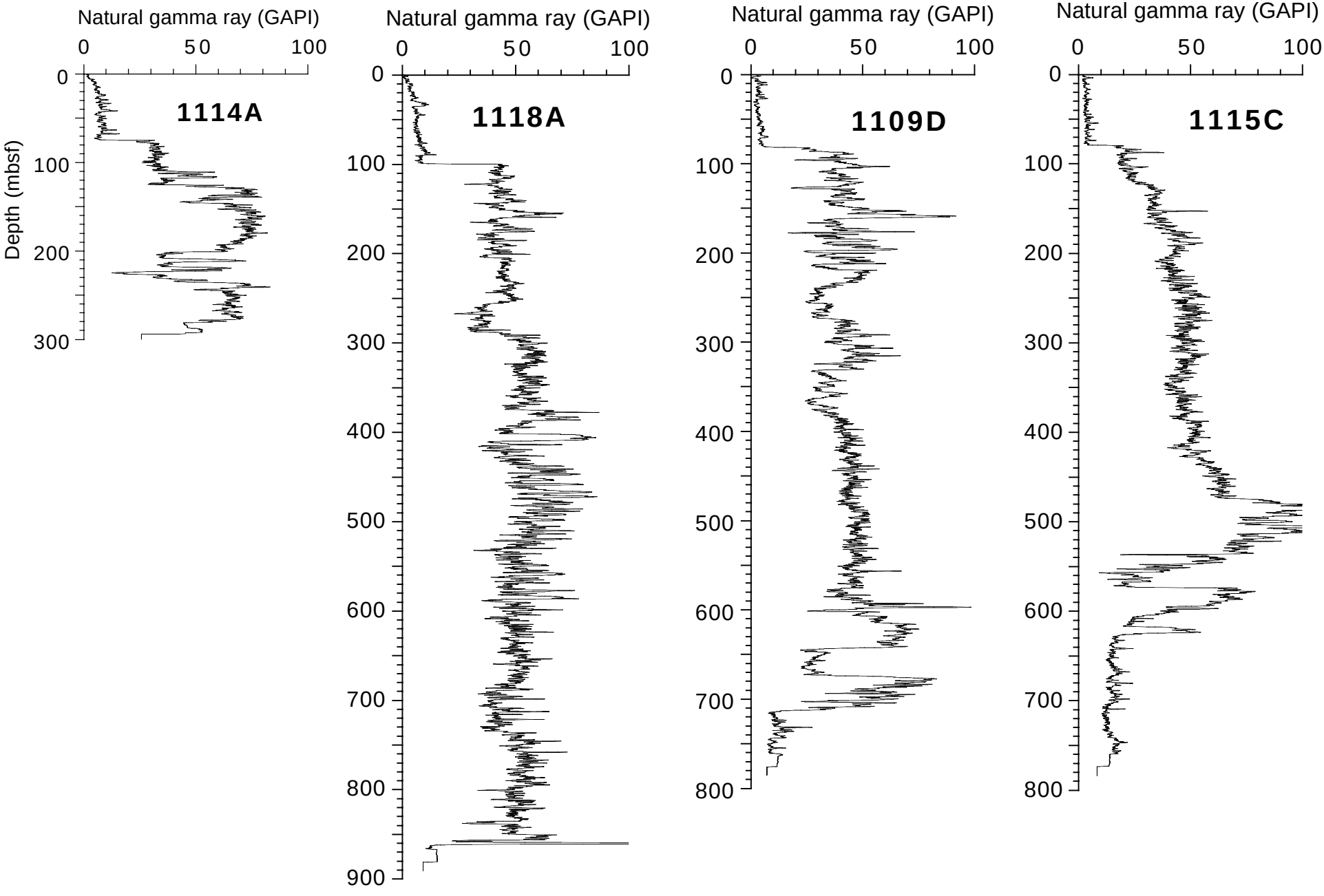
Natural gamma ray (GAPI)
0
50
100
Depth (mbsf)
1114A
1118A
1109D
1115C

Figure 33

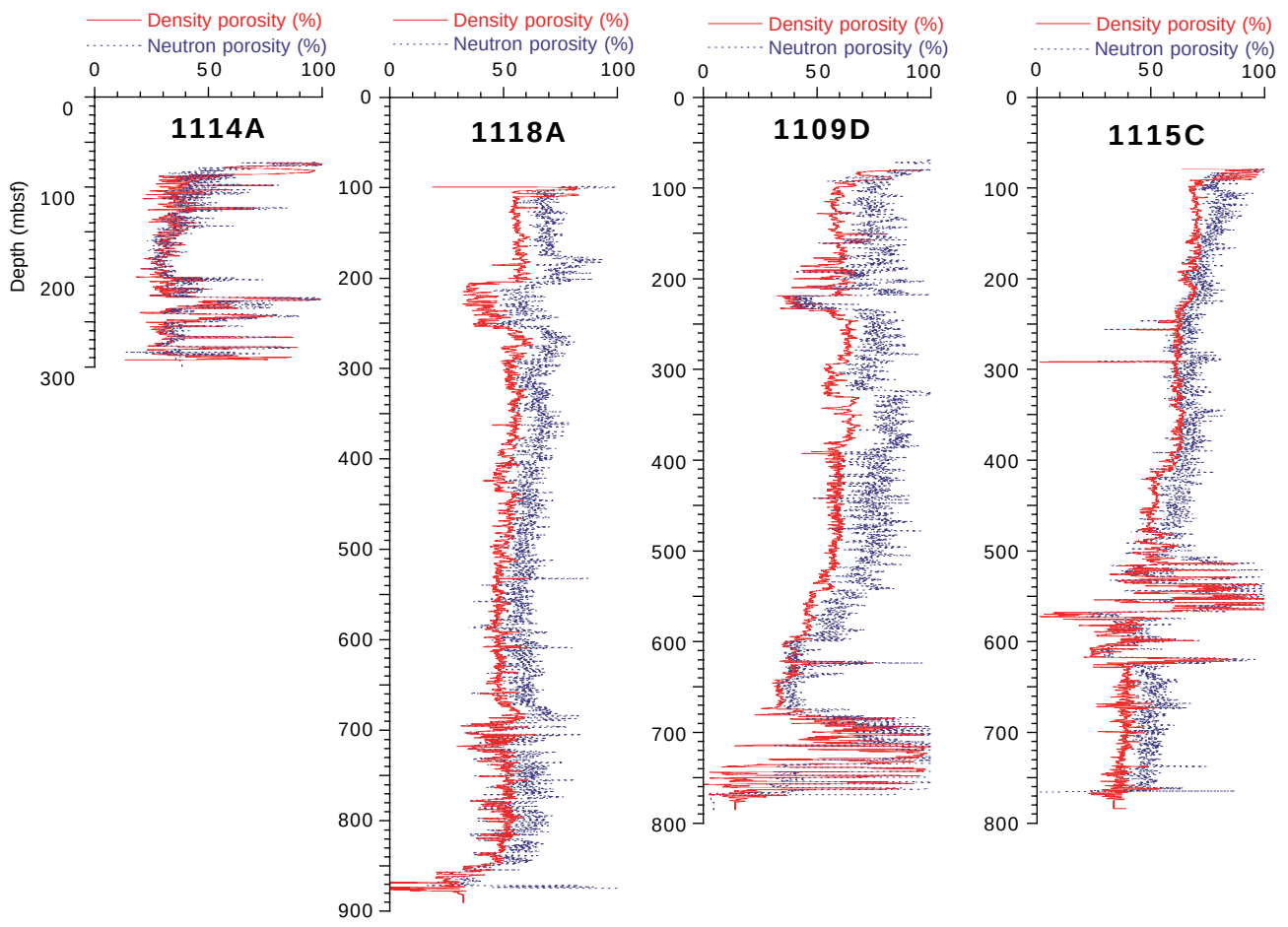
Density porosity (%)
Neutron porosity (%)
0
50
100
1114A
1118A
1109D
1115C
Depth (mbsf)
0
100
200
300
400
500
600
700
800
900

Figure 34

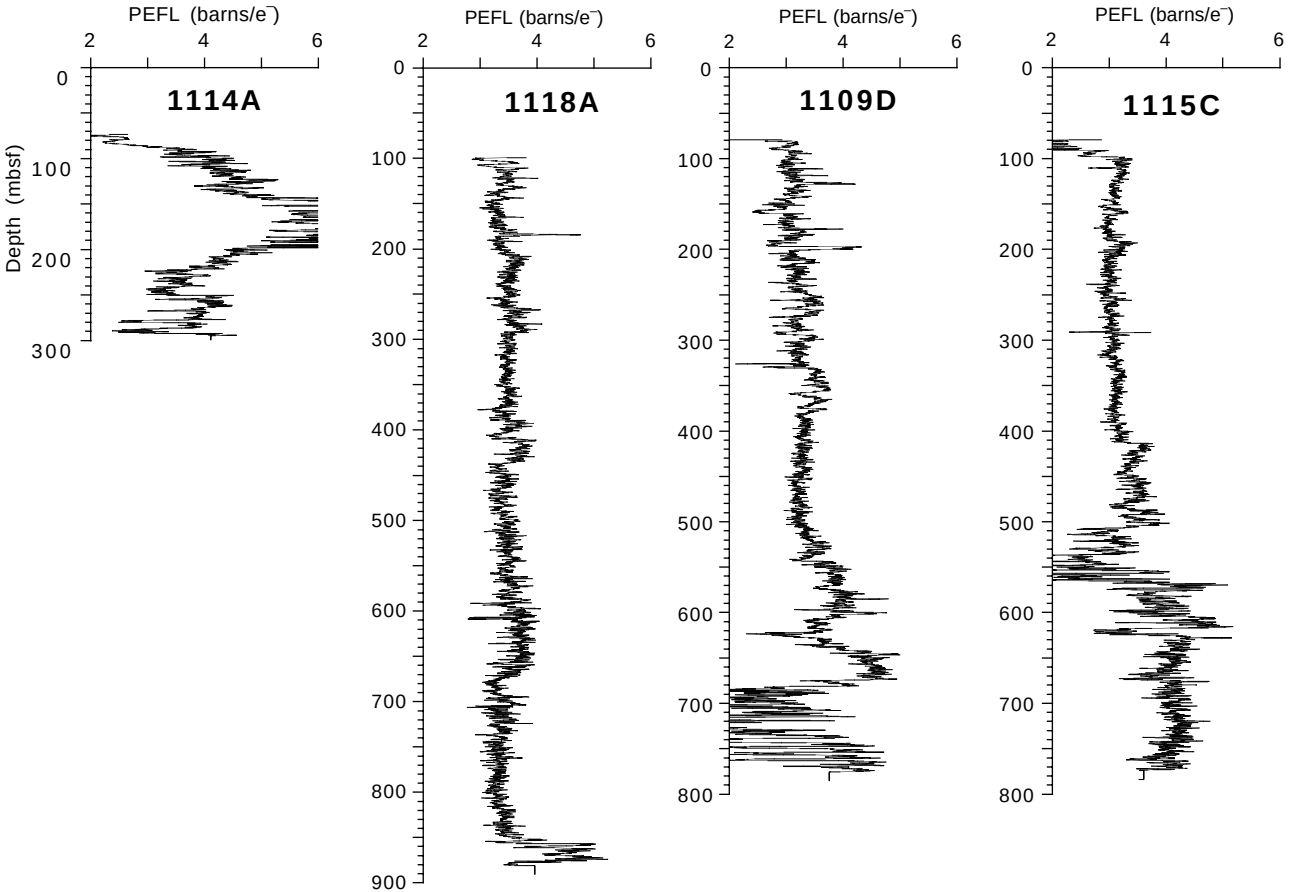
PEFL (barns/e⁻)
2
4
6
Depth (mbsf)
0
100
200
300
1114A
1118A
400
500
600
700
800
900
1109D
1115C

Figure 35

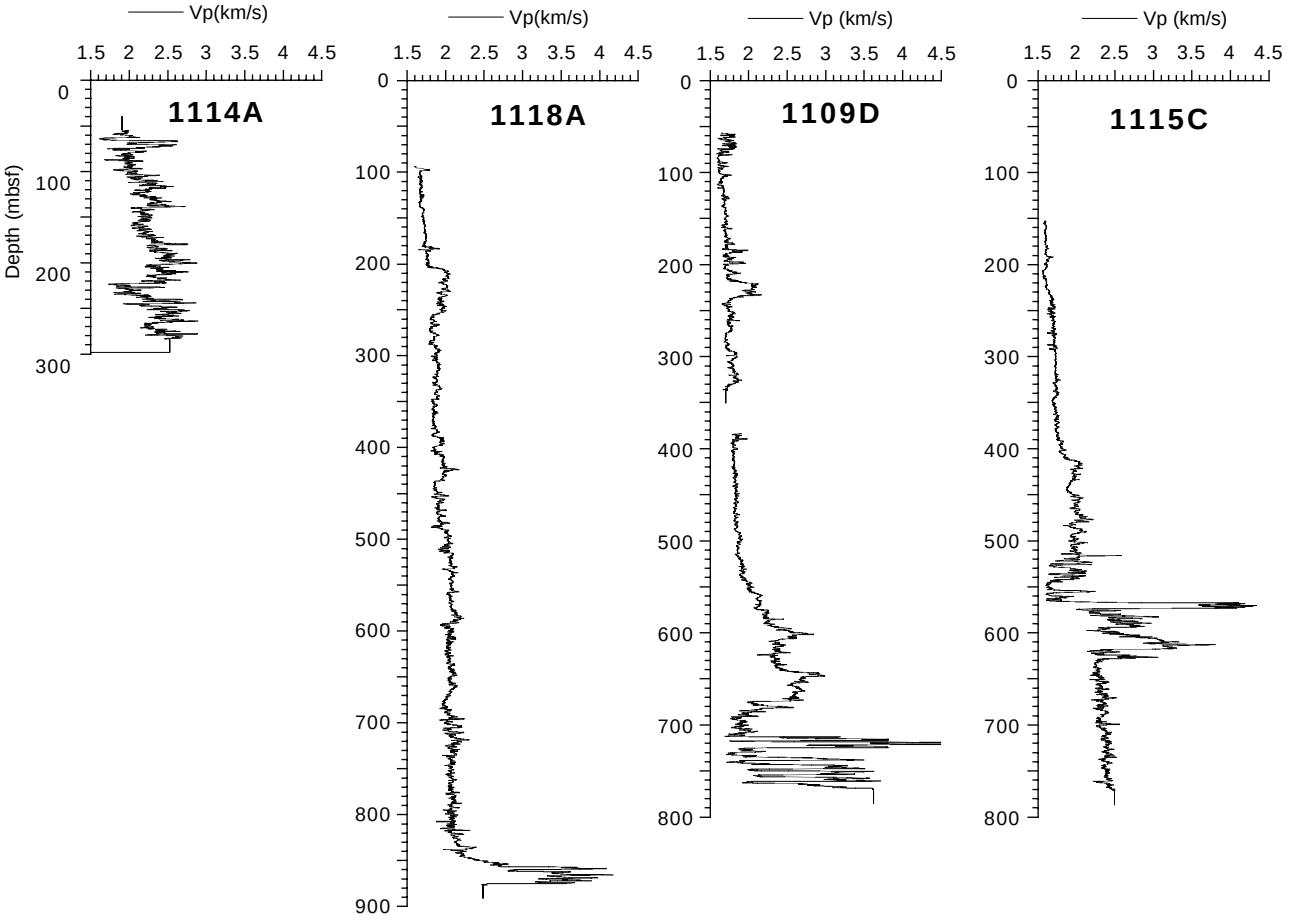
Vp(km/s)
1.5 2 2.5 3 3.5 4 4.5
1114A
Depth (mbsf)
0 100 200 300
Vp(km/s)
1.5 2 2.5 3 3.5 4 4.5
1118A
0 100 200 300 400 500 600 700 800 900
Vp (km/s)
1.5 2 2.5 3 3.5 4 4.5
1109D
0 100 200 300 400 500 600 700 800
Vp (km/s)
1.5 2 2.5 3 3.5 4 4.5
1115C
0 100 200 300 400 500 600 700 800

Figure 36

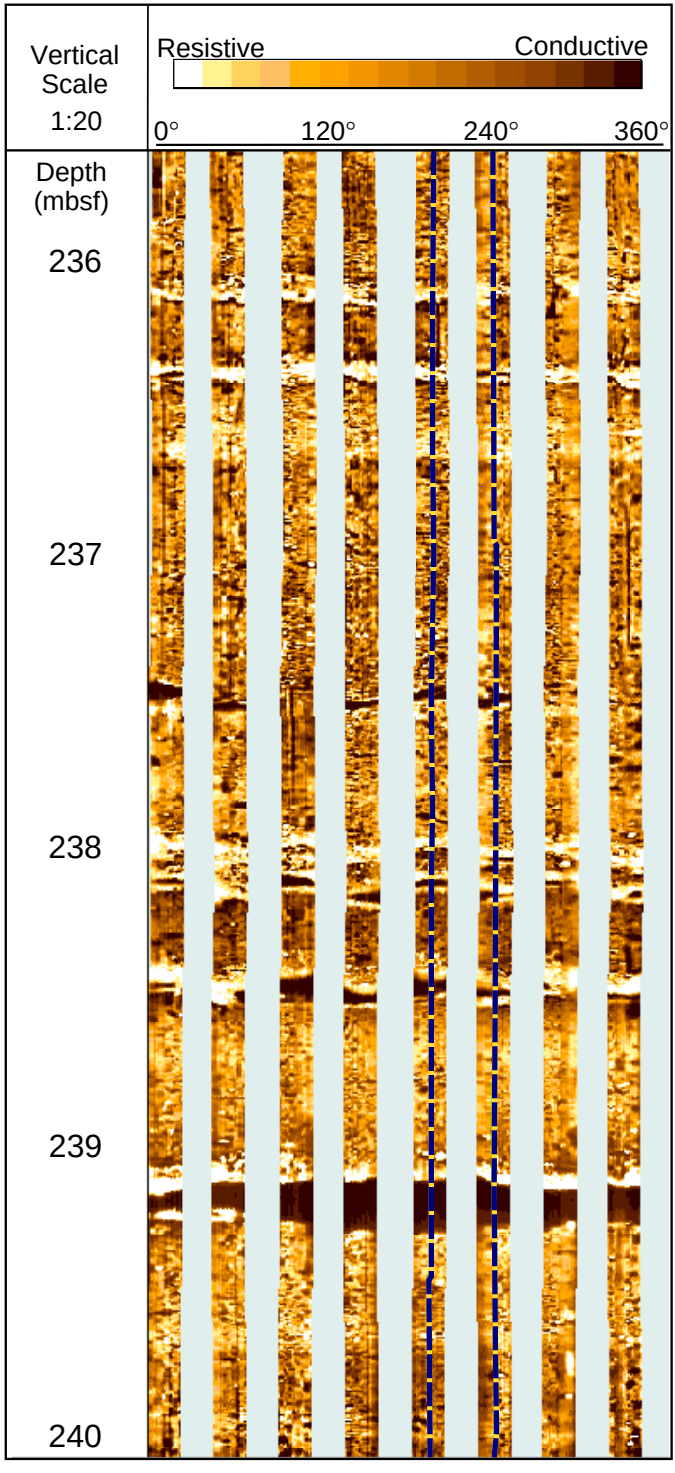
Vertical Scale 1:20
Resistive
Conductive
0°
120°
240°
360°
Depth (mbsf)
236
237
238
239
240

Figure 37

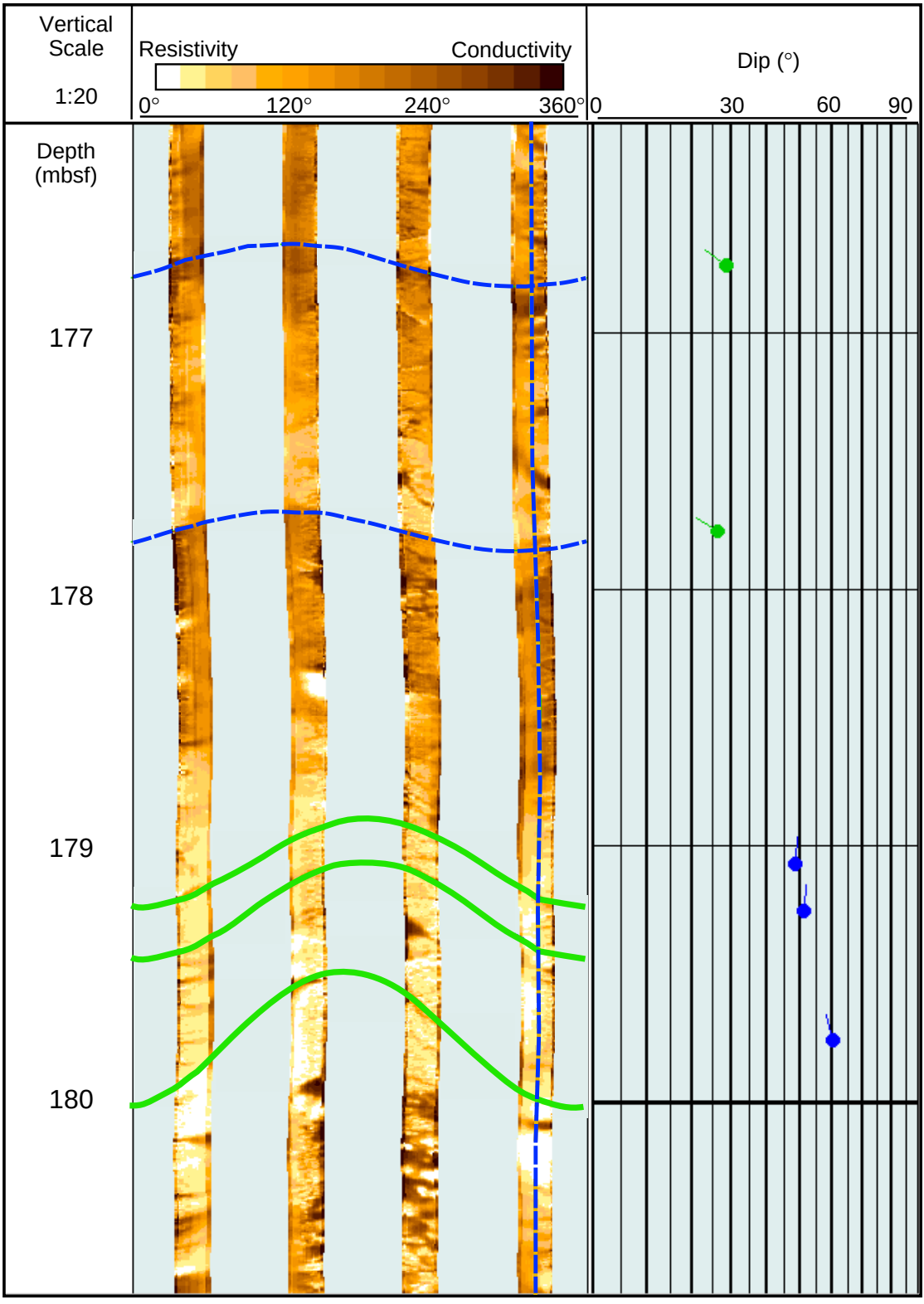
Vertical Scale
1:20
Resistivity
Conductivity
0°
120°
240°
360°
Dip (°)
0
30
60
90
Depth (mbsf)
177
178
179
180

Figure 38

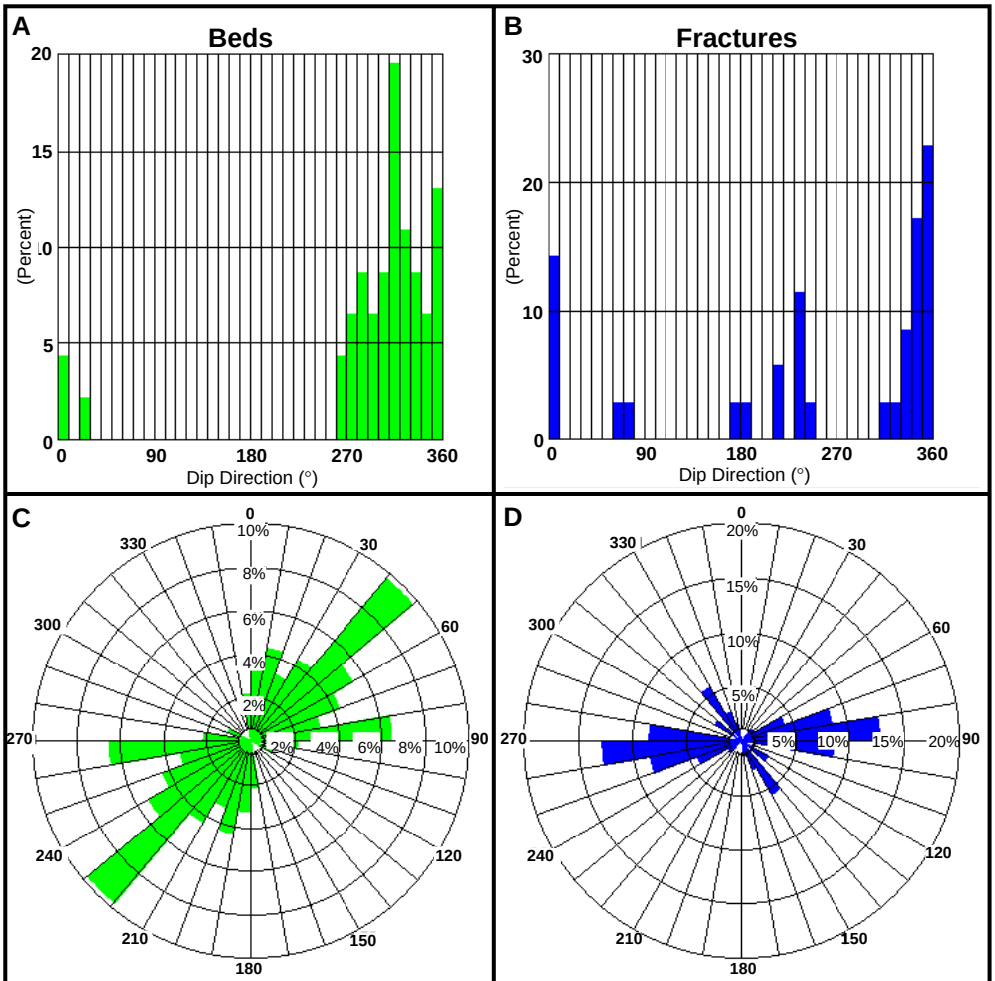
A
Beds
(Percent)
Dip Direction (°)
B
Fractures
(Percent)
Dip Direction (°)
C
D

Figure 39

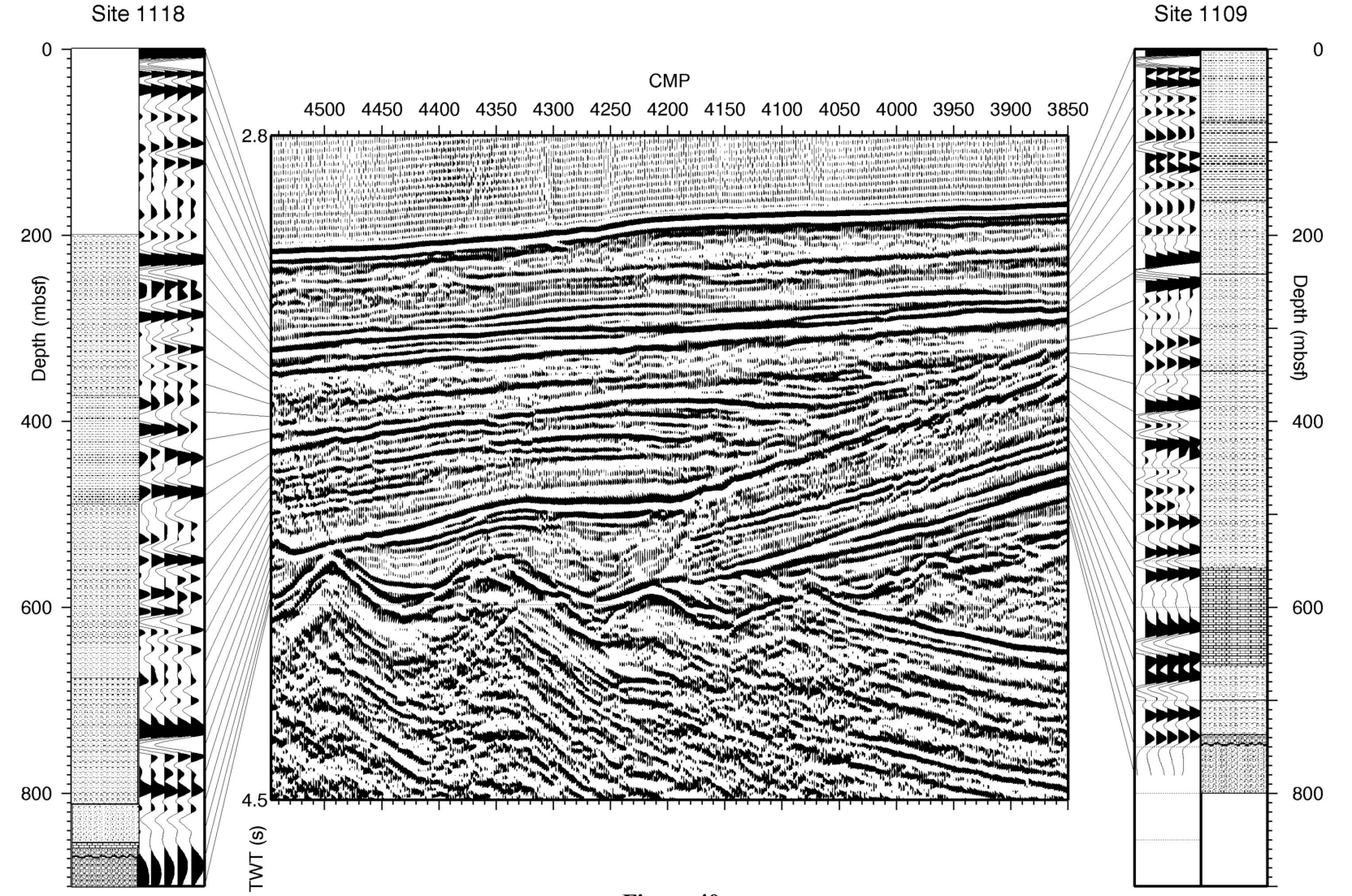
Site 1118
Site 1109
CMP
4500 4450 4400 4350 4300 4250 4200 4150 4100 4050 4000 3950 3900 3850
2.8
4.5
TWT (s)
Depth (mbsf)
0
200
400
600
800

Figure 40

OPERATIONS SYNOPSIS

The operations and engineering personnel aboard the *JOIDES Resolution* for Leg 180 were:

Operations Manager	Michael A. Storms
Operations Engineer	Derryl Schroeder

SUMMARY OF LEG 180 ENGINEERING AND DRILLING OPERATIONS

Port Call: Darwin, Australia

Leg 180 officially began with the first line ashore in Darwin, Australia, at 1630 hr on 7 June 1998. All times reported in the Leg 180 operations reports in this volume are local time (UTC + 10 hr). As soon as the ship was cleared through customs and immigration, the process of on- and offloading immediately began. Normal tasks of on/off loading surface and air freight took place. Among the major items off loaded were 22 boxes of core, twelve 9 1/2-in drill collars, twelve 6 3/4- in drill collars, SDS hammer drill hardware, 16 joints of 13 3/8-in flush joint casing, and a hard rock base with gimbal and 20-in casing hanger. Major items loaded included twenty 8 1/4-in drill collars, 41 joints of 16-in buttress casing, 8 joints of 20-in buttress casing. Bulk products included 30 metric tons of sepiolite drilling mud, 15 metric tons of bentonite gel mud, and 1250 sacks of blended cement all taken aboard via pneumatic trucks. In addition, 130 sacks of Kwikseal and 40 sacks calcium carbonate lost-circulation material were put aboard, along with an assortment of chemicals required for optimizing the cement program at proposed site ACE- 8A. Among other activities, Ocean Drilling, Ltd. (ODL) loaded the new anchor windlass motor and had the port side forward (No. 2) life raft refurbished during the port call. The ship took on 1034 metric tons of marine diesel fuel (low sulfur gas oil) and we topped off the drill water tanks.

Drilling Services Department personnel attended the port call to install a new shipboard inventory system as well as to meet with potential contractors reviewing the existing “passive” heave compensator system in preparation for bidding on conversion to an “active” system. Off-going Science Services Department personnel remained in port to train new physical properties and paleomagnetics laboratory marine specialists and to provide introductory training to scientists and technical staff for the new split-core multisensor track that was installed during Leg 179. Tours of the ship were given to ~100 geologists and students on the third day of the port call.

TRANSIT DARWIN TO SITE 1108 (ACE-8A)

At 0715 hr on 11 June the last line was released and we departed Darwin 2 days earlier than planned for our first drill location, Site 1108 (ACE-8A). The transit was uneventful and we made excellent time (averaging 11.5 nmi/hr) in calm seas. Because we would be operating in Papua New Guinea (PNG) waters, we were required to clear PNG customs and immigration before drilling operations could begin. A helicopter rendezvous with the ship was scheduled to minimize the time necessary to complete the requirement. We had to arrive at the rendezvous location early on the morning of 16 June, but our transit speeds were better than expected; therefore, on 15 June we reduced speed for several hours. We used this time to pick up and space out drill collars—an operation that would have had to take place once we arrived at our first site.

The first helicopter landed on the ship at 16 June 1998 south of Alotau at 10°55.0´S, 150°20.0´E. Passengers on this flight included a PNG customs agent, a PNG quarantine official, a representative from ODP's agent in PNG, and the ODP logistics coordinator. After the helicopter landed we immediately resumed full speed for the second rendezvous location ~20 nmi to the east. The helicopter departed from the ship at 0655 hr for Alotau to pick up the second PNG observer who was due to arrive about 0800 hr. Following the formalities of clearing the ship into PNG waters, the PNG officials were given a tour of the ship's laboratory facilities. The helicopter returned for the second rendezvous (11°10.0´S, 150°50.0´E) at ~1000 hr that same morning. This time the pilot did not shut down his engines. After the second PNG observer (Paul Kia, Geological Survey of PNG) disembarked, the PNG customs/quarantine officials and ODP's PNG agent boarded the helicopter and departed for PNG. As soon as the helicopter lifted off, we resumed full speed for Site 1108 (ACE-8A).

We left the Coral Sea and turned north entering the Solomon Sea via the Jomard Passage, picking up a favorable current along the way, which boosted our speed, temporarily at least, to nearly 14 nmi/hr. Overall, our transit speeds averaged 11.5 nmi/hr in calm seas. After arriving at the Global Positioning System (GPS) positions for Site 1108, we lowered the thrusters/hydrophones and switched into dynamic positioning (DP) mode. After stabilizing on the GPS position, we deployed a Datasonic commandable positioning beacon at 0115 hr.

SITE 1108

Hole 1108A

Hole 1108A was devoted strictly to obtaining information on the seafloor sediments for a reentry cone deployment planned for later in the leg. We fit together a bottom-hole assembly (BHA) with an 18 1/2-in tricone drill bit attached to the bottom stand of 8 1/4-in drill collars and lowered it to the seafloor. The subsea TV camera was deployed during the pipe trip, and while observing the seafloor, we spudded Hole 1108A at 0815 hr on 17 June.

The 3.5-kHz depth recorder indicated a seafloor depth of 3157.4 mbsl. We observed the drill bit tag the seafloor at 3162.7 mbsl. For the next hour and 40 min, we conducted a jet-in test into the moderately hard seafloor, eventually reaching a depth of 16.3 mbsf. The test was suspended at that point because little progress was being made at flow rates of up to 110 strokes per minute (spm). The drilling assembly was pulled clear of the seafloor at 1000 hr, the subsea television camera was recovered, and the hole officially ended at 1530 hr when the bit cleared the rig floor.

Hole 1108B

We had originally planned Hole 1108B as an advanced hydraulic piston corer/extended core barrel (APC/XCB) hole to ~600 mbsf. Since the jet-in test results indicated that APC coring was not possible and that XCB coring was unlikely to progress very far, we decided to start RCB coring. After putting together an rotary core barrel (RCB) drilling assembly (including a single stand of drill collars above a set of mechanical drilling jars), we lowered the drill string to the seafloor. During the pipe trip the ship was offset 50 m to the southeast on a bearing of 120°.

Upon reaching the 3162.7 mbsl seafloor depth of the previous hole, the driller had not recognized any indication of bottom (reduction of total drill string weight). Even after advancing another single joint of pipe to a depth of 3172.0 mbsl, no weight loss was observed. We checked the driller's pipe tally that was verified as correct and recovered the core barrel, which was empty. After adding another joint of drill pipe, the seafloor indication was tagged at a depth of 3177.3 m or 14.6 m, deeper than at the Hole 1108A jet-in test location.

Hole 1108B was officially spudded at 0100 hr on 18 June 1998 and continuous RCB coring began using very little weight on bit (WOB) and slow revolutions per minute (RPM). We were forced to proceed cautiously because of the lack of stabilization for the bottom-hole assembly (BHA) (it was still above the seafloor) and the hard surface sediments. The upper 50 m of the borehole was characterized by erratic torque, overpull and drag, poor recovery, and low rates of penetration (ROP). Typically 1–2 m of sediment filled the bottom of the borehole between connections. Liberal amounts of drilling mud (sepiolite) were used, and the hole condition gradually improved with depth. Because of the relatively unstable hole conditions and layers of semi-indurated sediments, we were unable to make temperature measurements in the formation.

At 91.3 mbsf (after Core 10R) we decided to make a wiper trip. The drilling in the last two cores had indicated that the formation was getting more lithified and appeared to be more stable. Drilling parameters became more consistent and core recovery continued to improve. The partial wiper trip was strictly precautionary because the drilling jars and last stand of drill collars were about to go below the mudline. We raised the drill string to a depth of 42.7 mbsf. At 47.7 mbsf the driller noted 70,000 lb overpull and was unable to rotate the drill string. After working the pipe for a few minutes, it became unstuck and a sepiolite pill was circulated. This portion of the hole was reamed several times until there was no longer any indication of drag or overpull. We then proceeded with running the pipe to bottom, where we encountered 3 m of fill. Another sepiolite pill was circulated while drilling out the fill. All drilling conditions were normal and the hole appeared to be in excellent condition at that point. When the bit was back on the bottom, a portion of the hole again apparently collapsed, trapping the pipe. The pipe was worked free and another sepiolite pill was circulated. Coring resumed some 2.75 hr later once the wiper trip was completed and the hole appeared to be stabilized.

The RCB coring continued through Core 41R to a depth of 389.0 mbsf. Higher than normal core barrel pump pressures (250–300 psi vs. normal values of 150 psi) and lower recovery led us to suspect that we may have lost some core in the pipe or that something was partially plugging the bit throat. A core barrel was pumped downhole and then recovered without advancing the drill bit. Upon recovery we found a small rock lodged in the lower core catcher. A bit deplugger with painted latch and landing shoulders (to document that it latched fully down and extended through the bit throat) was deployed. Once recovered, the deplugger indicated proper latching, and pump pressures returned to normal. The RCB coring progressed to 485.2 mbsf; however, core recovery and ROP deteriorated with depth possibly because of an increase in the degree of fractures in the formation. Toward the bottom of the hole, hydrocarbon headspace C_1/C_2 were decreasing and higher hydrocarbons such as *n*-C_5 (pentane) started to appear. We wondered what impact this trend might have regarding our plan to advance a reentry hole down to a projected depth of 1150 mbsf.

At 1630 hr on 22 June, the hole collapsed just after starting to cut Core 52R. The top drive continually stalled out and the pipe was pulled free with 30,000 lb of overpull. At that point, the annulus plugged off, preventing circulation. We pulled the pipe free again. This time with 110,000 lb overpull. Attempts to actuate the mechanical drilling jars were not successful, leading us to believe that the material holding the pipe had fallen in from above. The drilling assembly was literally dragged up the hole to a 253.7 mbsf using 20,000 to 60,000 lb overpull. At this depth we were able to resume circulation and torque/pump pressure returned to normal. We continued pulling the pipe to 114.7 mbsf without overpull. After recovering the core barrel (which had not been advanced before the pipe became stuck), we washed and drilled back to the bottom of the hole but could not pass 436.7 mbsf, which was 48.5 m above the bottom of the hole. At that point the hole packed off again, cutting off circulation and preventing top-drive rotation. The pipe was pulled back to 416.7 mbsf before we regained the ability to pump fluids and rotate the drill string. For the next

several hours, the pipe was cycled up and down in an unsuccessful attempt to get back to the original depth of the hole. Eventually, we decided that further coring in this hole was not possible. The pipe was placed at 379.0 mbsf and an Adara heat-flow shoe was deployed on a core barrel through the pipe to obtain a temperature gradient in the borehole. We knew that the data would not reflect accurate formation temperature but considered the data to be insurance in case the temperature-logging tool (TLT), which was to be run during the first wireline logging run, might not be able to be deployed very far into the hole. Temperatures were measured for 10 min each at 0, 388, 300, 200, and 100 mbsf with the circulating pumps shut off. Results of the Adara temperature profile, inside the drill pipe, indicated a linear temperature gradient of ~35.4°C/km. We later determined this to be significantly lower than the actual gradient.

Once the Adara temperature measurements were completed we made two wireline runs to activate the mechanical bit release (MBR) to drop the bit in the hole in preparation for logging. The hole was displaced with 150 bbl of sepiolite mud, and we pulled the drill string to a depth of 99.7 mbsf. During the pipe trip, the driller encountered overpulls of 20,000–40,000 lb to a depth of 225.7 mbsf.

After rigging up for logging, the triple combo was assembled and run in the hole. Unfortunately, the logging tools were only able to reach 62 m below the end of the pipe into the open hole. This section of hole was logged twice, and the remaining logging program for the hole was abandoned. Analysis of the temperature data, gathered with the TLT on the bottom of the triple combo and the Adara tool, yielded a temperature gradient of ~100°C/km. To displace the hole with weighted mud before abandoning this site, we attempted to lower the pipe further into the hole, but it could not be lowered more than 0.5 m before encountering an obstruction. After the hole was filled with 31 bbl of 10.5 pounds per gallon (ppg) bentonite gel mud, the pipe was pulled clear of the seafloor at 0415 hr on 23 June. Hole 1108B ended when the bit cleared the rig floor at 0900 hr. The acoustic positioning beacon was left on the seafloor in an active mode because we were planning to return to this site after drilling Site 1109.

A total of 51 cores were recovered from 485.2 m of section with a recovery of 148.6 m (30%). The average ROP was 12.3 m/hr.

TRANSIT TO SITE 1109 (ACE-9A)

An APC/XCB coring assembly was put together during the transit to Site 1109 in DP mode. The ship speed was ~4 nmi/hr for the 1.5 hr when the pipe was out of the water. At 1130 hr on 24 June we reduced speed to <1 nmi/hr and began lowering the drill pipe to the seafloor. A beacon was deployed at the GPS coordinates of Site 1109 (proposed site ACE-9A) at 1315 hr on 24 June 1998.

SITE 1109

Hole 1109A

The 3.5-kHz depth recorder indicated a seafloor depth of 2214 mbsl. Hole 1109A was spudded with the APC at 1630 hr on 24 June with the bit at 2210.9 mbsl. The core was virtually full, making an exact seafloor depth difficult to determine. However, there was no evidence of mud on the piston head and brown sediment inferred to be seafloor material was evident at the top; therefore, the seafloor was defined to be at 2210.9 mbsl. Recovery was 9.96 m, or 104.8%. To ensure we obtained the uppermost seafloor sediments, we decided to spud another hole.

Hole 1109B

Without offsetting the ship, we spudded Hole 1109B at 1715 hr with the bit at 2206.9 mbsl. Core 1H recovered 5.28 m; therefore, the seafloor was calculated to be at 2211.1 mbsl. This confirmed that Hole 1109A had indeed recovered nearly the entire mudline. We took a second APC core, which extended down to 14.8 mbsf. Total recovery was 15.14 m (102.3%). The cores were primarily intended to provide whole round samples for high-resolution microbiological and interstitial water (IW) chemistry studies. Hole 1109B ended when the bit was pulled clear of the seafloor at 1830 hr on 24 June.

Hole 1109C

Again without offset, we spudded Hole 1109C at 1900 hr. Core 1H was taken with the bit at 2208.9 mbsl and recovered 7.37 m, indicating a seafloor depth of 2211.0 mbsl. The APC coring continued through Core 11H (102.4 mbsf), which required 60,000 lb of overpull to get the barrel out of the formation. The APC core recovery was 107.55 m (105.0%). Cores 3H–11H were oriented with the tensor tool, and Adara temperature measurements were taken while obtaining Cores 3H, 5H, 7H, 9H, and 11H.

We began XCB coring with Core 12X, using soft formation cutting shoes through Core 37X at 346.6 mbsf. A single DVTP measurement was taken after Core 18X (169.7 mbsf). The probe tip was recovered with a very slight bend in it.

While removing the cutting shoe from Core 36X on the rig floor, the threaded connection of the shoe fractured. We suspected that the failure was caused by overheating during drilling and

subsequent quenching in seawater. This prompted us to switch to hard formation cutting shoes beginning with Core 38X because the Core 37X barrel had already been deployed. We wanted to continue XCB coring before switching to RCB because of the excellent XCB core recovery (99.3% for the day). A second cutting shoe failure occurred while cutting Core 40X, and it was returned to the rig floor without the lower part of the cutting shoe. We then attempted to advance a half core to see if we could push the junk to the side of the hole, but this attempt was not successful. Erratic torque and an abraded core cutting shoe indicated that we were pushing the broken parts of the cutting shoe tip downhole, and coring operations ceased at 375.7 mbsf. Pieces of the broken cutting shoe were recovered in Core 41X once it was split. The bit was pulled clear of the seafloor at 0430 hr on 27 June, and the hole officially ended at 0800 hr when the bit cleared the rig floor. Combined APC/XCB recovery for the hole was 234.32 m (82.2%).

Hole 1109D

We then converted to an RCB coring assembly, including a 9 7/8-in bit, a mechanical bit release, and an additional stand of drill collars. After lowering the pipe to the seafloor, we spudded Hole 1109D at 1245 hr on 27 June. Seafloor was established as 2211.1 mbsl, and we drilled without coring (using an RCB center bit) to a depth of 352.8 mbsf. The drilling took 12.25 hr at an average ROP of 28.8 m/hr. We then swept the hole clean with sepiolite mud, recovered the center bit, and at 0145 hr on 28 June we started RCB coring at 352.8 mbsf. This allowed an overlap of ~23 m with the cores from Hole 1109C. We continued through Core 35R to 676.4 mbsf with few problems. Sepiolite mud pills (30 bbl) were circulated every third core as a precautionary measure, and hole conditions remained good with no fill on connections, relatively constant torque, and no overpull or drag. The formation appeared to be quite variable, which affected core recovery and penetration rates. Coring continued through Core 45R (772.9 mbsf). In this interval we began to experience some fill (2–3 m) between connections. As a result, we increased the 30-bbl mud sweeps to every core. Recovery dropped off from the 54.9% of the day before to 47.3%, and ROP dropped from 12.9 m/hr to 3.9 m/hr while in a conglomerate. No hole stability problems were encountered until after cutting Core 46R (777.6 mbsf). During pulling off bottom, the driller noted high pump pressure and high torque, indicating a portion of the hole had caved in from above. After pulling the pipe back to 762.8 mbsf with 50,000 lb overpull the hole was swept with 30 bbl of sepiolite. High pump pressure was once again noted while retrieving the core barrel and a second 30-bbl sepiolite pill was circulated. After retrieving the core barrel, a bit deplugger was deployed to clear the bit throat. Drilling parameters returned to normal, and coring proceeded through Core 51R in hard and massive diabase to a total depth of 802.0 mbsf. Recovery was exceptional in this portion of the hole (88.9%); however, penetration rates were extremely slow (1.5 to 2.0 m/hr). Although the science party wanted to penetrate below the diabase into the inferred forearc sequence below, coring was terminated because there was no indication that we were approaching the bottom of the diabase.

After sweeping the hole with 40 bbl of sepiolite mud, a short wiper trip was made in the lower (problematic) portion of the hole. The bit was back reamed to 762.8 mbsf with 40,000–50,000 lb overpull before circulation could be established. Upon running the pipe back to the bottom of the hole, the bit encountered fill at 784.8 mbsf, indicating we had lost the lowermost ~17 m of the hole. We decided not to spend the time to clean out the bottom of the hole. Another 30-bbl sepiolite mud sweep was made and two wireline runs were made to release the bit. The hole was displaced with 217 bbl of sepiolite mud and the pipe was pulled up to 98.8 mbsf in preparation for logging.

After rigging up for logging, the triple combo with the TLT was assembled and lowered down the pipe. This tool suite was able to pass several tight spots between 326.8 and 376.8 mbsf to eventually reach 782.8 mbsf. Excellent logs were recovered over nearly the entire hole up to the bottom of the pipe. However, the caliper data indicated that the tight spots between 326.8 and 376.8 mbsf had narrowed to about the tool diameter of 4 in (10.16 cm). After the triple combo was rigged down, we assembled the Formation MicroScanner (FMS) sonic tool and ran it into the hole. Because of the constrictions, this tool could not be lowered past 349.8 mbsf and we logged up from that point. Once the FMS-sonic tool was out of the hole, the logging sheaves were pulled aside and the drill string (without the bit) was lowered to 377.8 mbsf and a second run of the FMS-sonic tool was made from 775.8 mbsf up to just below the end of the drill pipe.

The final logging run was with the well seismic tool (WST) to obtain a vertical seismic profile (VSP). Because of the light weight of this tool, it had to be lowered very slowly down the pipe. We tried pumping the tool down, but this did not help and actually made the tool appear lighter because of the pump-off effect from the oil saver. Eventually, we were able to work the tool down to 460.3 mbsf (82.5 m below the end of the pipe). The VSP was conducted at nine different depths with 7–12 shots at each level. All of the logging runs obtained quality data.

After the WST was retrieved and we were rigged down from logging, we filled the hole with 80 bbl of heavy mud. The pipe was then raised to 127.8 mbsf, and the hole plugged with cement (15 bbl). The drill pipe was pulled out of the hole, clearing the seafloor at 1945 hr on 3 July. The positioning beacon was recovered at 2130 hr, and the last thruster was raised when the end of the drill string cleared the rig floor at 0015 hr on 4 July 1998. Once the rig was secured we began the transit to Site 1110 (proposed site ACE-10A). At Hole 1109D, we cored 449.2 m of section and recovered 299.87 m (67%).

TRANSIT TO SITE 1110 (ACE-10A)

Because we had left a positioning beacon at Site 1108, we traveled to that site during the transit to Site 1110 (ACE-10A). The drilling line was slipped and cut while under way. Once arriving at Site 1108, we signaled the beacon to release and lowered the thrusters. The beacon was successfully recovered at 0245 hr on 4 July 1998. While the ship moved the final 3.3 nmi (6.1 km) to Site 1110 in dynamic positioning mode, we put together the APC/XCB coring assembly and began to run in the hole to save rig time.

SITE 1110

Hole 1110A

At 0600 hr on 4 July 1998 the positioning beacon for Site 1110 was deployed. The pipe was lowered the remaining distance to the seafloor and Hole 1110A was spudded at 0945 hr. Core 1H was taken with the bit at 3243.9 mbsl and recovered 7.03 m; therefore, the seafloor was calculated to be at 3246.4 mbsl. Core 2H failed to fully stroke and recovered 2.5 m of sand and gravel. We terminated this hole at a total depth of 9.5 mbsf, and Hole 1110A ended at 1100 hr when the pipe was pulled clear of the mudline.

Hole 1110B

Without offsetting the ship, we spudded Hole 1110B at 1130 hr on 4 July 1998. Core 1H was taken with the bit at 3241.9 mbsl and recovered 5.08 m; therefore, the seafloor was calculated to be at 3246.3 mbsl. We then switched to XCB coring. Core 3X took ~2.5 hr to cut and was recovered with the soft formation XCB cutting structure destroyed. High and erratic torque, slow ROP, and very low recovery was enough to convince us that the XCB system was not well suited to the formation. Coring was terminated at a total depth of 22.3 mbsf, the drill string recovered, and Hole 1110B ended at 2330 hrs on 4 July when the bit cleared the rig floor.

Hole 1110C

After assembling an RCB BHA, we tripped the pipe back to the seafloor. The ship was offset 30 m on a course of 280°, and we spudded Hole 1110C at 0545 hr on 5 July. A seafloor depth of 3246 mbsl was determined by tagging the seafloor with the drilling assembly. Repeated attempts were made to drill ahead with a center bit in place. After 7 hr of high torque, packing off, overpull, fill, and extremely slow penetration, it became painfully clear that a satisfactory hole was not going to be possible at this location. The hole was terminated after penetrating a mere 15.0 mbsf without even attempting to cut a single core. Hole 1110C ended at 1300 hr on 5 July when the bit cleared the mudline.

Hole 1110D

The center bit was recovered and a core barrel was deployed. The ship was offset 30 m north and 30 m east before we spudded Hole 1110D at 1430 hr on 5 July. The seafloor was tagged at 3245.8 mbsl, and drilling (without coring) proceeded to a depth of 22.7 mbsf. A single core was cut to a depth of 28.7 mbsf before we abandoned this hole for the same reason as Hole 1110C. High torque, packing off, overpull, and generally poor hole conditions prevailed once again. The drill pipe was pulled clear of the seafloor at 1845 hr officially ending Hole 1110C, and the core barrel was retrieved while we waited for the released positioning beacon to surface. Recovery for the 6.0-m interval cored was 0.16 m (2.7%).

TRANSIT TO SITE 1111 (ACE-11A)

The positioning beacon was recovered aboard at 1945 hr. With the drill bit positioned three stands above the seafloor we moved the ship ~1 km north to Site 1111 (proposed site ACE-11A). A positioning beacon was deployed at 2030 hr on 5 July 1998 at the Site 1111 GPS coordinates.

SITE 1111

Hole 1111A

The drill string was tripped the remaining distance to the seafloor and at 2230 hr on 5 July 1998 we spudded Hole 1111A. The seafloor was determined to be at 3200.8 mbsl. The RCB coring continued through Core 18R to 173.7 mbsf. Drilling rates in the upper part of the hole were 5–10 min per core, and recovery, with the exception of two isolated cores at 43%, was very low (1%–7%). A single temperature measurement was taken at 94 mbsf inside the drill pipe using the DVTP. Two additional measurements were taken using the DVTP with the probe pushed into the formation at 117.2 and 136.5 mbsf. A slow ROP (6.0 m/hr) and concerns over the potential for future instability of the hole led us to abandon the hole at 173.7 mbsf. The hole was displaced with 30 bbl of weighted mud, and the drill string was pulled clear of the mudline at 0335 hr on 7 July 1998. The beacon was released and the pipe trip continued to a depth of 2941 mbsl, where it was secured for the transit to the next site. The beacon was recovered at 0430 hr, ending Hole 1111A. Recovery for the hole was 15.19 m (8.7%).

TRANSIT TO SITE 1112 (ACE-12A)

The ~2.6-nmi transit to Site 1112 (proposed site ACE-12A) took 3 hr, and the positioning beacon was deployed at 0730 hr on 7 July.

SITE 1112

Hole 1112A

After picking up the top drive we advanced the pipe the remaining distance to the seafloor. Hole 1112A was spudded at 0900 hr, and the seafloor depth was established to be 3046.7 mbsl. The RCB coring continued through Core 11R to a depth of 101.8 mbsf. Although recovery was poor, the hole stability remained reasonably good until this point. At 0745 hr on 8 July, the hole packed off, preventing circulation, and the driller experienced high torque on the pipe. The pipe was pulled up to 39.0 mbsf and then reamed back to bottom. This wiper trip took ~1.25 hr and encountered 5.0 m of fill in the bottom of the hole. After washing out the fill, the hole was advanced two more cores to 116.4 mbsf. The bit was encountering resistance at 105.0 mbsf; therefore, the pipe was pulled back up to 96.0 mbsf and then reamed back to 116.4 mbsf. At this point we swept the hole with a double sepiolite mud pill (total of 50 bbl) and circulated it out of the hole before recovering the wash barrel. Once again the bit began to take weight at 105.0 mbsf and 2 hr more was spent pulling the pipe back to 96.0 mbsf then reaming back to 105.0 mbsf, where we circulated another 30-bbl sepiolite mud pill. Because there appeared to be a bad spot in the hole at 105 mbsf, we decided to pull the drill string back up the hole and change the spacing out of the drill string using a 20-ft knobby drilling joint. This was intended to enable us to drill past the trouble spot and make a connection without having to pull the pipe back above the bad spot. The hole packed off again during this process, and we ultimately had to pull the pipe to 77.0 mbsf before circulation could be restored. The bit was reamed down again and reached 116.4 mbsf after washing out 7.0 m of fill. Another 30-bbl sepiolite mud pill was circulated and we resumed coring with Core 14R. The hole was advanced to 122.4 mbsf, where high pump pressure and top drive stalling occurred with as little as 10,000 lb WOB. At this point, we decided that this hole was not salvageable; therefore, Core 14R was retrieved and we pulled out of the hole. Because this hole was never advanced beyond the unconsolidated “talus” material, it was not abandoned using heavy mud or cement. The seafloor was cleared at 2330 hr on 8 July, and the bit cleared the rig floor at 0430 hr on 9 July, officially ending Hole 1112A. Recovery for the hole was 5.85 m (4.8%).

Hole 1112B

After replacing the RCB core bit with a new C-4 bit, the pipe was lowered back to the seafloor. Before spudding Hole 1112B, a brief jet-in test was conducted in case a reentry cone was ultimately required at this site. The bit was advanced to a depth of 20 mbsf in ~50 min using up to 100 spm. The pipe was pulled clear of the mudline in preparation for spudding Hole 1112B.

Hole 1112B was spudded at 1130 hr on 9 July and the seafloor was determined to be at 3046.7 mbsl. The hole was drilled to 87.0 mbsf with a wash barrel (Core 1W) in place; however, at that depth the driller experienced high torque on the pipe and up to 30,000 lb of overpull. After working the pipe for 30 min, the hole appeared to be cleaned up and Core 1W was retrieved. We then continued drilling with a second wash barrel (Core 2W) to 126.1 mbsf. After Core 2W was recovered, we deployed a bit deplugger to ensure that the throat of the bit was unobstructed before initiating RCB coring. Cores 3R through 5R were then taken from 126.1 to 155.0 mbsf.

After recovering Core 5R, the hole again packed off and the top drive began to stall. The pipe was worked up and down the hole for the next 8.25 hr with overpulls of 20,000–40,000 lb. Several 30- to 50- barrel sepiolite pills were circulated, and the bit was eventually able to reach back to bottom after drilling out 6 m of fill on the bottom. Core 6R was then cut to 164.0 mbsf. Once again, the hole packed off and another 5.25 hr was spent fighting hole problems before we abandoned further attempts to deepen the hole. The pipe was pulled clear of the seafloor at 1400 hr on 11 July ending Hole 1112B. Recovery for the hole was 1.49 m (3.9%).

TRANSIT TO SITE 1113 (ACE-13A)

After raising the drill pipe to 2745 mbsl and recovering the positioning beacon, we began the DP transit to Site 1113 (proposed site ACE-13A). The positioning beacon was deployed at the GPS Site 1112 (ACE-12A) coordinates at 1645 hr on 11 July.

SITE 1113

Hole 1113

The vessel was positioned over the site as the drill pipe was lowered back to the seafloor. The top drive was picked up, and Hole 1113A was spudded at 2045 hr on 11 July 1998. The seafloor was tagged at a depth of 2915.6 mbsl, and we cut RCB Cores 1R and 2R to 20.2 mbsf. After making the drill pipe connection prior to cutting the next core, 7 m of sediment filled the bottom of the hole. The fill was washed out and Core 3R was cut to 25.2 mbsf. We decided to terminate the hole because of the extremely slow ROP (0.8 m/hr) and poor hole conditions at such shallow subseafloor depths. The pipe was pulled clear of the seafloor at 1345 hr on 12 July, and the bit cleared the rig floor, ending Hole 1113A at 2000 hr. Recovery for the hole was 0.44 m (1.7%).

TRANSIT TO SITE 1114 (ACE-14A)

During the ~3.6-nmi transit (in dynamic positioning mode) to Site 1114 (proposed site ACE-14A), an RCB BHA was made up with a new bit and a mechanical bit release. The ship arrived on location at 2015 hr on 12 July and a positioning beacon was deployed. However, this beacon could not be used for positioning because it had shifted into half repetition rate mode, possibly because of interference from one of the precision depth recorders (PDRs) (12 or 3.5 kHz). The ship returned to the GPS coordinates, and a second beacon was deployed at 2130 hr.

SITE 1114

Hole 1114A

While lowering the pipe to determine seafloor depth, the strong current caused the knobby drilling joints to drag in the guide horn. This allowed the heave compensator to close leading the driller to incorrectly assume the seafloor had been tagged. As a result several water cores were recovered before eventually spudding Hole 1114A at 406.5 mbsl at 0130 hr on 13 July.

The RCB Cores 1R through 31R were taken from 0 to 295.4 mbsf. The intervals l42–180 mbsf and 257–276 mbsf, were characterized by rapid ROP and extremely poor recovery (0%–4%). The small amount of recovery indicated the presence of sand in these intervals. Metamorphic rocks were first recovered at ~300.0 mbsf (Core 32R) and coring continued to 352.8 mbsf (Core 37R). While coring there were several episodes when we lost acoustic contact with the positioning beacons. A third positioning beacon was deployed at 1340 hr on 14 July, but contact with this beacon was lost almost immediately. At 1642 hr, a fourth beacon was deployed ~150 m upcurrent from Hole 1114A using the zodiac. The intent was for the beacon to drift with the >1.5 nmi/hr current while sinking to the bottom and to end up closer to the actual spud location. No further positioning problems were encountered.

While preparing to retrieve Core 37R, the hole collapsed, packing off the annulus and preventing circulation. The pipe was raised 80 m above the bottom of the hole on two separate occasions before circulation could be established. We spent 6.25 hr trying to get back to bottom to resume coring without success; therefore, we decided to run wireline logs in the portion of the hole that remained open. The bit release sleeve was shifted at 316.0 mbsf; however, the bit did not release. The pipe was picked up to 304.0 mbsf while rotating the pipe with the top drive. The bit released between 304 and 316 mbsf, and the hole was displaced with 90 bbl of sepiolite mud. The pipe was raised to 80.0 mbsf, and we rigged up for logging.

The first logging run with the triple combo was able to log from 304.0 mbsf up to ~60 mbsf. The second logging run with the FMS-sonic tool was able to log up from 299.0 mbsf. Once logging was completed (0545 hr on 16 July) we ran the open-ended drill pipe back in the hole as far as possible (107.0 mbsf) and displaced the hole with 35 bbl of 10.5-ppg bentonite gel mud. The

drill string was pulled clear of the seafloor at 0625 hr, and the four positioning beacons were recovered in 1.25 hr. At 0800 hr on 16 July, the drilling assembly cleared the rig floor and we began the transit to Site 1115 (proposed site ACE- l5A). Core recovery for Hole 1114A was 43.78 m (12%).

TRANSIT TO SITE 1115 (ACE-15A)

After the ~36 nmi (~3.75 hr) transit to Site 1115 (ACE-15A), a positioning beacon was deployed at the Site 1115 GPS coordinates at 1145 hr on 16 July.

SITE 1115

Hole 1115A

After preparing an APC coring assembly and lowering it to the seafloor, we spudded Hole 1115A at 1510 hr on 16 July. The single APC core taken at Hole 1115A recovered 4.43 m; therefore, the seafloor was 1149.6 mbsl. The bit was pulled clear of the mudline, immediately ending Hole 1115A, Core 1H was recovered, and the pipe was spaced out for spudding Hole 1115B.

Hole 1115B

At 1540 hr, Hole 1115B was spudded and Core 1H recovered 7.14 m, establishing the seafloor depth at 1148.8 mbsl. Cores 1H through 23H were taken to 216.2 mbsf. Core orientation (tensor tool) was performed on Cores 4H–23H, and Adara temperature measurements were taken after Cores 3H (26.2 mbsf), 5H (45.2 mbsf), 7H (64.2 mbsf), and 9H (83.2 mbsf) were recovered. APC coring was suspended after Core 23H when 70,000 lb overpull was required to extract the core barrel from the formation. APC core recovery was 225.67 m (104%).

Use of the XCB began with Core 24X and continued through Core 31X to a depth of 1453.4 m or 293.1 mbsf. A single DVTP temperature measurement was taken after Core 23X at a depth of 225.7 mbsf. Hole conditions remained excellent as did the ROP, which averaged 19.2 and 38.4 m/hr respectively on the last two cores. Recovery for the XCB portion of the hole was 80%. The hole was terminated after Core 31X because the formation had become indurated enough for successful RCB coring and because this section would have to be drilled again later in Hole 1115C. Total recovery for the hole was 286.84 m (98%).

The drill string was pulled clear of the seafloor at 1415 hr on 17 July, and the bit cleared the rig floor at 1615 hr that same day, ending Hole 1115B.

Hole 1115C

While we assembled the RCB BHA, the ship was offset 30 m to the west. The drill string was lowered to the seafloor and Hole 1115C was spudded at 2130 hr on 17 July. A seafloor depth of 1148.7 mbsl was established, based on a reduction in drill string weight. With a center bit in place, the hole was drilled without coring to 283.2 mbsf. The hole was flushed clean and the center bit recovered, preparing the way for RCB coring.

The RCB coring began at 0400 hr on 18 July 1998 and continued through Core 54R to 802.5 mbsf. Coring was terminated when the scientists considered that the primary scientific objectives had been achieved. Two zones of low recovery were encountered: 7% from 523.0 to 542.2 mbsf and from 1% to 2% from 628.8 to 657.8 mbsf. Bentonite gel mud sweeps (30 bbl each) were pumped every third core, and hole conditions remained excellent throughout the coring operations. Penetration rates were quite variable, ranging from 5.8 m/hr to 57.6 m/hr and averaged 18.0 m/hr. Total RCB core recovery was 291.63 m (56.2%).

A wiper trip up to 99.7 mbsf and then back to the bottom identified tight spots at 701.7 and 762.7 mbsf where the driller observed 40,000 lb overpull. The bit encountered 15 m of fill in the bottom of the hole, which we decided not to spend the time washing, reaming, and circulating out of the hole. The bit was released, the hole displaced with 215 bbl of sepiolite mud, and the drill pipe positioned at 99.7 mbsf in preparation for logging.

We began rigging up for logging at 0500 hr on 21 July 1998, and the first logging run consisted of the triple combo. The suite of tools reached a depth of 783.7 mbsf, which was 4.0 m above where the bit was released. The second tool string (FMS-sonic) also reached the same depth. Two logging passes were made with the FMS before pulling it out of the hole. The third logging string run was the ultrasonic borehole imager (UBI). This tool was put aboard by Schlumberger in lieu of a second borehole televiewer (BHTV) tool. The UBI is another form of borehole imager used extensively in industry, but this was the first time this tool had been deployed for ODP. The tool reached the same depth as the previous tool runs but, unfortunately, did not function correctly. It was recovered without obtaining any data. The final logging run was with the WST, but it failed to pass a bridge at 564.7 mbsf (probably because of its light weight). An air gun was deployed using the aft port side aft crane, and several stations were successfully occupied until the logging run had to be aborted because of an expected helicopter landing. During helicopter landings, the cranes must not be deployed for safety reasons. At 0600 hr, the WST was pulled up inside the pipe, the air gun was rigged down, and the crane used to deploy the air gun was retracted. The helicopter was bringing out a reporter from the Australian Broadcasting Commission (ABC) and a roustabout who had recovered from illness after having been evacuated from the ship earlier in the leg. We were notified by the ship's agent in PNG that the helicopter would depart Alotau at ~0630 hr on 22 July and would arrive on location within 30 min. By 0730 hr the helicopter had still not arrived and

the radio officer made several unsuccessful attempts to contact the helicopter via radio. He was able to hear conversations between other airborne helicopters but was not able to contact the helicopter destined for the *JOIDES Resolution.* At ~0845 hr the ship received a phone call from the agent that the helicopter had gone to the wrong site coordinates. Unable to locate the ship the helicopter had returned to Alotau. At ~0900 hr we resumed VSP logging operations. Subsequent VSP stations were not as successful as those earlier because of an unidentified source of noise in the system. After attempts to isolate and fix the cause of the noise, the VSP was terminated. The WST was pulled out of the hole and the air guns rigged down. All logging operations were completed, and the tools rigged down by 1345 hr on 22 July 1998.

The open-ended drill pipe was lowered to 483.7 mbsf, and the hole was displaced with 100 bbl of 10.5-ppg weighted gel mud. The drill string was pulled clear of the seafloor at 1630 hr, and the positioning beacon was recovered at 1745 hr. After recovering the drill string, the BHA drill collars and associated subs were subjected to the routine end of leg inspection for cracks (none were identified). Once the BHA inspection was completed, the final thruster was raised and we began the transit to Site 1116 (proposed site ACE-16A) at 2230 hr on 22 July 1998.

TRANSIT TO SITE 1116 (ACE-16A)

While under way to Site 1116 (ACE-16A), the drill crew prepared the RCB coring and BHA with a new C-4 core bit and MBR. At 0330 hr on 23 July, the seafloor positioning beacon was deployed, beginning Hole 1116A.

SITE 1116

Hole 1116A

After lowering the BHA to 1819.0 mbsl and picking up the top drive in preparation for spudding, the driller began the normal process of slowly circulating seawater ("slow circulating rates," SCRs) to establish baseline rig floor pressures for various flow rates before spudding. The pump pressure immediately rose to 600 psi (at 40 spm). Because this was abnormally high, the sinker bars were run in the hole to recover the core barrel. There was no sign of any sediment nor were any mechanical problems noted with the core barrel or its retrieval. Another core barrel was pumped to bottom, and the driller started circulating the seawater. This time the pump pressure rose immediately to 1400 psi and continued to climb until the driller shut down the pumps. It appeared that all of the bit nozzles were completely plugged. We decided not to make any more attempts to clear the blockage because in this relatively shallow water it would not take too long to retrieve the BHA to physically investigate the problem.

The bit reached the rig floor after a 4.5-hr pipe trip and a thorough inspection of all the BHA components failed to identify any mechanical problem or blockage. The bit, bit jets, support bearing, float valve, MBR, and core-barrel latch sleeve were all found to be unobstructed and in normal condition. Furthermore, there were no indications that any of these components had been below the seafloor, nor had the drillers seen any reduction in drill string weight to indicate that the bit had contacted the seafloor during the pipe trip.

While the drill crew was reassembling the original core barrel components for a rig floor flow test, the coring technician inspected another bit release assembly that was in the process of being rebuilt in the core technicians shop. He then noticed that when the lower support bearing was installed in the pocket of the bit disconnect, there appeared to be no flow path remaining for the circulating fluid. Upon checking the machine drawing of the bit disconnect it became apparent that this component had a manufacturing flaw. A 60% taper at the base of the pocket was missing, which prevented nearly all of the flow around the bearing. The only flow area remaining was that left between the inside diameter of the support bearing and the outside diameter of the core barrel landing sub. The difference in pump pressure between the first and second core barrel deployed may have resulted from different amounts of wear on the respective landing subs, resulting in a more or less internal flow area.

The rig crew reassembled the original outer core barrel components and when the circulating pumps were activated the pump pressure was significantly higher than normal (600 psi at 15 spm). This confirmed that there was a mechanical blockage somewhere in the coring assembly, and upon removing the suspect MBR for the second time, it too was missing the critical taper. After installing a new MBR with the correct taper, a rig floor flow test indicated normal pump pressures. The rest of the BHA was prepared and lowered to the seafloor.

Hole 1116A was spudded at 1915 hr on 23 July and, based on a reduction in drill string weight, seafloor depth was determined to be 1851.3 mbsl. Because of the indurated nature of the seafloor sediments, the first few cores progressed slowly. After a few drill collars were buried beneath the seafloor, the drillers were able to increase the WOB and the top drive rpm. The first 48 mbsf cut at an average rate of 2.5 m/hr with 5000–10,000 lb WOB and 40 to 50 rpm. RCB Cores 1R through 18R were taken from 0 to 158.9 mbsf. Core recovery in Hole 1116A was generally poor, ranging from 2% to 33% (average 21%), and the overall penetration rate was 3.8 m/hr.

When the drill string was being raised after cutting Core 18 (0215 hr on 26 July), the drill string started experiencing torque. The driller continued to raise the drill string up to 153.0 mbsf, where rotation was lost and the pipe became stuck. For the next 1.75 hr, the driller attempted to free the drill string. He was able to maintain circulation in the hole, but could not rotate or raise/lower the pipe. Initial attempts to actuate the drilling jars were unsuccessful, leading the drill crew to believe that the drill string may have been stuck above the jars. Overpulls of up to 200,000 lb were unable to free the drill string.

After recovering Core 18R, we resumed efforts to free the drill string. At 0600 hr, after working the pipe for another 1.25 hr, the drilling jars were successfully actuated with ~40,000 lb of overpull. Drill string rotation and vertical movement was immediately established; however, pump pressures remained slightly higher than normal.

A short wiper trip of the hole was made up to 91.0 mbsf and all drilling parameters returned to normal. At 0630 hr on 26 July, a core barrel was deployed and the driller prepared to run it back to bottom to resume coring. When pump pressures did not rise as normally occurs when the core barrel has landed, the driller began to suspect that the bit may have released during the efforts to free the drill string. Another explanation may have been that a drill string component had been bent and was keeping the core barrel from landing properly. The sinker bars were run in the hole to determine if the core barrel had landed properly, but the sinker bars passed below the depth where the top of the core barrel should have been and then passed even slightly below where the bit should have been. This confirmed that the bit had indeed released; therefore, we retrieved the drill string and abandoned the hole. The positioning beacon was recovered at 1030 hr, and the pipe trip was completed at 1100 hr, ending Hole 1116A.

At the rig floor the MBR was inspected. It was determined that the release sleeve had not shifted and the latch segments (“dogs”) remained in place. Brinelling (deformation of metal) evidenced on the upper surface of the segments indicated that the bit disconnect portion of the MBR had failed and been stripped over the latch segments. It is not clear whether the bit disconnect mechanically failed because of the jarring action or the overpull used in freeing the drill string. It is speculated that the bit was stuck in the hole and that the overpull had weakened or cracked the bit disconnect above the latch dog windows. Subsequent jarring with the mechanical drilling jars likely caused the disconnect to fail completely releasing the bit and freeing the drill string.

TRANSIT TO SITE 1117

After finishing operations at Site 1116, we began the transit to Site 1117 in dynamic positioning mode. During the transit, an RCB coring BHA with a MBR was assembled. Because the seafloor at Site 1117 was expected to be exposed metamorphic rocks with minimal talus, we used a C-7 core bit that was expected to do better in these harsh drilling conditions. As at earlier holes, the mechanical drilling jars were verified to be in good working condition and included in the BHA. The drill string, with a core barrel in place, was lowered to a depth of 1113.3 mbsl. While the pipe was being lowered to the seafloor, the positioning beacon was deployed at 1205 hr, and the ship was positioned over the site.

SITE 1117

Hole 1117A

The drill pipe was gently lowered until the bit encountered the seafloor at 1163.2 mbsl and we spudded Hole 1117A at 1535 hr on 26 July. Because hard rock was exposed at the seafloor, the first cored interval extended to 12.2 mbsf. This allowed the driller to maintain some rathole below his bit so that the bit would remain in the hole when recovering the first core barrel and making the next drill pipe connection. As on earlier attempts during this leg to spud directly into hard seafloor, initial progress was slow and it took >6 hr to cut the first core. The result was remarkable, with 4.07 m intact fault gouge being recovered. The success proved to be short-lived however, when an additional 13 cores recovered a total of 2.35 m (2.4%). Because of the hard, highly fractured formation and the poor recovery, it was thought that this hole was living on borrowed time almost from the start. It was pretty clear to everyone that once the drilling jars and the top of the BHA (8 1/4-in drill collars) became buried below the seafloor, 97.2 and 115.5 m respectively, the real problems would begin. The likelihood of the hole penetrating much below 100 mbsf was slight. Sure enough, at 0215 hr on 28 July 1998, while cutting Core 14R at 111.1 mbsf the driller began to experience excessive drilling torque. The pipe was pulled back to a depth 50.1 mbsf with 60,000 lb overpull. At that point rotation was lost and the pipe became firmly stuck. The pipe was worked for 15 min with up to 200,000 of overpull before rotation was regained and the pipe became free. We all knew that once these problems began it would be a diminishing return of penetration gained over time spent. Therefore, the bit was pulled clear of the seafloor at 0400 hr on 28 July. Total recovery for Hole 1117A was 6.42 m (5.8%).

Hole 1117B

Because of the keen interest in attempting to obtain another surface core containing fault gouge that could be used for whole-round sampling, we decided to cut another "mudline" core. Without offsetting the ship, Hole 1117B was spudded at 0445 hr on 28 July. The bit tagged the seafloor at the same depth as Hole 1117A (1163.2 mbsl). Core 1R was cut in 3.5 hr to a depth of 9.5 mbsf. The bit was pulled clear of the seafloor at 0830 hr. When Core 1R was recovered, it did not contain any fault gouge and only 5 cm of metamorphic rock.

Hole 1117C

We decided to make one more try to obtain more fault gouge. Again without offsetting the ship, Hole 1117C was spudded at 0900 hr. Core 1R took <2.25 hr to advance to 9.5 mbsf. The bit was pulled clear of the mudline and the core barrel was recovered. Core 1R recovered only 10 cm of metamorphic rock and, unfortunately, no fault gouge. The rig crew began to retrieve the drill string; the positioning beacon was recovered at 1245 hr on 28 July, and the ship began the transit to Site 1118 (proposed site ACE-1C).

TRANSIT TO SITE 1118 (ACE-1C)

During the ~11.5 nmi transit from Site 1117, an RCB BHA with drilling jars and a MBR was put together and run down to the seafloor.

SITE 1118

Hole 1118A

After the positioning beacon was deployed (1830 hr on 28 July), Hole 1118 was spudded at 2030 hr on 28 July. A seafloor depth of 2303.6 mbsl was determined by reduction in drill string weight. This was 3.0 m shallower than the 3.5-kHz PDR depth. With a center bit in place, we drilled without coring to 205.0 mbsf with an average ROP of 51.3 m/hr.

Once the center bit was retrieved and the hole circulated with a 20-bbl gel mud sweep, RCB coring began at 0330 hr on 29 July. Cores 1R-73R were taken from 205.0 to 897.5 mbsf. When the driller raised the bit off bottom to recover Core 73R, he observed 30,000 lb overpull, high torque, high pump pressure, and 3.0 m of fill in the bottom of the hole. Core 74R also had similar overpull and fill. Coring was stopped after reaching 926.6 mbsf (Core 76R) to allow enough time for a wiper trip, hole conditioning, and a full wireline logging program. Overall ROP for the cored portion of the hole was 15.3 m/hr. Total recovery for the hole was 466.21 m (65%).

After circulating the hole clean with a 40-bbl pill of bentonite gel mud, a wiper trip was conducted up to 98.6 mbsf. When the bit was lowered back down, 36.0 m of fill was encountered in the bottom of the hole. We decided not to take the time to clean out the fill and released the bit at 892.6 mbsf. In preparation for logging, the hole was displaced with 300 bbl of sepiolite mud and the drill string raised up to 98.6 mbsf. Overpulls of 20,000–30,000 lb were required to pull the pipe from 491.6 to 434.6 mbsf; therefore, an additional 20-bbl pill of 10.5 ppg mud was spotted in the pipe before continuing up to logging depth.

We began rigging up for logging at 1030 hr on 3 August 1998. The first logging was with the triple combo tool and was able to reach 887.6 mbsf, which was 5.0 m above where the bit was released. The loggers requested that the pipe be raised 20 m to log more of the shallow section, but this was rejected because the pipe was experiencing up to 30,000 lb overpull. A second pass was made with the triple combo to get more detailed temperature data, and the tool was stopped for 10 min each at 410.0 mbsf, 620.0 mbsf, and 830.0 mbsf.

After the triple combo run was finished, the FMS-sonic tool string was run and also reached 887.6 mbsf. The lowermost 50.0 m of the hole was logged twice, and the logs were collected up to the pipe depth (98.6 mbsf). Caliper data from the FMS tool indicated some tight spots (4–5 in diameter) down as far as 298.6 mbsf. During the FMS-sonic run, the drill string began taking weight (10–20,000 lb) and overpull of 10–20,000 lb. After the FMS-sonic run was finished and it

was in the pipe being retrieved, the pipe was raised slightly but could only be lowered back down to within 6 in of the dual-elevator stool, even with slow circulation (higher circulation could not be used with the logging tool inside the drill pipe). We decided to pull back up about 1.0 m with the pipe hung off the elevator bales and retrieve the FMS-sonic tool string by pulling it through the blocks. Once the tools were laid down, the top drive was picked up and the pipe lowered back down to 309.6 mbsf; however, no resistance was encountered and the pipe was pulled back to 107.6 mbsf in preparation for the VSP logging with the WST. The WST was run in the hole but could not pass 691.6 mbsf (due to its light weight). A total of 20 stations occupied between 691.6 and 107.6 mbsf. The WST was retrieved and logging was completed at 1845 hr on 4 August.

While we were logging, PNG customs and immigration officials came aboard to clear the ship and personnel out of PNG territorial waters. One of the two PNG observers departed the ship on the helicopter with the PNG officials.

The drill string was lowered to 395.6 mbsf and the hole was displaced with 144 bbl of 10.5 ppg mud. After the drill pipe was retrieved and the BHA taken apart and secured, the positioning beacon was recovered at 0337 hr on 5 August. At 0430 hr on 5 August the vessel began the transit to Sydney, Australia.

TRANSIT TO SYDNEY, AUSTRALIA

During the transit, the heave compensator was taken apart in preparation for the planned replacement of seals while in Sydney. At 1523 hr on 8 August, a three-person documentary film crew (Australian Broadcasting Corporation) visited the ship for two hours. After the 6.04-day transit (1524 nmi), Leg 180 ended with the first line ashore in Sydney, Australia, at 0530 hr on 11 August.